Stability of Systems with Stochastic Delay

by

Mehdi Sadeghpour

A dissertation submitted in partial fulfillment
of the requirements for the degree of
Doctor of Philosophy
(Mechanical Engineering)
in The University of Michigan
2018

Doctoral Committee:

Professor Gábor Orosz, Chair
Professor Matthew R. Bennett, Rice University
Professor Allen P. Liu
Professor Jeffrey T. Scruggs

Mehdi Sadeghpour

mehsad@umich.edu

ORCID iD: 0000-0003-3946-960X

To Hadi

A C K N O W L E D G M E N T S

I am thankful to my advisor and mentor, Gábor Orosz, who guided and supported me as I walked down the path to my PhD degree. I thank my collaborators in research, Marcella Gomez, Matthew Bennett, Krešimir Josić, Richard Murray, and Dimitri Breda who I gained a lot of insight and guidance from. I thank my colleagues, Chaozhe He, Sergei Avedisov, Wubing Qin, Jin Ge, and Linjun Zhang, who I received help and feedback from in our lab and group meetings.

I am thankful to my family, especially my parents, who always supported me unconditionally. I thank my dear wife, Kate, who has always been supporting me with her helpful advice and positive thoughts and inputs.

TABLE OF CONTENTS

Dedication . . . . . **ii**

Acknowledgments . . . . . **iii**

List of Figures . . . . . **vi**

Abstract . . . . . **xi**

Chapter

1 Introduction and motivation **1**

2 Stochastic delays in discrete time **4**

2.1 Introduction 4
2.2 Problem statement 5
2.2.1 Semi-discretization technique 7
2.2.2 Discretization of the stochastic system 9
2.3 Stability conditions 10
2.3.1 Convergence of spectra and stability charts – an illustrative example 14
2.4 Stochastic versus distributed delay 19
2.4.1 Evolution matrices 20
2.4.2 A numerical example 24
2.5 Generalization to random dwelling times and Markov jumps 26
2.5.1 Problem setup 26
2.5.2 Moment equations 27
2.5.3 An example 33
2.6 Discussion 34

3 Stochastic delays in continuous time **37**

3.1 Introduction 37
3.2 Problem statement 38
3.3 Solution operator representation of the system 39
3.4 Stability analysis 41
3.5 Finite-dimensional approximations 49
3.6 Examples 51
3.6.1 Scalar system 51
3.6.2 A vector (2-D) system 52
3.7 Note on almost-sure stability 54

3.8 Discussion . . . 57

4 Applications of the method on gene regulation dynamics . . . 58

4.1 Introduction . . . 58
4.2 Stochastic delays in a gene regulatory network . . . 58
4.3 Model of an auto-regulatory gene circuit . . . 60
4.4 Auto-regulatory gene network with mRNA dynamics and dual delayed feedback . . . 66
4.5 Discussion . . . 69

5 Dynamics of microbial consortia . . . 70

5.1 Introduction . . . 70
5.2 Dynamics of a two-strain co-repressive consortium . . . 71
5.2.1 Bistability in the absence of metabolic loading . . . 74
5.2.2 Impact of metabolic loading on population toggle dynamics . . . 76
5.3 Small population effects . . . 79
5.3.1 Stochastic dynamics in the absence of metabolic loading . . . 81
5.3.2 The impact of metabolic loading on stochastic growth dynamics . . . 83
5.4 Discussion . . . 84

6 Conclusion . . . 87

Appendix . . . 88

Bibliography . . . 93

LIST OF FIGURES

2.1 (a) A sample path of the delay with two values τ_1 and τ_2 and dwelling time $t_{\rm d}$. (b) The dwelling time $t_{\rm d}$ is discretized to ℓ time steps such that $t_{\rm d} = \ell\Delta t$, ($\ell = 3$ in this case). 7

2.2 Left column: stability charts for system (2.33) with delay distribution $w(\sigma) = \frac{1}{3}\delta(\sigma - 0.2) + \frac{1}{3}\delta(\sigma - 0.3) + \frac{1}{3}\delta(\sigma - 0.4)$ and the dwelling time $t_{\rm d} = 0.1$ for different values of the discretization step Δt as indicated on the left. Blue curves are the stability boundaries for the mean while the red curves are the stability boundaries for the second moment. The dashed black curves are stability boundaries for the mean in the continuous limit (system (2.36)). Light gray shading indicates mean stability and dark gray shading indicates second moment stability. Middle column: Eigenvalues for the discretized mean dynamics (matrix $\bar{\mathbf{A}}$) corresponding to point P located at $(a, b) = (-1, -6.5)$. Right column: Eigenvalues for the second moment dynamics (matrix $\bar{\bar{\mathbf{A}}}$) at point P. Stable eigenvalues are plotted as green while unstable eigenvalues are plotted as red. 16

2.3 The spectral radii of the matrices $\bar{\mathbf{A}}$ and $\bar{\bar{\mathbf{A}}}$ as functions of $1/\Delta t$ shown in panels (a) and (b), respectively. The horizontal dashed red line in (a) shows the value of $\left|\mathrm{e}^{s_{1,2}t_{\rm d}}\right|$ where $s_{1,2}$ are the leading characteristic roots of (2.37). . . 18

2.4 (a–d) Comparison of the spectra of the matrix $\mathbf{M}_{\rm dd}$ in (2.50) (indicated by $\circ$), associated with the distributed-delay system (2.43), and the spectra of the matrix $\mathbf{M}_{\rm sd}$ in (2.48) (indicated by $\times$) associated with the mean of the stochastic-delay system (2.42), for different dwelling times $t_{\rm d}$ as indicated. The spectra are obtained for point P shown in the bottom panels and only the 10 largest eigenvalues in magnitude are shown in the complex plane. (e–f) Stable regions of the distributed-delay system (2.43) obtained using the eigenvalues of the matrix $\mathbf{M}_{\rm dd}$ in (2.50) (bounded by dashed green curves) and the mean of the stochastic-delay system (2.42) obtained using the eigenvalues of the matrix $\mathbf{M}_{\rm sd}$ in (2.48) (bounded by solid blue curves), for different dwelling times. The light gray area is a parameter domain where both (2.42) and (2.43) are stable. The dark gray area is where (2.42) is stable but (2.43) is not. The red area is where (2.42) is not stable but (2.43) is stable. 25

2.5 (a) A sample realization of the time evolution of the delay τ with $J = 3$ possible values. (b) A sample realization of the approximated delay process. . 28

2.6 Stability chart in the plane of parameters a and b. Dark shaded area is the region of stability; *i.e.* the second moment (and the mean) are stable. Light shaded area shows the region in which only the mean (but not the second moment) is stable. The black dashed curve shows the boundary of stability region of a deterministic system with a fixed average delay $\tau_{\text{avg}} \approx 8.33$. Simulations for points A and B are displayed in panels (a) and (b) of Fig. 2.7, respectively. . 34
2.7 (a) Simulation results for system (2.82) using the parameters at point A in Fig. 2.6. (b) Simulation results using the parameters at point B in Fig. 2.6. The black curve shows the mean and the red curves show the mean plus and minus the standard deviation based on the gray sample trajectories. 35

3.1 **a** Two sample paths of the delay with dwelling time $t_{\text{d}} = 1$ and delay values $\{0.5, 1, 1.5\}$. **b** Trajectories of the scalar version of system (3.1) with $\mathbf{a} = -1$ and $\mathbf{b} = -2$ corresponding to sample paths of the delay shown in Fig. 3.1a and initial condition $\phi(\theta) = 0.1$, $-1.5 \leq \theta \leq 0$. 39
3.2 Stability charts for system (3.67). The blue curve is the boundary of the mean stable area. The red curve is the boundary of the second moment stable area. For comparison, the stable areas of deterministic versions of system (3.67) with delays equal to $\tau = 0.5$ and $\tau = 1$ are shown with dashed and solid black boundaries, respectively. 52
3.3 Stability charts for system (3.70-3.71). The red curve is the boundary of the second moment stable area. For comparison, the stability boundary of a deterministic version of system (3.70-3.71) with delay $\tau = 1$ (the average delay) is also shown by a black curve. **a** Stable and unstable areas in the (k_1, k_2) space for system parameters associated with point Q in panel b. **b** Stable and unstable areas in the (a_1, a_2) space for control gains indicated by point P in panel a. 54
3.4 Stable and unstable regions of system (3.67) in the sense of the second moment and almost sure stability where the red curve is the boundary of the second moment stable area and the cyan curve is the boundary of the almost sure stable area. **a** The parameters are the same as in Fig. 3.2. **b** The parameters are the same as in Fig. 3.2 except that $t_{\text{d}} = 2$ (slower delay switchings). For comparison, stable regions of the deterministic version of system (3.67) with delays $\tau = 0.5$ and $\tau = 1$ are also shown by dashed and solid black curves, respectively. 56

4.1 An auto-regulatory gene network. The target gene codes for the protein *LacI* that represses its own production by blocking the RNA polymerase from binding. 60
4.2 (a) A normalized histogram of the delay obtained with running a Gillespie simulation for system (4.1) with $N = 50$ reactions and $c = 5$ reactions per second using the initial condition $P_0 = 10000$, $P_i = 0$, for $i = 1, \ldots, N$. The black curve shows the Erlang distribution (4.2) for the same parameters with mean $E = N/c = 10\,[\text{s}]$ and variance $V = N/c^2 = 2\,[\text{s}^2]$. (b) Discretization of the Erlang distribution using Dirac deltas separated by $\Delta t = 1\,[\text{s}]$. 61

4.3 Stability charts for system (4.8),(4.9) when the delay follows the Erlang distribution (4.2) for different values of the mean delay $E = N/c$ and relative variance $R = 1/N$. The dwelling time is set to $t_{\mathrm{d}} = 1\,[\mathrm{s}]$ and $\Delta t = 1\,[\mathrm{s}]$. The dark gray region is where the second moment and the mean are stable. The light gray region is where the mean is stable but not the second moment. The dashed black curve is the boundary of the stability for the continuous-time mean dynamics described by Eqs. (4.13). 64

4.4 (a–c) Numerical simulations of the linear model (4.8),(4.9) for points A $(\gamma, \kappa) = (1.5, 600)$, B $(\gamma, \kappa) = (2.5, 600)$, and C $(\gamma, \kappa) = (3.5, 600)$ marked in Fig. 4.3(g). (d–f) Corresponding simulation results of the nonlinear model (4.6). In each panel (a–f), the black trajectory indicates the mean while the red trajectories enclose mean $\pm$ standard deviation for 1000 runs and the gray curve shows a sample realization. 65

4.5 Top panels: stability boundaries for the linearized system (2.2,4.19) with $\tau_1 = 10\,[\mathrm{s}]$ and $\tau_2 = 20\,[\mathrm{s}]$ and probability distribution $w_1 = u$, $w_2 = 1 - u$ for (a) $u = 1$, (b) $u = 0$, and (c) $u = 0.75$. Bottom panels: simulation results of the nonlinear model (4.16) for parameter values associated with point Q: $(\gamma_p, \alpha_m) = (0.5, 70)$. A sample trajectory of proteins as a function of time for (d) $u = 1$, (e) $u = 0$, and (f) $u = 0.75$. Note that panels (d) and (e) correspond to the deterministic systems with the single delay $\tau = 10\,[\mathrm{s}]$ and $\tau = 20\,[\mathrm{s}]$, respectively. 68

4.6 (a) The spectral radius of $\bar{\bar{\mathbf{A}}}$ versus the weight u in the probability distribution. (b) The spectral radius of $\bar{\bar{\mathbf{A}}}$ versus the dwelling time t_{d}. 69

5.1 Single- and two-strain toggle switch. **a** Gene circuit diagram of a single cell co-repressive toggle switch [23]. **b** Proposed synthetic microbial consortium with a co-repressive network. Each strain contains a transcriptional inverter (mediated by LacI) and an enzyme that creates a quorum sensing molecule. Repression occurs when the quorum sensing molecule from one strain diffuses into the other strain, up-regulating the target transcriptional inverter (green dashed arrows). That inverter down-regulates production of the second, orthogonal quorum sensing molecule. 72

5.2 Two-strain population toggle with equal growth rates. **a** The equilibrium x_1^* as a function of population ratio r. The dashed and solid lines correspond to unstable and stable equilibria, respectively. **b** Two trajectories of Eq. (5.1) approaching one of the two stable equilibria marked by ♦ and ■ based on the initial conditions. The third, unstable equilibrium is denoted by ○. The gray dashed line shows the separatrix between the two basins of attraction of the stable equilibria. The parameters are chosen as $\beta_1 = \beta_2 = 0.023\,[\mathrm{min}^{-1}]$ corresponding to *E. coli*'s cell cycle of approximately 30 minutes, $\alpha = 10\,[\mathrm{min}^{-1}]$, $\theta = 500$, $N = 200$, and $n = 2$. The simulations are carried out for constant population ratio $r = 0.4$ and initial conditions $\big(x_1(0), x_2(0)\big) = (100, 200)$ proteins per cell and $\big(x_1(0), x_2(0)\big) = (300, 100)$ proteins per cell. 75

5.3 Two-strain population toggle with different growth rates. Simulations of system (5.1),(5.2),(5.4),(5.6) with $\beta_0 = 0.023\,[\text{min}^{-1}]$ and different ϵ values as indicated. Other parameters are the same as in Fig. 5.2. Initial protein concentrations are $\big(x_1(0), x_2(0)\big) = (100, 200)$ proteins per cell and initial population ratio is $r(0) = 0.1$. 76
5.4 Metabolic loading leading to relaxation oscillations. Simulations of system (5.1),(5.2),(5.4),(5.7) for different values of ϵ and ρ as indicated. Parameters are $\beta_0 = 0.023\,[\text{min}^{-1}]$, $\alpha = 10\,[\text{min}^{-1}]$, $\theta = 500$, $N = 200$, and $n = 2$. Initial conditions are $\big(x_1(0), x_2(0)\big) = (100, 200)$ proteins per cell and $r(0) = 0.4$. 77
5.5 Bifurcation diagrams for the two-strain toggle under metabolic load. In panels **a,b,d,e**, solid and dashed lines denote stable and unstable equilibria, respectively. In panels **d,e,f**, the markers $\times$ and $*$ indicate transcritical and Hopf bifurcations, respectively. The solid magenta line in panels **c,f** shows the amplitude of the periodic solution. In panel **f** the periodic solution emerges from a Hopf bifurcation. Parameters are the same as in Fig. 5.4. 78
5.6 Stochasticity in the dynamics of the two-strain toggle consortium. **a,b** Simulations of system (5.8)-(5.11) with no metabolic loading ($\rho = 0$) and equal growth rates ($\epsilon = 0$) for different population sizes as indicated. The blue and green curves show the mean number of proteins in strains 1 and 2, respectively. The red curve shows the population ratio. Simulations of the deterministic system (5.1),(5.2),(5.4) are also shown using gray curves. Parameters are the same as in Fig. 5.4. Initial protein counts are $x_{1,i}(0) = 100$, $i = 1, \ldots, n_1$, $x_{2,j}(0) = 200$, $j = 1, \ldots, n_2$, and initial ratio of strain 1 is $r(0) = 0.4$. **c,d** Stochastic simulations of the population ratio r corresponding to the parameters in panels **a,b**, respectively. The mean of the simulations (μ_r) and the mean plus and minus the standard deviation ($\mu_r \pm \sigma_r$) are also shown as functions of time. 81
5.7 Simulations of the stochastic system (5.8)-(5.11) with unequal growth rates of the strains and no metabolic loading ($\rho = 0$) with different ϵ and N values as indicated. The gray curves show the simulations of the corresponding deterministic model (5.1),(5.2),(5.4),(5.6). Parameters are the same as in Fig. 5.4. Initial conditions are $x_{1,i}(0) = 100$ proteins, $i = 1, \ldots, n_1$, $x_{2,j}(0) = 200$ proteins, $j = 1, \ldots, n_2$, and initial ratio of strain 1 is $r(0) = 0.1$. 83
5.8 Effects of the metabolic load on the stochastic dynamics of the two-strain toggle. Simulations of the stochastic system (5.8)-(5.11) with metabolic loading $\rho = 0.5$ and $\epsilon = 0$ for different populations sizes as indicated. The gray curves show the simulations of the corresponding deterministic model (5.1),(5.2),(5.4),(5.7). Parameters are the same as in Fig. 5.4. Initial conditions are $x_{1,i}(0) = 100$ proteins, $i = 1, \ldots, n_1$, $x_{2,j}(0) = 200$ proteins, $j = 1, \ldots, n_2$, and initial ratio of strain 1 is $r(0) = 0.4$. 84

5.9 Effects of the metabolic load on the extinction times of the two-strain consortium. Normalized histograms of the extinction times for different values of metabolic loading ρ obtained from 500 simulations of the stochastic model (5.8)-(5.11) with $N = 40$ and $\epsilon = 0$. Parameters are the same as in Fig. 5.4. Initial conditions are $x_{1,i}(0) = 100$ proteins, $i = 1, \ldots, n_1$, $x_{2,j}(0) = 200$ proteins, $j = 1, \ldots, n_2$, and initial population ratio is $r(0) = 0.5$. 85

ABSTRACT

Stability of systems with stochastic delays is addressed in this dissertation. A linear delay differential equation is considered where the delay takes values from a finite set of numbers according to a probability distribution function. Exact stability conditions for the resulting system are obtained. These conditions depend on the parameters of the system, the delay values and the probability distribution function governing the delay. The stability criteria are first obtained in a discrete-time setting after discretizing the continuous-time system. Then, the stability conditions are obtained in a continuous-time setting where an operator description of delay differential equations is used.

The stability results are applied to models of gene regulatory networks. The results can determine whether a steady state protein production is stable or oscillations in protein levels may arise as a result of stochastic fluctuations in reaction times. Finally, the interplay between noise in the gene expression level and noise in the population level in microbial consortia is investigated. The results suggest a mechanism for creating robust oscillations in multicellular environments.

CHAPTER 1

Introduction and motivation

Today there are an astonishingly large number of labs where biologists do experiments on biological entities spanning from bacteria to human cells in order to understand the principles based on which the living systems function, improve the current medicine, and explore the frontiers of science. An important question hovering over all areas of life sciences is: what are the design principles of biological systems allowing them to function in a remarkably robust manner? To answer this question, one needs to have a quantitative evaluation of the key biological processes underlying the behaviors of biological systems. This is where the motivation for this research is stemming from.

One of the most important areas of study of biological systems at the cellular level is to understand the function of gene regulatory networks—networks of genes and their protein products that respond to environmental signals and perform logical functions in cells. Mathematical modeling of these networks is deemed capable of answering questions such as: why and when do genes turn on or off and how do they influence the functionality of the cell? Correct mathematical modeling of biological events is, however, not straightforward. In particular, if one wishes to model every biological process that is involved in a biological system, one will end up with a highly complicated, large-dimensional model that cannot be analyzed either analytically or numerically. In an attempt to tackle this issue, a sequence of consecutive biological events or reactions that lead to a specific product can be replaced with one delayed reaction where the delay is the total time needed for all the reactions to take place. This way the complexity of the mathematical model reduces significantly.

This reduction is used in modeling, for instance, transcription and translation processes that are key processes in gene regulatory networks. Put briefly, transcription is the process of reading a gene by an enzyme and producing an RNA strand that has the same nucleotide sequence as the original gene. Translation is the process of reading this RNA strand by another enzyme and producing a chain of amino acids based on the nucleotide sequence of the RNA. The chain of amino acids, after some modifications, becomes a protein. Instead of modeling the process of reading the gene or RNA strand by an enzyme as a series of

reactions where each reaction represents reading one nucleotide at a time, one can use a single delayed reaction for the entire transcription or translation process. The delay is the time it takes for the enzyme to finish reading the genetic sequence of the DNA or RNA. On the other hand one should note that a very important aspect of biological systems is the inherent randomness that exists at the molecular level. Whether two reactant molecules are going to collide or not as well as "when" they collide are probabilistic events by nature. As a result, the time it takes for all necessary reactions for reading a genetic sequence to take place is a random quantity.

Using delayed reactions in lieu of many consecutive reactions leads to dealing with delay differential equations. Even though the theory for the analysis of delay differential equations is well developed when the delays are known [30, 16], it is lacking when the delays are random or stochastic. This observation serves as a motivation for us to study the dynamics and stability of systems described by delay differential equations where the delays are subject to stochastic variations. Mathematical analysis of the dynamics and stability of systems with stochastic delays has not gained much attention in literature. Therefore, not only we study this problem in a mathematically rigorous manner providing theorems and proofs, but also we provide numerical techniques to investigate different aspects of the problem in an efficient manner.

We use our developed methods to investigate stability properties of some gene regulatory networks and illustrate how our theory can be used to elucidate the effects of stochasticity in signaling times on the dynamics of these systems. Not only in the design of biological circuits, our theoretical results are expected to be useful for any system where information flow may experience random delays. Additionally, we also study other aspects of noise in biological systems; in particular, we study the interplay between intracellular and population level dynamics in a noisy multicellular environment. The structure of the thesis is as follows.

In Chapter 2, we consider a nonlinear system of delay differential equations where the delay is a stochastic process. We study the local stability of the system through linearizing around the steady state. We discretize the continuous-time system using a semi-discretization process, and obtain necessary and sufficient conditions for the stability of the discretized system. We characterize the stability of the mean as well as the second moment of the stochastic system. We illustrate the application of the method on a generic scalar system. We show that when the discretization time step tends to zero, the stability charts converge.

In Chapter 3, we consider a linear continuous-time system with stochastic delay. We study the stability of the system in continuous time directly rather than discretizing the

system first. The goal is to obtain an expression for the continuous-time version of stability conditions that we obtained in Chapter 2. We take advantage of the theory of the solution operators of delay differential equations as well as tensor products of Banach spaces to achieve this goal.

In Chapter 4, the theoretical tools are applied to some models of gene regulatory networks with negative feedback. In particular, we consider an auto-regulatory gene with single and dual negative feedback pathways.

In Chapter 5, we study the interactions between the intracellular dynamics of gene expression and the population level dynamics in multicellular systems. In particular, we consider two strains of cells that are in the same container and study their growth dynamics as they compete in a noisy environment. We propose a model that captures both intracellular dynamics and intercellular signaling and sheds light on mechanisms that lead to different dynamic behaviors such as steady-state or oscillations.

In Chapter 6, conclusions are provided.

CHAPTER 2

Stochastic delays in discrete time

2.1 Introduction

Time delays are a well-known source of instability in dynamical systems and can make control design a challenging task. When the delays are assumed to be constant or distributed, there are well established methods to analyze stability and bifurcations of equilibria and periodic orbits [30, 16, 39, 11]. When the delays depend on time or on the state of the system, stability analysis becomes more difficult and may require averaging or numerical techniques [7, 33, 55]. However, in some cases delays vary stochastically in time, making it very challenging to characterize stability. We target the problem of stability analysis of systems with stochastically changing delays. In addition to biological systems such as gene regulatory networks [29, 34], stochastic delays also arise in applications such as networked control systems [42, 60] and connected vehicle systems [66].

When investigating dynamics under stochastic delay variations, key factors include the stochastic process describing the time evolution of the delay and the type of stability investigated. In early works, random delays modeled by continuous-time Markov chains were incorporated into delay differential equations [36, 47] and Lyapunov stability theorems were used to obtain sufficient conditions of stability. Lyapunov-based approaches were extended to nonlinear systems [40] and also were applied to discrete-time systems where sufficient stability conditions were presented in the form of matrix inequalities [22, 63, 90]. These conditions are typically very conservative making it difficult to evaluate the true effect of the stochastic delays on the dynamics. Additionally, a design based on the worst case scenario (*e.g.* largest delay) can lead to unnecessary conservativeness or may simply give erroneous results. Even ensuring stability for each value of the delay does not necessarily give the stability of the stochastic system [24, 69].

We consider a relatively broad class of delay processes and focus on moment (mean and second moment) stability. We use a time-discretization technique, called semi-discretization

that is developed in [32], to create a discretized version of the continuous-time system. Using the discretized system, we obtain stability conditions based on which we classify different stability losses and draw stability charts.

2.2 Problem statement

Consider a system of the form

$$\dot{\chi}(t) = f\big(\chi(t), \chi(t-\tau(t))\big)\,, \tag{2.1}$$

where the dot denotes the derivative with respect to time t, $\chi \in \mathbb{R}^n$, $f\colon \mathbb{R}^n \times \mathbb{R}^n \to \mathbb{R}^n$, and the delay $\tau(t) \in \mathbb{R}$ varies in time stochastically. More precisely, we assume that the delay follows a stationary stochastic process with probability distribution $w(\sigma)$, $\sigma \in [\tau_{\min}, \tau_{\max}]$. Thus, the initial condition is given by $\chi(t) = \chi_0(t)$, $t \in [-\tau_{\max},\ 0]$. Due to the stochasticity in the delay, the vector $\chi(t)$ is also a stochastic process.

Linearizing Eq. (2.1) about an equilibrium $\chi(t) \equiv \chi_*$ results in the system

$$\dot{x}(t) = \mathbf{a}\, x(t) + \mathbf{b}\, x(t-\tau(t))\,, \tag{2.2}$$

where $x(t) = \chi(t) - \chi_*$, $\mathbf{a} = \partial_1 f(\chi_*, \chi_*), \mathbf{b} = \partial_2 f(\chi_*, \chi_*) \in \mathbb{R}^{n\times n}$, and ∂_1 and ∂_2 represent derivatives with respect to the first and second variables, respectively. We will analyze the time evolution of the first and the second moment of the linear system (2.2) by discretizing it in time. Note that we cannot express in closed form the time evolution of the first and the second moment of the nonlinear system (2.1) in general.

We consider a class of delay processes where the delay trajectories are piece-wise constant functions of time. Namely, we assume that the delay $\tau(t)$ may only take J possible discrete values from the set $\Omega = \{\tau_1, \tau_2, \ldots, \tau_J\}$ where $\tau_1 < \tau_2 < \cdots < \tau_J$, and the probability density function (pdf) of the delays is $\mathbb{P}\big(\tau(t) = \tau_j\big) = w_j$ where $\mathbb{P}$ denotes probability and $\sum_{j=1}^{J} w_j = 1$. This pdf can also be expressed in terms of Dirac delta function, that is,

$$w(\sigma) = \sum_{j=1}^{J} w_j\, \delta(\sigma - \tau_j)\,. \tag{2.3}$$

From here on, we use the term probability density function and delay distribution interchangeably. Note that one can approximate continuous delay distributions by increasing the density of the Dirac deltas, *i.e.* picking more discrete points from the distribution. Additionally, we assume that the delay stays constant for a time $t_{\rm d}$ (called switching time or

dwelling time) before switching to a new value (or possibly staying at the same value). A sample realization of the delay is shown in Fig. 2.1 for $J = 2$ delay values. As seen in Fig. 2.1, the delay is constant in the time intervals $[kt_{\rm d}, (k+1)t_{\rm d})$, $k = 0, 1, 2, \ldots$ that we call dwelling intervals. Since the probability distribution function (2.3) is not changing with time, the delay values in different dwelling intervals for $k = 0, 1, 2, \ldots$ are independent and identically distributed (*i.i.d.*). We focus on stability analysis of linear systems in the form of (2.2) with stated assumptions on the delay behavior. The stability of system (2.2) is a local stability result for the nonlinear system (2.1).

Let us first take the expected value, denoted by $\mathbb{E}$, of system (2.2) which gives us

$$\frac{\rm d}{{\rm d}t}\mathbb{E}[x(t)] = \mathbf{a}\,\mathbb{E}[x(t)] + \mathbf{b}\sum_{j=1}^{J}\mathbb{P}\big(\tau(t)=\tau_j\big)\;\mathbb{E}[x(t-\tau_j)|\tau(t)=\tau_j]\,. \tag{2.4}$$

If the dwelling time $t_{\rm d}$ is smaller than the minimum delay, *i.e.* $t_{\rm d} < \tau_1$, then $x(t-\tau_j)$ is independent of $\tau(t)$ due to the *i.i.d.* assumption on the delay values. To see this, assume that $kt_{\rm d} \le t < (k+1)t_{\rm d}$ for some k. Now if the dwelling time is less than the minimum delay, then $\tilde{k}_j t_{\rm d} \le t-\tau_j < (\tilde{k}_j+1)t_{\rm d}$ for some $\tilde{k}_j < k$. In other words, $t-\tau_j$ will fall in one of the dwelling intervals proceeding the current interval k. Note that $x(t-\tau_j)$ depends only on the delay values in the dwelling intervals $[\hat{k}t_{\rm d},\ (\hat{k}+1)t_{\rm d})$, $\hat{k} = 0, 1, \ldots, \tilde{k}_j$. Since the delays are chosen based on a fixed probability distribution at each switching, the delays at different dwelling intervals are mutually independent. Therefore $x(t-\tau_j)$ is independent of $\tau(t)$ and $\mathbb{E}\big[x(t-\tau_j)|\tau(t)=\tau_j\big] = \mathbb{E}\big[x(t-\tau_j)\big]$. Hence, introducing the notation $\bar{x} = \mathbb{E}[x]$, (2.4) reduces to the distributed delay system

$$\dot{\bar{x}}(t) = \mathbf{a}\,\bar{x}(t) + \mathbf{b}\sum_{j=1}^{J} w_j\,\bar{x}(t-\tau_j) \tag{2.5}$$

which describes the dynamics of the mean and it can be analyzed using standard stability and bifurcation analysis tools [19, 72, 74]. The mean dynamics can provide some information about the effect of stochastic delays as they explicitly contain the delay distribution. However, to characterize the stochastic stability only the mean dynamics are not enough and one needs to analyze other stochastic stability criteria. We will focus on the stability of the second moment that is a well-known stability criterion for stochastic systems. Note that the distributed delay system (2.5) is only valid for the mean $\bar{x}(t)$ in the case when $t_{\rm d} < \tau_1$. Nonetheless, our stability analysis method for system (2.2), that will be presented in Chapters 2 and 3, works for the general case, *i.e.* for arbitrary $t_{\rm d}$.

In order to analyze the second moment of the continuous-time system (2.2), we dis-

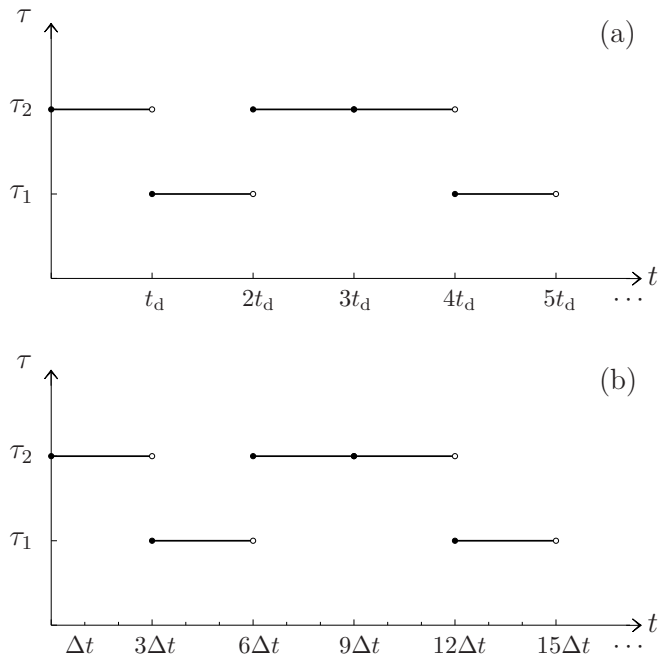

Figure 2.1: (a) A sample path of the delay with two values τ_1 and τ_2 and dwelling time t_d. (b) The dwelling time t_d is discretized to ℓ time steps such that $t_\mathrm{d} = \ell\Delta t$, ($\ell = 3$ in this case).

cretize system (2.2) by dividing the holding intervals of length t_d into $\ell \in \mathbb{N}$ subintervals of length $\Delta t = t_\mathrm{d}/\ell$; see Fig. 2.1b. Then, using semi-discretization technique from [32], we construct a discrete-time map as a discretization of (2.2) which allows us to obtain conditions for the stability of the mean and the second moment. We also demonstrate, using a numerical example, the convergence of the stability charts, that are obtained using our proposed stability conditions, when $\Delta t \to 0$.

2.2.1 Semi-discretization technique

To explain the discretization method, we first discretize the deterministic system

$$\dot{x}(t) = \mathbf{a}x(t) + \mathbf{b}x(t-\tau), \tag{2.6}$$

that has only a single fixed delay. Note that by substituting the trial solution $x(t) = \kappa \mathrm{e}^{st}$, $\kappa \in \mathbb{C}^n$, $s \in \mathbb{C}$, in (2.6), we obtain the characteristic equation

$$s\mathbf{I} - \mathbf{a} - \mathbf{b}\,\mathrm{e}^{-s\tau} = 0 \tag{2.7}$$

where s is a characteristic root. System (2.6) is stable if and only if all (infinitely many) characteristic roots are located in the left-half complex plane.

Now consider the mesh $t_i = i\Delta t$, $i = 0, 1, 2, \ldots$. Let $m = \lfloor \tau/\Delta t \rfloor$. In the time interval $[i\Delta t, (i+1)\Delta t)$, we use the approximation $x(t-\tau) \approx x(i\Delta t - m\Delta t)$ (a zeroth-order approximation) in (2.6), and solve the approximate system

$$\dot{\tilde{x}}(t) = \mathbf{a}\tilde{x}(t) + \mathbf{b}\tilde{x}\big(i\Delta t - m\Delta t\big), \qquad t \in [i\Delta t, (i+1)\Delta t) \tag{2.8}$$

that yields

$$\tilde{x}\big((i+1)\Delta t\big) = \boldsymbol{\alpha}\tilde{x}(i\Delta t) + \boldsymbol{\beta}\tilde{x}\big((i-m)\Delta t\big), \tag{2.9}$$

where

$$\boldsymbol{\alpha} = \mathrm{e}^{\mathbf{a}\Delta t}, \qquad \boldsymbol{\beta} = \big(\int_0^{\Delta t} \mathrm{e}^{\mathbf{a}(\Delta t - t)}\mathrm{d}t\big)\mathbf{b}, \tag{2.10}$$

If $\mathbf{a}^{-1}$ exists, then the second formula in (2.10) results in $\boldsymbol{\beta} = \big(\mathrm{e}^{\mathbf{a}\Delta t} - \mathbf{I}\big)\mathbf{a}^{-1}\mathbf{b}$, where $\mathbf{I}$ is the n-dimensional identity matrix.

Now we define the augmented state vector $X(i) = \big[\tilde{x}^{\mathrm{T}}(i\Delta t),\, \tilde{x}^{\mathrm{T}}\big((i-1)\Delta t\big),\, \ldots,\, \tilde{x}^{\mathrm{T}}\big((i-m)\Delta t\big)\big]^{\mathrm{T}} \in \mathbb{R}^{n(m+1)}$, that contains the history of the state back to the last m time steps. Here T denotes the transpose. Now using Eq. (2.9), we can write

$$X(i+1) = \mathbf{T}X(i), \tag{2.11}$$

where

$$\mathbf{T} = \begin{bmatrix} \boldsymbol{\alpha} & & & \boldsymbol{\beta} \\ \mathbf{I} & & & \\ & \mathbf{I} & & \\ & & \ddots & \\ & & \mathbf{I} & \end{bmatrix} \in \mathbb{R}^{n(m+1)\times n(m+1)}. \tag{2.12}$$

Note that the block sub-diagonal elements are all given by the $n \times n$ identity matrix $\mathbf{I}$. The stability of matrix $\mathbf{T}$ determines the stability of the approximate system (2.8)-(2.9), *i.e.* if all the eigenvalues of $\mathbf{T}$ are inside the unit circle, then the linear system (2.8)-(2.9) is stable. In fact, the matrix $\mathbf{T}$ is a finite-dimensional approximation of the infinite-dimensional solution operator of the linear system (2.6). Assume z is an eigenvalue of $\mathbf{T}$. Then, as $\Delta t \to 0$, $\tilde{s} = \frac{1}{\Delta t}\ln z$ approaches the characteristic roots given by (2.7); *i.e.* $\tilde{s} \to s$; therefore, the stable region (in the plain of some parameters) of the approximate system (2.8) converges to the stable region of the original system (2.6) as the time step goes to zero ($\Delta t \to 0$). In

practice, one can obtain stability charts for system (2.6) by making Δt small until achieving a desired accuracy. See [32] and [11] for more information on the discretization of the delay differential equations and approximating their spectra and [16] for more information about the solution operators and infinitesimal generators of delay differential equations.

2.2.2 Discretization of the stochastic system

Now we use the discretization method explained in the previous section to create a discrete-time map as a discretization of the stochastic system (2.2). Consider the same mesh $t_i = i\Delta t$, $i = 0, 1, 2, \ldots$, and let $m_j = \lfloor \frac{\tau_j}{\Delta t} \rfloor$, $j = 1, \ldots, J$. The delay values are in fact rounded off to the mesh size Δt. Here the approximate system is

$$\dot{\tilde{x}}(t) = \mathbf{a}\,\tilde{x}(t) + \mathbf{b}\,\tilde{x}(i\Delta t - m(i)\Delta t), \quad t \in [i\Delta t, (i+1)\Delta t), \tag{2.13}$$

where $m(i) \in \{m_1, \ldots, m_J\}$, for $i = 0, 1, 2, \ldots$. Solving (2.13) yields

$$\tilde{x}(i+1) = \boldsymbol{\alpha}\,\tilde{x}(i) + \boldsymbol{\beta}\,\tilde{x}(i - m(i))\,, \tag{2.14}$$

where $\boldsymbol{\alpha}$ and $\boldsymbol{\beta}$ were introduced in (2.10) and the notation $\tilde{x}(i) = \tilde{x}(i\Delta t)$ is used. Let us define $X(i) = [\,\tilde{x}^{\mathrm{T}}(i)\,,\ \tilde{x}^{\mathrm{T}}(i-1)\,, \ldots\,, \tilde{x}^{\mathrm{T}}(i-m_J)\,]^{\mathrm{T}} \in \mathbb{R}^{n(m_J+1)}$ as an augmented state vector that contains the history of the state up to the last m_J time steps (corresponding to the largest delay in the system). Note that in the case when $t_{\mathrm{d}} > \tau_J$, *i.e.* when the dwelling time is larger than the maximum delay, we define the augmented state vector in a way that it contains the history of the state up to the last ℓ time steps. Recall that we choose Δt such that $t_{\mathrm{d}} = \ell\Delta t$. Therefore, in the case of $t_{\mathrm{d}} > \tau_J$, m_J will be replaced with ℓ in the formulation in the remainder of this chapter.

Eq. (2.14) can be written in a vector-matrix form

$$X(i+1) = \mathbf{G}(i)\,X(i), \tag{2.15}$$

where the matrix $\mathbf{G}(i)$, $i = 0, 1, 2, \ldots$ can take one of the values

$$\mathbf{G}_j = \begin{bmatrix} \boldsymbol{\alpha} & \mathbf{0} & \cdots & \boldsymbol{\beta} & \cdots & \mathbf{0} \\ \mathbf{I} & \mathbf{0} & \mathbf{0} & \cdots & \mathbf{0} & \mathbf{0} \\ \mathbf{0} & \mathbf{I} & \mathbf{0} & \cdots & \mathbf{0} & \mathbf{0} \\ \mathbf{0} & \mathbf{0} & \mathbf{I} & \cdots & \mathbf{0} & \mathbf{0} \\ \vdots & \vdots & \vdots & \ddots & \vdots & \vdots \\ \mathbf{0} & \mathbf{0} & \mathbf{0} & \cdots & \mathbf{I} & \mathbf{0} \end{bmatrix} \in \mathbb{R}^{n(m_J+1)\times n(m_J+1)}, \tag{2.16}$$

$j = 1, \ldots, J$, based on the probability distribution $\mathbb{P}(\mathbf{G}(i) = \mathbf{G}_j) = w_j$. The location of the block element $\boldsymbol{\beta} \in \mathbb{R}^{n\times n}$ is in the first block-row and the $(m_j + 1)$-th block-column. Indeed, $\mathbf{G}(i) = \mathbf{G}_j$ occurs if $m(i) = m_j$ that corresponds to $\tau(t) = \tau_j$ in the interval $[i\Delta t, (i + 1)\Delta t)$.

Now recall that the delay is constant within each of the dwelling intervals $\big[kt_{\rm d}, (k + 1)t_{\rm d}\big)$ and $t_{\rm d} = \ell\Delta t$. Therefore, from system (2.15) we can write

$$X((k + 1)\ell) = \big(\mathbf{G}_j\big)^{\ell} X(k\ell), \quad k = 0, 1, 2, \ldots, \tag{2.17}$$

given that $\tau(t) = \tau_j$ in the time interval $[kt_{\rm d}, (k + 1)t_{\rm d})$. By defining $\tilde{X}(k) = X(k\ell)$, this yields

$$\tilde{X}(k + 1) = \mathbf{A}(k)\, \tilde{X}(k), \tag{2.18}$$

where $\mathbf{A}(k)$ takes values

$$\mathbf{A}_j = \big(\mathbf{G}_j\big)^{\ell} \in \mathbb{R}^{n(m_J+1)\times n(m_J+1)}, \tag{2.19}$$

based on the probability distribution $\mathbb{P}\big(\mathbf{A}(k) = \mathbf{A}_j\big) = w_j$, $j = 1, \ldots, J$. Since the delays at different dwelling intervals are *i.i.d.*, the matrices $\mathbf{A}(k)$ are *i.i.d.* and $\mathbf{A}(k)$ is independent of $\tilde{X}(k)$.

It should be noted that if one uses different discretization techniques, one will end up with different finite-dimensional matrices than the ones in (2.16). Other common discretization techniques used for delay differential equations are Runge-Kutta methods (see [7]) and linear multi-step methods (see [18] and references therein). Although different discretization techniques have different convergence properties, the theory developed in this dissertation works for any type of discretization scheme as long as a constant step-size mesh is used. We are using the semi-discretization technique from [32] for its simplicity. Also the semi-discretization method converges faster than full discretization methods with the same order such as forward difference, backward difference, and central difference schemes as shown in [32].

2.3 Stability conditions

In this section, we establish conditions for stability of the stochastic dynamical system (2.18), that is a discretization of system (2.2). Let us start with some definitions.

Definition 2.1. A random sequence $\{X(k) \in \mathbb{R}^n\}_{k=0}^{+\infty}$ converges to 0 almost surely if $\mathbb{P}\big(\lim_{k\to\infty} X(k) = 0\big) = 1$ or equivalently $\mathbb{P}\big(\forall\, \epsilon > 0,\ \|X(k)\| > \epsilon$ happens only finitely often$\big) =$

1. If sequences generated by a stochastic dynamical system converge to 0 almost surely, then the trivial solution $X(k) \equiv 0$ is almost surely stable. Almost sure convergence is also called convergence with probability one.

Definition 2.2. A random sequence $\{X(k) \in \mathbb{R}^n\}_{k=0}^{+\infty}$ converges to 0 in the mean if $\lim_{k\to\infty} \mathbb{E}\big[X(k)\big] = 0$ and converges to 0 in the second moment if $\lim_{k\to\infty} \mathbb{E}\big[X(k)X^{\mathrm{T}}(k)\big] = 0$. If sequences generated by a stochastic dynamical system converge to 0 in the mean or in the second moment, then the trivial solution $X(k) \equiv 0$ is stable in the mean or in the second moment, respectively.

Stability in the second moment is sufficient for the stability in the mean, but in general, there is no relationship between second moment stability and almost sure stability. However, in the special case described by system (2.18) where $\mathbf{A}(k)$ are *i.i.d.*, stability in the second moment does imply almost sure stability (see [44] page 217). We remark that for vector-valued sequences, moments higher than 2 are rarely used in the literature; see [66].

We begin by characterizing the dynamics of the mean $\mathbb{E}[\tilde{X}(k)]$ of (2.18). Stability of the mean provides a necessary condition for the stability of the stochastic system, that is, if the mean is unstable then the system is unstable. Therefore, the stability region for the mean in the parameter space contains the true stable region. We next derive the dynamics of the second moment $\mathbb{E}[\tilde{X}(k)\tilde{X}^{\mathrm{T}}(k)]$ and provide a necessary and sufficient condition for the second moment stability and sufficient for almost sure stability.

Since $\mathbf{A}(k)$ is *i.i.d.*, it is independent of $\tilde{X}(k)$. Thus, taking the expected value of both sides of (2.18), we obtain

$$\begin{aligned}\mathbb{E}\big[\tilde{X}(k+1)\big] &= \mathbb{E}\big[\mathbf{A}(k)\tilde{X}(k)\big] = \mathbb{E}\big[\mathbf{A}(k)\big]\mathbb{E}[\tilde{X}(k)] \\ &= \Big(\sum_{j=1}^{J} \mathbb{P}\big[\mathbf{A}(k) = \mathbf{A}_j\big]\mathbf{A}_j\Big)\mathbb{E}[\tilde{X}(k)] \\ &= \Big(\sum_{j=1}^{J} w_j \mathbf{A}_j\Big)\mathbb{E}[\tilde{X}(k)].\end{aligned} \tag{2.20}$$

Using the notation

$$\bar{\tilde{X}}(k) := \mathbb{E}[\tilde{X}(k)] \in \mathbb{R}^{n(m_J+1)}, \tag{2.21}$$

we can write the discretized mean dynamics (2.20) in the form

$$\bar{\tilde{X}}(k+1) = \bar{\mathbf{A}}\,\bar{\tilde{X}}(k), \tag{2.22}$$

where

$$\bar{\mathbf{A}} = \sum_{j=1}^{J} w_j \, \mathbf{A}_j = \sum_{j=1}^{J} w_j \big(\mathbf{G}_j\big)^{\ell}, \tag{2.23}$$

and $\bar{\mathbf{A}} \in \mathbb{R}^{n(m_J+1)\times n(m_J+1)}$; cf. (2.19). Thus,

$$\lim_{k\to\infty} \bar{\tilde{X}}(k) = 0 \qquad \text{if and only if} \qquad \rho\big(\bar{\mathbf{A}}\big) < 1, \tag{2.24}$$

where $\rho(.)$ denotes the spectral radius. Note that

$$\rho(\mathbf{A}) = \max_i \{|\lambda_i|\}, \tag{2.25}$$

where λ_i are the eigenvalues of $\mathbf{A}$. Condition (2.24) is a necessary and sufficient condition for the stability of the mean of the stochastic system (2.18) that is a discretization of the continuous-time system (2.2).

To analyze the second moment of (2.18), we proceed as follows

$$\begin{aligned}
\mathbb{E}\big[\tilde{X}(k+1)\tilde{X}^{\mathrm{T}}(k+1)\big] &= \mathbb{E}\big[\mathbf{A}(k)\tilde{X}(k)\tilde{X}^{\mathrm{T}}(k)\mathbf{A}^{\mathrm{T}}(k)\big] \\
&= \sum_{j=1}^{J} \mathbb{P}\big[\mathbf{A}(k) = \mathbf{A}_j\big]\mathbb{E}\big[\mathbf{A}(k)\tilde{X}(k)\tilde{X}^{\mathrm{T}}(k)\mathbf{A}^{\mathrm{T}}(k)|\, \mathbf{A}(k) = \mathbf{A}_j\big] \\
&= \sum_{j=1}^{J} w_j \mathbf{A}_j \mathbb{E}\big[\tilde{X}(k)\tilde{X}^{\mathrm{T}}(k)|\, \mathbf{A}(k) = \mathbf{A}_j\big]\mathbf{A}_j^{\mathrm{T}} \\
&= \sum_{j=1}^{J} w_j \mathbf{A}_j \mathbb{E}\big[\tilde{X}(k)\tilde{X}^{\mathrm{T}}(k)\big]\mathbf{A}_j^{\mathrm{T}}\,,
\end{aligned} \tag{2.26}$$

where in the last step we used the independence of $\tilde{X}(k)$ and $\mathbf{A}(k)$. In order to vectorize Eq. (2.26), we introduce the vec operator. Let $\mathbf{H} = [\, h_1 \; h_2 \; \cdots \; h_m \,] \in \mathbb{R}^{n\times m}$, where $h_i \in \mathbb{R}^n$ denotes the i-th column vector. Then,

$$\mathrm{vec}(\mathbf{H}) = \begin{bmatrix} h_1 \\ h_2 \\ \vdots \\ h_m \end{bmatrix} \in \mathbb{R}^{nm}\,. \tag{2.27}$$

The following is a property of the vec operator. Assume $\mathbf{A}$, $\mathbf{B}$, and $\mathbf{C}$ are matrices such

that the product $\mathbf{ABC}$ is defined. Then,

$$\mathrm{vec}(\mathbf{ABC}) = \big(\mathbf{C}^{\mathrm{T}} \otimes \mathbf{A}\big)\mathrm{vec}(\mathbf{B}), \tag{2.28}$$

where $\otimes$ denotes the Kronecker product.

Now using the vec operator, we define the vectorized form of the second moment as

$$\bar{\tilde{X}}(k) := \mathrm{vec}\big(\mathbb{E}\big[\tilde{X}(k)\tilde{X}^{\mathrm{T}}(k)\big]\big) \in \mathbb{R}^{n^2(m_J+1)^2}. \tag{2.29}$$

Then using (2.27), (2.28), and (2.29), Eq. (2.26) becomes

$$\bar{\tilde{X}}(k+1) = \bar{\bar{\mathbf{A}}}\, \bar{\tilde{X}}(k)\,, \tag{2.30}$$

where

$$\bar{\bar{\mathbf{A}}} = \sum_{j=1}^{J} w_j \mathbf{A}_j \otimes \mathbf{A}_j = \sum_{j=1}^{J} w_j \big(\mathbf{G}_j\big)^{\ell} \otimes \big(\mathbf{G}_j\big)^{\ell}, \tag{2.31}$$

and $\bar{\bar{\mathbf{A}}} \in \mathbb{R}^{n^2(m_J+1)^2 \times n^2(m_J+1)^2}$. From (2.30), we know that

$$\lim_{k\to\infty} \bar{\tilde{X}}(k) = 0 \qquad \text{if and only if} \qquad \rho\big(\bar{\bar{\mathbf{A}}}\big) < \mathbf{1}. \tag{2.32}$$

Condition (2.32) is a necessary and sufficient condition for the stability of the second moment of the stochastic system (2.18) that is a discretization of the continuous-time system (2.2). Moreover, condition $\rho\big(\bar{\bar{\mathbf{A}}}\big) < \mathbf{1}$ is a sufficient condition for the almost sure stability of the stochastic system (2.18).

Remark 2.1. In the case when $t_{\mathrm{d}} > \tau_J$, the size of the corresponding matrices in (2.16) will be $n(\ell+1) \times n(\ell+1)$, while they will have the same structure. However, we state without proof that the eigenvalues of the matrices $\bar{\mathbf{A}}$ in (2.23) and $\bar{\bar{\mathbf{A}}}$ in (2.31) with the size $n(\ell+1) \times n(\ell+1)$ will be the same as the eigenvalues of the matrices $\bar{\mathbf{A}}$ and $\bar{\bar{\mathbf{A}}}$ with the size $n(m_J+1) \times n(m_J+1)$, respectively. This observation is especially beneficial in the case that the dwelling time is very large, $t_{\mathrm{d}} \gg \tau_{\max}$, as it can reduce the computational burden significantly. Also note that if $J = 1$, conditions $\rho\big(\bar{\mathbf{A}}\big) < 1$ and $\rho\big(\bar{\bar{\mathbf{A}}}\big) < \mathbf{1}$ reduce to the asymptotic stability condition of a deterministic system with one single delay, *i.e.* $\rho(\mathbf{G}_1) < 1$.

Remark 2.2. We provided necessary and sufficient stability conditions for the mean and the second moment (conditions (2.24) and (2.32), respectively) of the stochastic system (2.18) that is a discretization of the continuous-time system (2.2). The stable parameter domain of

the stochastic discretized system (2.18) converges to that of the stochastic continuous-time system (2.2) as $\Delta t \to 0$. We demonstrate this convergence using spectra of operators $\bar{\mathbf{A}}$ and $\bar{\bar{\mathbf{A}}}$ and stability charts for an example provided in the next section.

2.3.1 Convergence of spectra and stability charts – an illustrative example

Let us consider an example in order to illustrate the stability analysis method established in the previous section. Consider the scalar case of system (2.2), that is

$$\dot{x}(t) = a\,x(t) + b\,x(t-\tau(t))\,, \tag{2.33}$$

where a and b are scalars. Assume that the delay takes the values $\tau_1 = 0.2$, $\tau_2 = 0.3$, and $\tau_3 = 0.4$ with equal probability $w_1 = w_2 = w_3 = 1/3$, and assume the dwelling time is $t_\mathrm{d} = 0.1$. We want to obtain stability charts for system (in the (a, b) parameter space. Here the matrix in (2.16) is

$$\mathbf{G}_j = \begin{bmatrix} \alpha & 0 & \cdots & \beta & \cdots & 0 \\ 1 & 0 & 0 & \cdots & 0 & 0 \\ 0 & 1 & 0 & \cdots & 0 & 0 \\ 0 & 0 & 1 & \cdots & 0 & 0 \\ \vdots & \vdots & \vdots & \ddots & \vdots & \vdots \\ 0 & 0 & 0 & \cdots & 1 & 0 \end{bmatrix} \in \mathbb{R}^{(m_3+1)\times(m_3+1)}, \tag{2.34}$$

where $m_3 = \lfloor \tau_3/\Delta t \rfloor$ and

$$\alpha = \mathrm{e}^{a\Delta t}\,, \qquad \beta = \big(\mathrm{e}^{a\Delta t} - 1\big)\frac{b}{a}\,, \qquad (\beta = b\Delta t \text{ if } a = 0), \tag{2.35}$$

cf. Eq. (2.10). To evaluate the stability of the mean of system (2.33), we study the eigenvalues of matrix $\bar{\mathbf{A}}$ in (2.23), and to evaluate the stability of the second moment of system (2.33), we study the eigenvalues of matrix $\bar{\bar{\mathbf{A}}}$ in (2.31).

As shown in Eq. (2.5), the mean dynamics of system (2.33) can also be described by

$$\dot{\bar{x}}(t) = a\,\bar{x}(t) + b\sum_{j=1}^{3} w_j\,\bar{x}(t-\tau_j)\,, \tag{2.36}$$

as condition $t_\mathrm{d} < \tau_1$ holds in this example. We also study the stability of system (2.36) directly (without using the semi-discretization method) for comparison. The characteristic

equation of system (2.36) can be obtained by plugging the trial solution $\bar{x}(t) = \kappa \mathrm{e}^{st}$, $\kappa, s \in \mathbb{C}$ in (2.36) that yields

$$s - a - b \sum_{j=1}^{3} w_j \, \mathrm{e}^{-s\tau_j} = 0 \,. \tag{2.37}$$

Here, two different kinds of stability losses may occur. (i) When a real eigenvalue crosses the imaginary axis at 0 that is referred to as fold stability loss. Substituting $s = 0$ into the characteristic equation (2.37), we find that the fold stability loss occurs when crossing the boundary

$$b = -a \,. \tag{2.38}$$

(ii) When a pair of complex conjugate eigenvalues crosses the imaginary axis at $\pm \mathrm{i}\omega$ that is referred to as Hopf stability loss. Substituting $s = \mathrm{i}\omega$ into the characteristic equation (2.37), the Hopf stability loss boundary is obtained as

$$\begin{aligned} a &= \frac{\omega \sum_{j=1}^{3} w_j \, \cos(\omega \tau_j)}{\sum_{j=1}^{3} w_j \, \sin(\omega \tau_j)} \,, \\ b &= \frac{-\omega}{\sum_{j=1}^{3} w_j \, \sin(\omega \tau_j)} \,. \end{aligned} \tag{2.39}$$

The parameter ω is varied continuously to obtain the Hopf stability boundary (2.39). The stability curves corresponding to (2.38) and (2.39) are plotted as dashed black curves in the left column of Fig. 2.2. These curves are exact mean stability boundaries as we obtained them analytically. Next we obtain the mean and second moment stability boundaries using the semi-discretization method.

In order to obtain the stable region for the mean of system (2.33) using the corresponding discretized system (2.22), we study the characteristic equation

$$\det \left(z \bar{\mathbf{I}} - \bar{\mathbf{A}} \right) = 0 \,, \tag{2.40}$$

where $\bar{\mathbf{I}}$ is the $(m_3 + 1)$-dimensional identity matrix where $m_3 = \lfloor \tau_3 / \Delta t \rfloor$. The characteristic equation (2.40) can be obtained by substituting the trial solution $\bar{\tilde{X}}(k) = K z^k$, $K \in \mathbb{C}^{m_3+1}, z \in \mathbb{C}$, in (2.22). Equation (2.40) has $m_3 + 1$ solutions for the eigenvalues z.

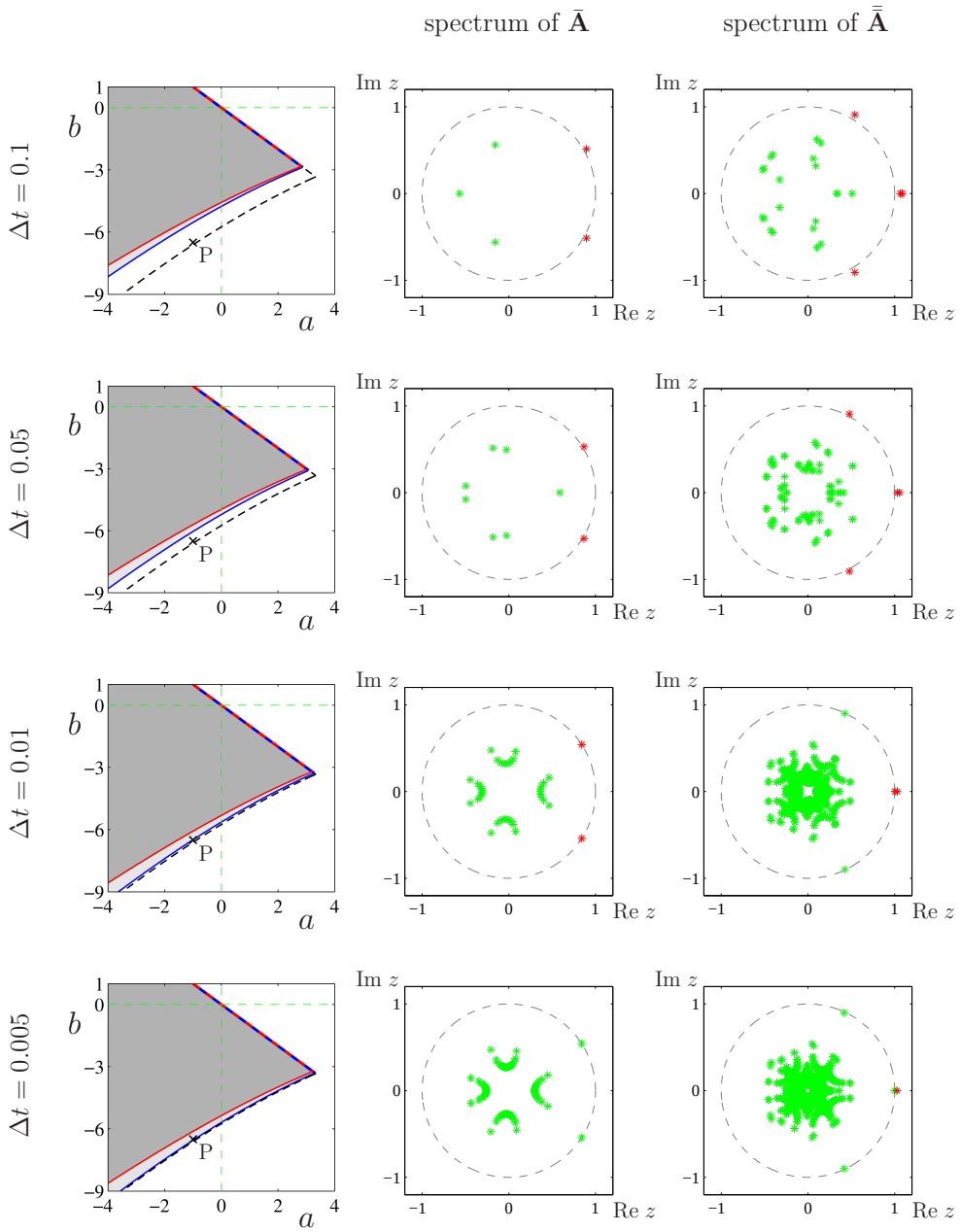

Figure 2.2: Left column: stability charts for system (2.33) with delay distribution $w(\sigma) = \frac{1}{3}\delta(\sigma-0.2)+\frac{1}{3}\delta(\sigma-0.3)+\frac{1}{3}\delta(\sigma-0.4)$ and the dwelling time $t_{\mathrm{d}} = 0.1$ for different values of the discretization step Δt as indicated on the left. Blue curves are the stability boundaries for the mean while the red curves are the stability boundaries for the second moment. The dashed black curves are stability boundaries for the mean in the continuous limit (system (2.36)). Light gray shading indicates mean stability and dark gray shading indicates second moment stability. Middle column: Eigenvalues for the discretized mean dynamics (matrix $\bar{\mathbf{A}}$) corresponding to point P located at $(a, b) = (-1, -6.5)$. Right column: Eigenvalues for the second moment dynamics (matrix $\bar{\bar{\mathbf{A}}}$) at point P. Stable eigenvalues are plotted as green while unstable eigenvalues are plotted as red.

To investigate stability bounds in the (a, b) parameter space, we note that there can be three different kinds of stability losses defined by the movement of eigenvalues across the unit circle: (i) a real eigenvalue crosses the unit circle at 1; (ii) a real eigenvalue crosses the unit circle at -1; (iii) a pair of complex conjugate eigenvalues crosses the unit circle at $\mathrm{e}^{\pm \mathrm{i}\phi}$, $\phi \in (0, \pi)$. We refer to these as fold, flip, and Hopf stability losses, respectively, based on the nomenclature of the corresponding bifurcations in nonlinear systems. A Hopf bifurcation for discrete-time systems is often called a Neimark-Sacker bifurcation. To obtain the corresponding stability curves in cases (i) and (ii), we substitute $z = 1$ and $z = -1$ into the characteristic equation (2.40) and solve for b as a function of a. This may not be obtained analytically, therefore we use numerical continuation to obtain the solution. Considering a fixed value for a, we make an initial guess for b and then correct this initial guess using the Newton-Raphson method. Once we found a solution for b, we can use it as an initial guess for a nearby value of a. Be varying a and continuing this process, one can obtain the desired boundary in (a, b) parameter domain. To do this continuation process, we use the software package DDE-BIFTOOL that is implemented in Matlab; see [17] and [71] for more details about this software. In case (iii), we substitute $z = \mathrm{e}^{\mathrm{i}\phi}$ into the characteristic Eq. (2.40), separate the real and imaginary parts, and solve the equations for a and b as a function of ϕ. Again, we use numerical continuation to trace the curves in the (a, b)-plane while varying ϕ.

The corresponding curves are plotted on the (a, b) parameter plane in the left column of Fig. 2.2 for different values of Δt as indicated. The dashed blue curve corresponds to fold stability loss and the solid blue curve corresponds to Hopf stability loss. The zero solution is mean stable in all shaded domains. The corresponding angular frequency $\omega = \phi/t_{\mathrm{d}}$ increases along the Hopf curve when moving away from the dashed blue curve. Notice that as Δt decreases the boundary moves but it converges to the dashed black curve. The convergence can be further observed by looking at the eigenvalues in the second column of Fig. 2.2 corresponding to the point P located at $(a, b) = (-1, -6.5)$. Indeed the number of eigenvalues increases but the leading eigenvalues converge with decreasing Δt while more and more eigenvalues appear in the vicinity of the origin. To better visualize the convergence of the leading eigenvalues, we plot the spectral radius of $\bar{\mathbf{A}}$ as a function of $1/\Delta t$ in Fig. 2.3(a). We also calculate the leading eigenvalues of the continuous-time mean dynamics (2.36) from the characteristic equation (2.37) using the package DDE-BIFTOOl for point P; these are $s_{1,2} = -0.037102 \pm \mathrm{i}\, 5.781085$. Then the corresponding leading eigenvalues of $\bar{\mathbf{A}}$ shall converge to $z_{1,2} = \mathrm{e}^{s_{1,2} t_{\mathrm{d}}}$ as $\Delta t \to 0$ and consequently $\rho(\bar{\mathbf{A}})$ converges to $\left|\mathrm{e}^{s_{1,2} t_{\mathrm{d}}}\right| = 0.996297$ (dashed horizontal red line in Fig. 2.3(a)). Note that while the parameters α and β depend on Δt in matrix $\mathbf{G}_j$ in (2.34), the size of the matrix $\mathbf{G}_j$ is

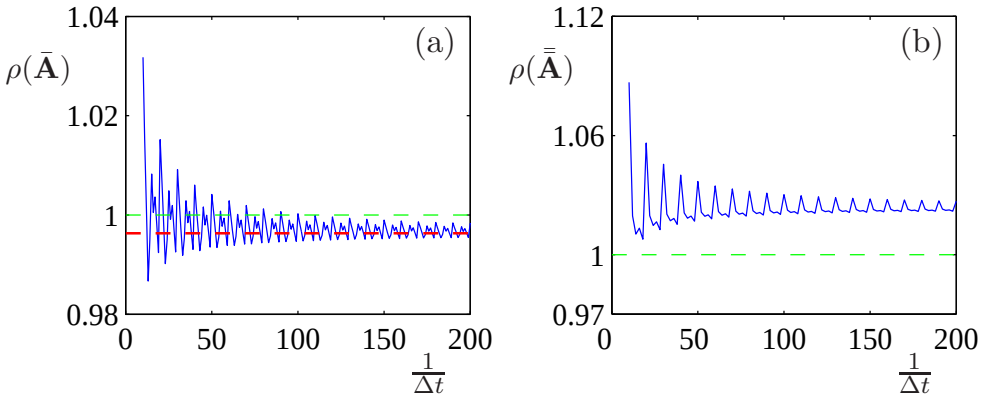

Figure 2.3: The spectral radii of the matrices $\bar{\mathbf{A}}$ and $\bar{\bar{\mathbf{A}}}$ as functions of $1/\Delta t$ shown in panels (a) and (b), respectively. The horizontal dashed red line in (a) shows the value of $\left|\mathrm{e}^{s_{1,2}t_\mathrm{d}}\right|$ where $s_{1,2}$ are the leading characteristic roots of (2.37).

also proportional to $1/\Delta t$. Therefore, we see discontinuities in the spectral radius of $\bar{\mathbf{A}}$ as Δt changes. We remark that in the case $t_\mathrm{d} > \tau_1$, the mean dynamics are not described by system (2.36) anymore. However, we still observe that the leading eigenvalues and stability charts converge to a limit as $\Delta t \to 0$. An example for the case $t_\mathrm{d} > \tau_1$ is given in Section 2.4.

In order to obtain the stable region for the second moment of system (2.33), we use the corresponding discretized system (2.30) and study the characteristic equation

$$\det\left(z\bar{\bar{\mathbf{I}}} - \bar{\bar{\mathbf{A}}}\right) = 0\,, \tag{2.41}$$

where $\bar{\bar{\mathbf{I}}}$ is the $(m_3+1)^2$-dimensional identity matrix. The characteristic equation (2.41) can be obtained by substituting the trial solution $\bar{\bar{X}}(k) = Kz^k$, $K \in \mathbb{C}^{(m_3+1)^2}, z \in \mathbb{C}$, in (2.30). Here we have $(m_3+1)^2$ solutions for the eigenvalues z. Again, one may investigate the three possible stability losses but it turns out that only fold type occurs in this case. The corresponding curves are plotted as red curves in the (a,b)-plane in the left column of Fig. 2.2 where the second moment stable region is indicated by dark gray shading. The eigenvalues of matrix $\bar{\bar{\mathbf{A}}}$ at point P are plotted in the right column, showing convergence of the leading eigenvalues with decreasing Δt. The spectral radius of $\bar{\bar{\mathbf{A}}}$ is also plotted in Fig. 2.3(b). By decreasing Δt the spectral radius converges. However, since the size of $\bar{\bar{\mathbf{A}}}$ grows with $(1/\Delta t)^2$, the smallest value of Δt for which we could compute $\rho(\bar{\bar{\mathbf{A}}})$ was 0.005 due to our hardware limitations. More details about the computational limitations of the method are given in Section 4.3. Unlike the case of the mean for which Eq. (2.36) describes the continuous-time mean dynamics, we do not have an equation to describe the

continuous-time second moment dynamics. Although, we still observe that the spectral radius of $\bar{\bar{\mathbf{A}}}$ converges to a limit. In Chapter 3, we will find this limit. In the next section, we provide a useful observation regarding the differences between systems with stochastic delay and systems with distributed delay.

2.4 Stochastic versus distributed delay

In stability analysis and control design for a system with stochastic delay, it might seem intuitive to approximate the stochastic system with a deterministic, distributed-delay system where the weights of the delayed terms are the same as the probability distribution function of the stochastic delay. In particular, as mentioned in Section 2.2, one might consider system (2.5) as an approximation for the mean of system (2.2). In Section 2.2, we showed that this approximation is valid when $t_{\rm d} < \tau_1$. In this section, by considering a scalar linear system, we show that the above mentioned approximation loses its grounds when the delay dwelling time $t_{\rm d}$ gets larger than the minimum delay in the system.

Consider the scalar case of the linear system (2.2) which we repeat here for easy reference

$$\dot{x}(t) = a\,x(t) + b\,x(t-\tau(t)), \tag{2.42}$$

where the delay $\tau(t)$ stochastically changes in a finite set $\Omega = \{\tau_1, \tau_2, \ldots, \tau_J\}$ following a probability distribution $\mathbb{P}(\tau(t) = \tau_j) = w_j$, $j = 1, \ldots, J$, and resides at each value for a constant time $t_{\rm d}$. One might speculate that one would get satisfactory approximate results if one considers, instead, the deterministic, distributed-delay system

$$\dot{x}(t) = a\,x(t) + b\sum_{j=1}^{J} w_j\,x(t-\tau_j), \tag{2.43}$$

where the delays have the same weights w_j. In the following, using a simple scalar linear system, we show that this approximation can be completely misleading.

In particular, assume that the delay $\tau(t)$ switches between only two delay values τ_1 and τ_2 where $0 < \tau_1 < \tau_2$; see Fig. 2.1 where an example realization of the delay is shown. The probability distribution is $\mathbb{P}(\tau = \tau_1) = w_1$, $\mathbb{P}(\tau = \tau_2) = w_2$, where $w_1 + w_2 = 1$. Using this simplistic behavior for the delay, we aim to show that the dwelling time $t_{\rm d}$ can have a substantial effect on the stability of the stochastic system (2.42) that cannot be captured by the corresponding deterministic, distributed-delay system (2.43). To highlight this effect from a computational point of view, we use the discretizations of systems (2.42) and (2.43) and compare their corresponding spectra (in particular, leading eigenvalues).

2.4.1 Evolution matrices

We first apply the discretization method described in Section 2.2.2 to the stochastic system (2.42). Therefore, by choosing Δt such that $t_{\rm d} = \ell\Delta t$, $\ell \in \mathbb{N}$, assuming $\tau_1 = m_1\Delta t$ and $\tau_2 = m_2\Delta t$, $m_1, m_2 \in \mathbb{N}$, and defining the augmented vector $X(i) = \big[x(i\Delta t),\, x\big((i-1)\Delta t\big),\, \ldots,\, x\big((i-m_2)\Delta t\big)\big]^{\rm T}$, the evolution matrix of system $\dot{x}(t) = ax(t) + bx(t-\tau_1)$ becomes

$$\mathbf{G}_1(\Delta t) = \begin{bmatrix} \alpha & \overset{\text{column } m_1+1}{\overset{\downarrow}{\beta}} & & & \\ 1 & & & & \\ & 1 & & & \\ & & \ddots & & \\ & & & 1 & \end{bmatrix}_{(m_2+1)\times(m_2+1)}, \tag{2.44}$$

and the evolution matrix of system $\dot{x}(t) = ax(t) + bx(t-\tau_2)$ becomes

$$\mathbf{G}_2(\Delta t) = \begin{bmatrix} \alpha & & & \overset{\text{column } m_2+1}{\overset{\downarrow}{\beta}} \\ 1 & & & \\ & 1 & & \\ & & \ddots & \\ & & & 1 \end{bmatrix}_{(m_2+1)\times(m_2+1)}, \tag{2.45}$$

where α and β were introduced in (2.10). Here we have used the notation $\mathbf{G}_1(\Delta t)$ and $\mathbf{G}_2(\Delta t)$, rather than $\mathbf{G}_1$ and $\mathbf{G}_2$ to emphasize on the fact that these matrices depend on Δt. Now recall that the delay changes every ℓ time steps (see Fig. 2.1). Therefore, similar to Section 2.2.2, we define $\tilde{X}(k) = X(k\ell)$, so that $\tilde{X}(k+1) = \mathbf{G}_j(\ell\Delta t)\tilde{X}(k) = (\mathbf{G}_j(\Delta t))^{\ell}\tilde{X}(k)$ given that $\tau(t) = \tau_j$ in $[k\ell\Delta t, (k+1)\ell\Delta t]$, $j = 1$ or 2. Then, system

$$\tilde{X}(k+1) = \mathbf{A}(k)\tilde{X}(k), \tag{2.46}$$

$k = 0, 1, 2, \ldots$, is a discretization of system (2.42), where $\mathbf{A}(k) = (\mathbf{G}_j(\Delta t))^{\ell}$ with probability w_j, $j = 1$ and 2. Now taking the expectation of both sides of (2.46), similar to Section 2.2.2, we arrive at

$$\bar{\tilde{X}}(k+1) = \mathbf{M}_{\rm sd}\bar{\tilde{X}}(k), \tag{2.47}$$

where $\bar{\tilde{X}} = \mathbb{E}\big[\tilde{X}(k)\big]$ and $\mathbf{M}_{\rm sd} = \mathbb{E}\big[\mathbf{A}(k)\big]$, and

$$\mathbf{M}_{\rm sd} = w_1\big(\mathbf{G}_1(\Delta t)\big)^{\ell} + w_2\big(\mathbf{G}_2(\Delta t)\big)^{\ell}. \tag{2.48}$$

System (2.47) describes the mean dynamics of system (2.46) that is a discretization of system (2.42). Therefore one can analyze the stability of the mean of the stochastic system (2.42) by investigating if all of the eigenvalues of matrix $\mathbf{M}_{\rm sd}$ fall inside the unit circle (stable) or not (unstable). In practice, this is done by making Δt small enough to observe convergence up to a desired accuracy. Note that the matrix $\mathbf{M}_{\rm sd}$ is the same as the matrix $\bar{\mathbf{A}}$ in (2.23) for $J = 2$. Here we used the notation $\mathbf{M}_{\rm sd}$ to emphasize that it is associated with a stochastic delay system.

Note that if $\ell > m_2$, *i.e.* if the dwelling time $t_{\rm d}$ is larger than the maximum delay in the system, we define the augmented state vector as $X(i) = \big[x(i\Delta t),\, x\big((i{-}1)\Delta t\big),\, \ldots,\, x\big((i{-}\ell)\Delta t\big)\big]^{\rm T}$, that contains the history of the state back to the last ℓ time steps. In this case, the evolution matrices $\mathbf{G}_1(\Delta t)$ in (2.44) and $\mathbf{G}_2(\Delta t)$ in (2.45) will have the same structure with the same places for elements α and β except that the sub-diagonal of 1's will extend further such that the size of the matrices becomes $(\ell+1)\times(\ell+1)$.

Now consider system (2.43) with two delays τ_1 and τ_2. Applying the discretization method described in Section 2.2.2 to system (2.43), and in the same fashion used to obtain matrices in (2.44) and (2.45), we obtain the evolution matrix for system (2.43) as

$$\mathbf{G}_{\rm dd}(\Delta t) = \begin{array}{l} \text{column: } m_1+1 \quad m_2+1 \\ \qquad\quad\ \downarrow \qquad\ \downarrow \\ \begin{bmatrix} \alpha & w_1\beta & w_2\beta \\ 1 & & \\ & 1 & \\ & & \ddots \\ & & & 1 \end{bmatrix}_{(m_2+1)\times(m_2+1)} \end{array}. \tag{2.49}$$

To compare the stability of system (2.43) with that of the mean of system (2.42), we consider the ℓ-step evolution matrix $\mathbf{M}_{\rm dd} = \mathbf{G}_{\rm dd}(\ell\Delta t) = \big(\mathbf{G}_{\rm dd}(\Delta t)\big)^{\ell}$. Observe that $\mathbf{G}_{\rm dd}(\Delta t) = w_1\mathbf{G}_1(\Delta t) + w_2\mathbf{G}_2(\Delta t)$, and thus

$$\mathbf{M}_{\rm dd} = \big(w_1\mathbf{G}_1(\Delta t) + w_2\mathbf{G}_2(\Delta t)\big)^{\ell}. \tag{2.50}$$

Our goal is to demonstrate the effect of the delay dwelling time $t_{\rm d}$ on the spectra, and thus on the stability, of the stochastic delay system (2.42) and the corresponding determin-

istic, distributed-delay system (2.43). To this end, we compare the spectra of matrices $\mathbf{M}_{\rm sd}$ defined in (2.48) (associated to system (2.42)) and $\mathbf{M}_{\rm dd}$ defined in (2.50) (associated to system (2.43)) for a fixed time step Δt while changing ℓ (recall that $t_{\rm d} = \ell \Delta t$).

For $\ell = 1$ it is easy to check that $\mathbf{M}_{\rm sd} = \mathbf{M}_{\rm dd}$. In fact, owing to the cyclic-like structures of matrices $\mathbf{G}_1(\Delta t)$, $\mathbf{G}_2(\Delta t)$ and $\mathbf{G}_{\rm dd}(\Delta t)$, we have

$$\mathbf{M}_{\rm sd} = \mathbf{M}_{\rm dd} \quad \text{for} \quad \ell = 0, 1, \ldots, m_1 + 1. \tag{2.51}$$

For instance, for $\ell = 2$

$$\mathbf{M}_{\rm sd} = \mathbf{M}_{\rm dd} = \begin{array}{c} \begin{array}{ccccccc} & & & \text{column: } m_1+1 & & & m_2+1 \\ & & & \downarrow & & & \downarrow \end{array} \\ \begin{bmatrix} \alpha^2 & & & w_1\beta & \alpha w_1\beta & w_2\beta & \alpha w_2\beta \\ \alpha & & & & w_1\beta & & w_2\beta \\ 1 & & & & & & \\ & 1 & & & & & \\ & & \ddots & & & & \\ & & & & & & \\ & & & & & & \\ & & & & & & \\ & & & & & & \\ & & & & 1 & & \end{bmatrix} \end{array}, \tag{2.52}$$

and for $\ell = 3$

$$\mathbf{M}_{\rm sd} = \mathbf{M}_{\rm dd} = \begin{bmatrix} \alpha^3 & w_1\beta & \alpha w_1\beta & \alpha^2 w_1\beta & w_2\beta & \alpha w_2\beta & \alpha^2 w_2\beta \\ \alpha^2 & & w_1\beta & \alpha w_1\beta & & w_2\beta & \alpha w_2\beta \\ \alpha & & & w_1\beta & & & w_2\beta \\ 1 & & & & & & \\ & 1 & & & & & \\ & & \ddots & & & & \\ & & & & & & \\ & & & & & & \\ & & & & & & \\ & & & & 1 & & \end{bmatrix}. \tag{2.53}$$

Once ℓ gets larger than $m_1 + 1$ the equality (2.51) does not hold anymore. For $\ell > m_1 + 1$, $\mathbf{M}_{\rm sd} \neq \mathbf{M}_{\rm dd}$ and therefore their spectra are different. Note that this observation

holds independent of Δt. Moreover, observe that

$$\ell \leq m_1 + 1 \;\Rightarrow\; \ell \Delta t \leq (m_1 + 1)\Delta t \;\Rightarrow\; t_{\rm d} \leq \tau_1 + \Delta t. \tag{2.54}$$

Since Δt can be made arbitrarily small, we conclude from (2.54) that

$$t_{\rm d} \leq \tau_1. \tag{2.55}$$

Eq. (2.55) provides a condition under which $\mathbf{M}_{\rm sd} = \mathbf{M}_{\rm dd}$. Therefore if the delay dwelling time is less than the smallest delay value, the spectra of (the mean of) the stochastic system (2.42) and the deterministic system (2.43) are equal and so are their stability properties. However if $t_{\rm d} > \tau_1$, the spectra of the two systems (2.42) and (2.43) are different. In fact, the difference between matrices $\mathbf{M}_{\rm sd}$ and $\mathbf{M}_{\rm dd}$ gets larger as $t_{\rm d}$ increases further. In Section 2.4.2, we provide a numerical example to further demonstrate this observation.

An important result of the observation above is that one may consider the distributed-delay, deterministic system (2.43) an approximate version of the stochastic delay system (2.42) (in the sense of average), if the delay dwelling time is less than the minimum delay in the system, *i.e.* $t_{\rm d} \leq \tau_1$. However, this approximation is groundless for dwelling time $t_{\rm d} > \tau_1$. In fact it can lead to completely erroneous results as will be demonstrated in Section 2.4.2. Before proceeding to the next section, we shall make some remarks.

Remark 2.3. We showed that the spectra of (the mean of) the stochastic-delay system (2.42) and the deterministic, distributed-delay system (2.43) are equal when $t_{\rm d} \leq \tau_1$, using evolution matrices of the corresponding systems. This fact no longer holds, when $t_{\rm d} > \tau_1$. This observation can also be verified by taking the expectation of both sides of (2.42) that yields

$$\begin{aligned} \frac{\rm d}{{\rm d}t}\big(\mathbb{E}[x(t)]\big) &= a\,\mathbb{E}[x(t)] + b\,\mathbb{E}[x(t-\tau(t))] \\ &= a\,\mathbb{E}[x(t)] + b\sum_{j=1}^{J} \mathbb{P}(\tau(t)=\tau_j)\mathbb{E}\big[x(t-\tau_j)|\tau(t)=\tau_j\big]; \end{aligned} \tag{2.56}$$

cf. (2.4). Now as described in the paragraph after (2.4), if the dwelling time is less than the minimum delay, *i.e.* $t_{\rm d} \leq \tau_1$, system (2.56) reduces to

$$\dot{\bar{x}}(t) = a\,\bar{x}(t) + b\sum_{j=1}^{J} w_j\,\bar{x}(t-\tau_j), \tag{2.57}$$

where $\bar{x} = \mathbb{E}[x(t)]$ and $w_j = \mathbb{P}(\tau(t)=\tau_j)$; cf. (2.5). System (2.57) is indeed the same as

system (2.43). Note that this reduction is not possible if $t_{\rm d} > \tau_1$.

Remark 2.4. We showed that one may consider the deterministic system (2.43) as an approximate system for the stochastic system (2.42) when the delay dwelling time is less than the smallest delay in the system. This approximation is based on the fact that the stability of the mean of a stochastic system is a necessary condition for the stability of the system. Exact stability regions of the stochastic system (2.42), that lie inside the region of mean stability, can be obtained by investigating the stability of the second moment that provides a stronger stability condition. Therefore one should note that even under the assumption of the delay dwelling time being less than the minimum delay, the exact stability regions of system (2.42) can be quite smaller than the ones obtained by the approximate system (2.43).

Remark 2.5. All the results in Section 2.4 hold in the vector case too, *i.e.* if $x \in \mathbb{R}^n$ where n is the dimension of the vector x. Additionally, all the results hold if there are more than two delays, *i.e.* $J > 2$ in (2.43), and also if $\tau_j/\Delta t$ is not an integer for some j (in which case one can use $m_j = \lfloor \tau_j/\Delta t \rfloor$). In this section, we used a scalar system with only two delays for brevity and simplicity of the notation .

2.4.2 A numerical example

In this section, we consider the linear system (2.42) with two delays $\tau_1 = 0.4$ and $\tau_1 = 0.8$ with probability distribution function $w_1 = w_2 = 1/2$. Then, for different dwelling times $t_{\rm d} = 0.3$, $t_{\rm d} = 0.6$, $t_{\rm d} = 1$, and $t_{\rm d} = 2$, we construct stability charts in the (a, b) parameter space using the spectra of matrices $\mathbf{M}_{\rm dd}$ (associated with the distributed-delay system (2.43)) and $\mathbf{M}_{\rm sd}$ (associated with the mean of the stochastic-delay system (2.42)). The goal is to demonstrate the effect of the parameter $t_{\rm d}$ on the fidelity of the approximation of system (2.42) by system (2.43).

Fig. 2.4(a–d) show the spectra of matrices $\mathbf{M}_{\rm dd}$ (indicated by $\circ$) and $\mathbf{M}_{\rm sd}$ (indicated by $\times$) for $(a, b) = (-1.2, -5.5)$ (marked by P in the bottom panels). Note that only the first 10 leading eigenvalues are shown. The value $\Delta t = 0.005$ is used for all panels. When the dwelling time $t_{\rm d} = 0.3$ is less than the smallest delay $\tau_1 = 0.4$, the matrices $\mathbf{M}_{\rm dd}$ and $\mathbf{M}_{\rm sd}$ are equal and their spectra are the same, as shown in Fig. 2.4(a). In this case, the approximation of system (2.42) by system (2.43) is meaningful, since system (2.43) is indeed the average of the stochastic system (2.42). As Fig. 2.4(e) shows, the stable area of the mean of system (2.42), enclosed by the solid blue boundary, is the same as the stable area of system (2.43), enclosed by the dashed green boundary. The stable region is

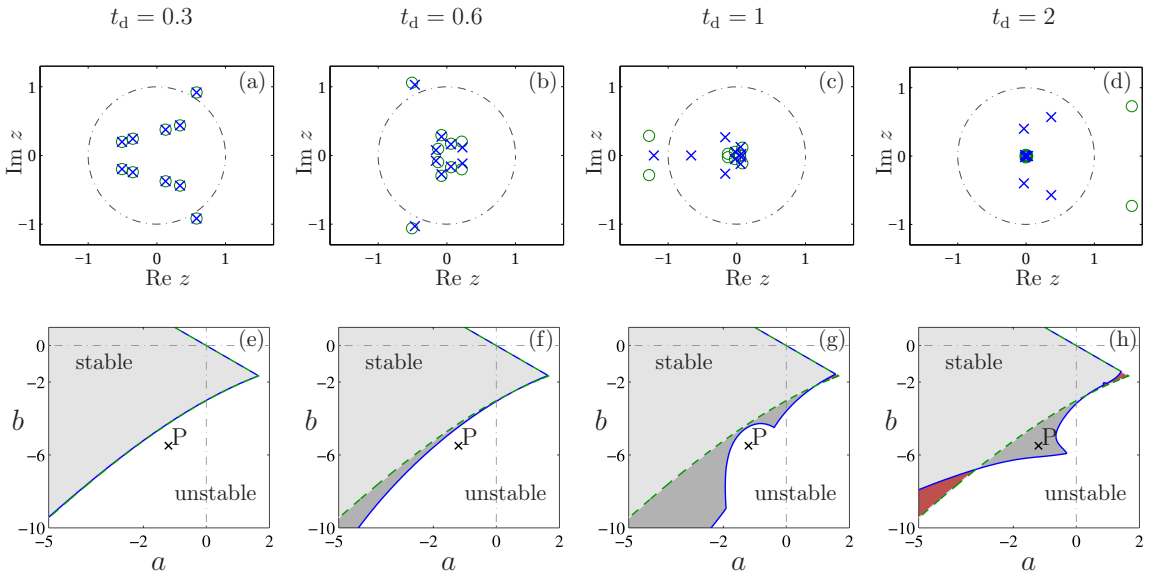

Figure 2.4: (a–d) Comparison of the spectra of the matrix $\mathbf{M}_{\rm dd}$ in (2.50) (indicated by $\circ$), associated with the distributed-delay system (2.43), and the spectra of the matrix $\mathbf{M}_{\rm sd}$ in (2.48) (indicated by $\times$) associated with the mean of the stochastic-delay system (2.42), for different dwelling times $t_{\rm d}$ as indicated. The spectra are obtained for point P shown in the bottom panels and only the 10 largest eigenvalues in magnitude are shown in the complex plane. (e–f) Stable regions of the distributed-delay system (2.43) obtained using the eigenvalues of the matrix $\mathbf{M}_{\rm dd}$ in (2.50) (bounded by dashed green curves) and the mean of the stochastic-delay system (2.42) obtained using the eigenvalues of the matrix $\mathbf{M}_{\rm sd}$ in (2.48) (bounded by solid blue curves), for different dwelling times. The light gray area is a parameter domain where both (2.42) and (2.43) are stable. The dark gray area is where (2.42) is stable but (2.43) is not. The red area is where (2.42) is not stable but (2.43) is stable.

shaded light gray. Note that the crossing of the boundary from stable to unstable region is equivalent to the crossing of the unit circle by the leading eigenvalue from inside to outside.

When the dwelling time is $t_{\rm d} = 0.6$, we have $\tau_1 < t_{\rm d} < \tau_2$. In this case the matrices $\mathbf{M}_{\rm dd}$ and $\mathbf{M}_{\rm sd}$ are different and so are their spectra, as shown in Fig. 2.4(b). This is because when $t_{\rm d} > \tau_1$, system (2.43) is no longer the average of system (2.42). Therefore, the stable area obtained through investigating the eigenvalues of $\mathbf{M}_{\rm dd}$ (the dashed green boundary) is different than the stable area obtained using matrix $\mathbf{M}_{\rm sd}$ (the solid blue boundary). The region shaded as dark gray is the parameter domain where the distributed-delay system is unstable but the mean of the stochastic-delay system is stable.

As the dwelling time $t_{\rm d}$ gets larger relative to the delay values, the approximation of system (2.42) by system (2.43) gets worse. Fig. 2.4(c–d) show the cases $t_{\rm d} = 1$ and $t_{\rm d} = 2$ for which the dwelling time is larger than the maximum delay, $t_{\rm d} > \tau_2$. In these cases, the spectra of matrices $\mathbf{M}_{\rm dd}$ and $\mathbf{M}_{\rm dd}$ are very different. Correspondingly, the stable

areas of systems (2.43) and the mean of system (2.42), shown by Fig. 2.4(g–h), are significantly different. The region shaded by dark gray is again a parameter domain where the distributed-delay system (2.43) is unstable but the mean of the stochastic-delay system (2.42) is stable. On the other hand, the region shaded by red is where the distributed-delay system is stable but the mean of the stochastic-delay system is not.

The example given in this section is simple in the sense that the system is scalar with only two delay values. Despite this simplicity, we observed a big difference between stability properties of systems (2.42) and (2.43). One may expect that for vector-valued systems and a larger number of delay values, one would find bigger differences between systems (2.42) and (2.43). This example may therefore act as a warning if one wants to use a distributed-delay system as an approximation of a stochastic-delay system.

2.5 Generalization to random dwelling times and Markov jumps

So far in this chapter, we assumed that the delay dwelling time is fixed. In this section, we consider the case where the dwelling time t_{d} is a random variable. The delay process therefore has two sources of randomness: randomness in switching between delay values and randomness in the duration of the times the delay dwells at a value. Moreover, we assume that the switchings in the delay values follow a Markov rule which is more general than *i.i.d.* assumption. We again consider a linear continuous-time system that is discretized using the semi-discretization technique in the same fashion as the previous sections in this chapter. We then find stability conditions for the mean and the second moment of the system. We show the results by studying an example at the end of the section.

2.5.1 Problem setup

The probability transition matrix which governs the jumps between the delay values is given by

$$\mathbf{Q} = \begin{bmatrix} q_{11} & q_{21} & \cdots & q_{J1} \\ q_{12} & q_{22} & \cdots & q_{J2} \\ \vdots & \vdots & \ddots & \vdots \\ q_{1J} & q_{2J} & \cdots & q_{JJ} \end{bmatrix}, \tag{2.58}$$

where the probability of jumping from $\tau = \tau_i$ to $\tau = \tau_j$ is denoted by q_{ij}, $i, j = 1, 2, \ldots, J$. Note that, for each column, the sum of the elements is 1. We assume that the matrix $\mathbf{Q}$ is

not changing with time.

Here we assume that the dwelling time $t_{\rm d}$ is a random variable. Fig. 2.5a shows a sample realization of the delay with a random dwelling time where the dwelling time follows some probability distribution function. Let $t_{\rm d}(k) = t_{k+1} - t_k$ where t_k, $k = 0, 1, 2, \ldots$, are the times at which a switch occurs in the delay value. Suppose that at time $t = 0$ the delay is $\tau_{s(0)}$, $s(0) \in \{1, \ldots, J\}$. Then a random real number $t_{\rm d}(0) = t_1$ is generated from a probability distribution function governing $t_{\rm d}$, and the delay is kept constant along the time interval $0 \leq t < t_1$. Then it switches to a new value $\tau_{s(1)}$, $s(1) \in \{1, \ldots, J\}$. The new delay value $\tau_{s(1)}$ is chosen based on the transition probabilities $q_{s(0)j}, j = 1, \ldots, J$, introduced in Eq. (2.58). Now another random number $t_{\rm d}(1)$ is generated, independently of $t_{\rm d}(0)$, based on the probability distribution function governing $t_{\rm d}$. The delay is held at the new value during the interval $t_1 \leq t < t_2$, and so forth. Note that $t_2 = t_{\rm d}(0) + t_{\rm d}(1)$. The random variable $s(k)$, $k = 0, 1, 2, \ldots$, is a Markov chain with the transition probability matrix $\mathbf{Q}$ in (2.58) that determines the delay values at the next switchings.

Recall that we discretize system (2.2) to obtain stability conditions. We use the mesh $t_i = i\Delta t$, $i = 0, 1, 2, \ldots$. To use the same discretization technique presented in the previous sections, we need to discretize the delay process too. We do this by assuming that the dwelling times are multiples of Δt, *i.e.* $t_{\rm d}(k) \approx \ell(k)\Delta t$ where $\ell(k)$ is a random integer; see Fig. 2.5(b). We assume that $\ell(k) \in \{1, 2, \ldots, L\}$ is a random integer with a fixed probability distribution function at each k, $k = 0, 1, 2, \ldots$. After applying the approximation $t_{\rm d}(k) \approx \ell(k)\Delta t$, we denote the switching times by t'_k, that is, $t'_{k+1} - t'_k = \ell(k)\Delta t$. The delay remains constant at the value $\tau_{s(0)}$ along the time interval $0 \leq t < \ell(0)\Delta t = t'_1$ and at $\tau_{s(1)}$ along the interval $\ell(0)\Delta t \leq t < \big(\ell(0) + \ell(1)\big)\Delta t = t'_2$, and so on.

The assumption that the dwelling times are $t_{\rm d}(k) = \ell(k)\Delta t$, where $\ell(k)$ is a random variable, changes system (2.18)-(2.19) to the following system

$$X(k+1) = \big(\mathbf{G}_{s(k)}\big)^{\ell(k)} X(k), \tag{2.59}$$

where $\mathbf{G}_{s(k)} \in \{\mathbf{G}_j,\ j = 1, \ldots, J\}$, and $\mathbf{G}_j$ are defined in (2.16). Note that here the augmented vector $X(k) \in \mathbb{R}^{n(M+1)}$ where $M = \max\{m_J, L\}$. In the following section, we derive equations for the first and second moments of system (2.59).

2.5.2 Moment equations

Here, we establish conditions for the stability of the trivial solution of the stochastic system (2.59) that is a discretization of system (2.2) when the delay has random dwelling times and follows a Markov switching rule. First we derive equations for the time evolution of the

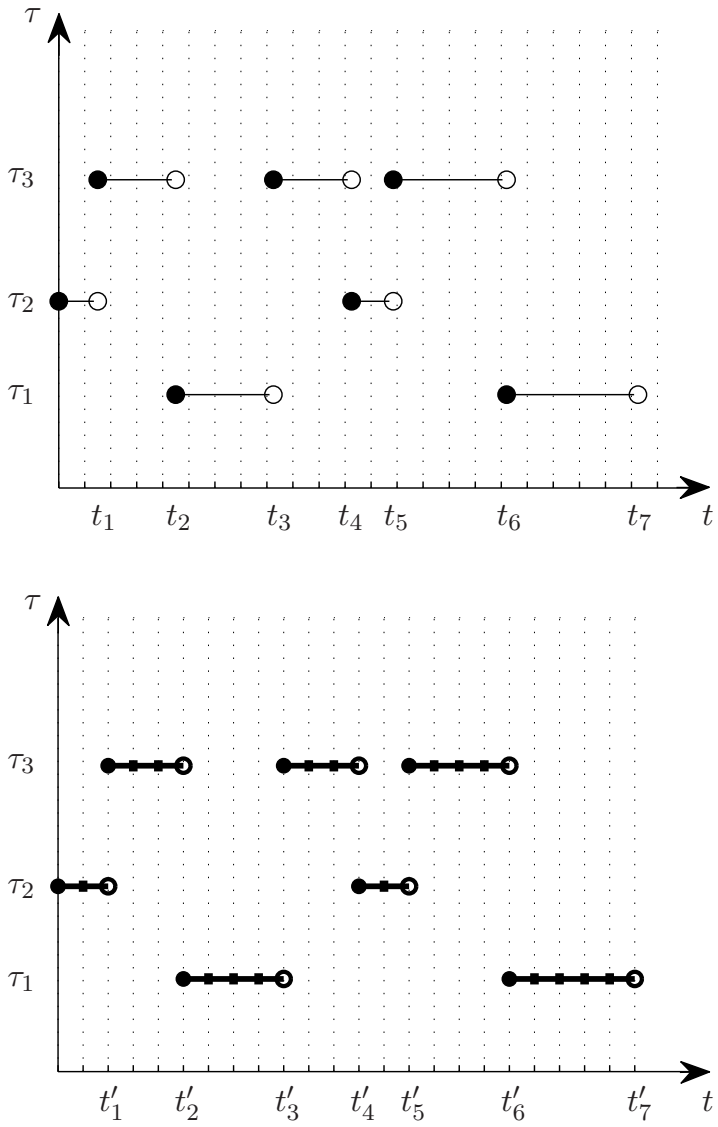

Figure 2.5: (a) A sample realization of the time evolution of the delay τ with $J = 3$ possible values. (b) A sample realization of the approximated delay process.

mean. Then the dynamics of the second moment are derived from which necessary and sufficient stability conditions for the second moment are obtained.

2.5.2.1 Dynamics of the mean

First we characterize the dynamics of the mean of system (2.59), *i.e.* $\mathbb{E}[X(k)]$. Recall that stability of the mean provides a necessary condition for the stability of the stochastic

system. Using (2.59) we proceed as follows

$$\begin{aligned}
&\mathbb{E}\big[X(k+1)|\, s(k+1)=j\big] = \mathbb{E}\big[(\mathbf{G}_{s(k)})^{\ell(k)}X(k)|\, s(k+1)=j\big] \\
&= \sum_{i=1}^{J} \mathbb{E}\big[(\mathbf{G}_{s(k)})^{\ell(k)}X(k)|\, s(k+1)=j, s(k)=i\big] \\
&\times \mathbb{P}\big(s(k)=i|\, s(k+1)=j\big). \qquad (2.60)
\end{aligned}$$

We exploit the independence of $\ell(k)$ and $X(k)$ along with Bayes' rule in (2.60) to obtain

$$\begin{aligned}
&\mathbb{E}\big[X(k+1)|\, s(k+1)=j\big] \\
&= \sum_{i=1}^{J} \mathbb{E}\big[(\mathbf{G}_i)^{\ell(k)}|\, s(k+1)=j, s(k)=i\big]\, \mathbb{E}\big[X(k)|\, s(k+1)=j, s(k)=i\big] \\
&\times \frac{\mathbb{P}\big(s(k+1)=j|\, s(k)=i\big)\mathbb{P}\big(s(k)=i\big)}{\mathbb{P}\big(s(k+1)=j\big)}. \qquad (2.61)
\end{aligned}$$

Now, we note that $\ell(k)$, $k=0,1,\ldots$, are independent, identically distributed (*i.i.d.*), and they are also independent of $s(k)$, $k=0,1,\ldots$. Hence, $\mathbb{E}\big[(\mathbf{G}_i)^{\ell(k)}|\, s(k+1)=j, s(k)=i\big] = \mathbb{E}\big[(\mathbf{G}_i)^{\ell(k)}\big]$. Further note that based on Eq. (2.59), $X(k)$ depends on $s(k-1)$. Moreover, since the jump occurs from $s(k-1)$ to $s(k)$, information about $s(k)$ gives information about $s(k-1)$. However, due to the Markov property of the jump process, information about $s(k+1)$ gives no extra information about $s(k-1)$, given that $s(k)$ is already known. This yields $\mathbb{E}\big[X(k)|\, s(k+1)=j, s(k)=i\big] = \mathbb{E}\big[X(k)|\, s(k)=i\big]$. Thus, (2.61) simplifies to

$$\begin{aligned}
&\mathbb{E}\big[X(k+1)|\, s(k+1)=j\big] \\
&\qquad = \sum_{i=1}^{J} \mathbb{E}\big[(\mathbf{G}_i)^{\ell(k)}\big]\mathbb{E}\big[X(k)|s(k)=i\big]\frac{q_{ij}\,\mathbb{P}(s(k)=i)}{\mathbb{P}(s(k+1)=j)}, \qquad (2.62)
\end{aligned}$$

where we used the substitution $q_{ij}=\mathbb{P}\big(s(k+1)=j|\, s(k)=i\big)$; cf. (2.58).
Now we define

$$f(\mathbf{G}_i) := \mathbb{E}\big[(\mathbf{G}_i)^{\ell(k)}\big] = \sum_{\ell=1}^{L} (\mathbf{G}_i)^{\ell}\mathbb{P}\big(\ell(k)=\ell\big). \qquad (2.63)$$

Using (2.63) in (2.62), we obtain

$$\begin{aligned}\mathbb{E}\big[X(k+1)|\, s(k+1)=j\big]\,\mathbb{P}(s(k+1)=j)\\ =\sum_{i=1}^{J} f(\mathbf{G}_i)\,q_{ij}\,\mathbb{E}\big[X(k)|\, s(k)=i\big]\,\mathbb{P}(s(k)=i).\end{aligned}\tag{2.64}$$

Let $\bar{x}_j(k) := \mathbb{E}\big[X(k)|\, s(k)=j\big]\,\mathbb{P}\big(s(k)=j\big)$. Then, Eq. (2.64) can be written as

$$\bar{x}_j(k+1)=\sum_{i=1}^{J} q_{ij}\, f(\mathbf{G}_i)\,\bar{x}_i(k),\quad j=1,\ldots,J.\tag{2.65}$$

Now defining $\hat{\bar{x}}(k) := \big[\bar{x}_1(k)^{\mathrm{T}},\quad \ldots\quad ,\bar{x}_J(k)^{\mathrm{T}}\big]^{\mathrm{T}} \in \mathbb{R}^{nJ(M+1)}$, we can write (2.65) in the compact form

$$\hat{\bar{x}}(k+1)=\mathbf{M}\,\hat{\bar{x}}(k),\tag{2.66}$$

where $\mathbf{M}\in\mathbb{R}^{nJ(M+1)\times nJ(M+1)}$ is given by

$$\begin{aligned}\mathbf{M}&=\begin{bmatrix} q_{11}f(\mathbf{G}_1) & q_{21}f(\mathbf{G}_2) & \cdots & q_{J1}f(\mathbf{G}_J)\\ q_{12}f(\mathbf{G}_1) & q_{22}f(\mathbf{G}_2) & \cdots & q_{J2}f(\mathbf{G}_J)\\ \vdots & \vdots & \ddots & \vdots\\ q_{1J}f(\mathbf{G}_1) & q_{2J}f(\mathbf{G}_2) & \cdots & q_{JJ}f(\mathbf{G}_J)\end{bmatrix}\\ &=\big(\mathbf{Q}\otimes\mathbf{I}_{n(M+1)}\big)\mathrm{diag}\big(f(\mathbf{G}_i)\big).\end{aligned}\tag{2.67}$$

Here $\otimes$ denotes the Kronecker product, $\mathbf{I}_{n(M+1)}$ is the $n(M+1)\times n(M+1)$ identity matrix, and $\mathrm{diag}\big(f(\mathbf{G}_i)\big)$ is a block diagonal matrix with $f(\mathbf{G}_1),\cdots,f(\mathbf{G}_J)$ as diagonal elements. Now notice that

$$\mathbb{E}\big[X(k)\big]=\sum_{j=1}^{J}\mathbb{E}\big[X(k)|\, s(k)=j\big]\,\mathbb{P}\big(s(k)=j\big)=\sum_{j=1}^{J}\bar{x}_j(k).\tag{2.68}$$

Hence, if the spectral radius of matrix $\mathbf{M}$ in (2.67), *i.e.* $\rho(\mathbf{M})$, is less than 1, then system (2.66) is stable meaning that $\hat{\bar{x}}(k)\to 0$ as $k\to\infty$. This implies $\mathbb{E}\big[X(k)\big]\to 0$ as $k\to\infty$ in light of (2.68). We summarize these results as the following.

Consider system (2.59) that is a discretization of system (2.2) when the delay has random dwelling times and the switches in the delay values occur based on a Markov chain rule. The variable $s(k)$ that represents delay values is a Markov chain with transition matrix $\mathbf{Q}$ in (2.58) and domain $\{1,\ldots,J\}$. The dwelling times are $\ell(k)\Delta t$ where $\ell(k)$,

$k = 0, 1, 2, \ldots$, are *i.i.d.* random variables with domain $\{1, \ldots, L\}$. We assume that $\ell(k)$ are independent of $s(k)$ and $X(k)$. Then,

$$\mathbb{E}[X(k)] \to 0 \quad \text{as} \quad k \to \infty \qquad \text{if} \qquad \rho(\mathbf{M}) < 1, \tag{2.69}$$

where $\mathbf{M}$ is defined in (2.67). Condition (2.69) provides a necessary condition for the stability of the mean of system (2.59).

2.5.2.2 Dynamics of the second moment

Our main quest is to find necessary and sufficient criteria for the stability of the stochastic system (2.59). We use the second moment stability, that is, system (2.59) is second moment stable if for any initial probability distributions on $X(0)$ and $s(0)$ we have

$$\mathbb{E}\big[X(k)X(k)^{\mathrm{T}}\big] \to 0 \quad \text{as} \quad k \to \infty, \tag{2.70}$$

where $\mathbb{E}\big[X(k)X(k)^{\mathrm{T}}\big]$ is the second moment matrix of system (2.59). To derive the dynamics of the second moment, we proceed as follows

$$\begin{aligned}
&\mathbb{E}\big[X(k+1)X(k+1)^{\mathrm{T}} | s(k+1) = j\big] \\
&= \mathbb{E}\Big[(\mathbf{G}_{s(k)})^{\ell(k)} X(k)X(k)^{\mathrm{T}} \big((\mathbf{G}_{s(k)})^{\ell(k)}\big)^{\mathrm{T}} |\, s(k+1) = j\Big] \\
&= \sum_{i=1}^{J} \mathbb{E}\Big[(\mathbf{G}_{s(k)})^{\ell(k)} X(k)X(k)^{\mathrm{T}} \big((\mathbf{G}_{s(k)})^{\ell(k)}\big)^{\mathrm{T}} |\, s(k+1) = j, s(k) = i\Big] \\
&\times \mathbb{P}\Big(s(k) = i \,\Big|\, s(k+1) = j\Big).
\end{aligned} \tag{2.71}$$

Now we use the law of total probability along with the Bayes' rule to write (2.71) as

$$\begin{aligned}
&\mathbb{E}\big[X(k+1)X(k+1)^{\mathrm{T}} | s(k+1) = j\big] \\
&= \sum_{i=1}^{J} \sum_{\ell=1}^{L} \mathbb{E}\Big[(\mathbf{G}_i)^{\ell(k)} X(k)X(k)^{\mathrm{T}} \Big((\mathbf{G}_i)^{\ell(k)}\Big)^{\mathrm{T}} \Big| s(k+1) = j, s(k) = i, \ell(k) = \ell\Big] \\
&\times \mathbb{P}\Big(\ell(k) = \ell | s(k+1) = j, s(k) = i\Big) \frac{q_{ij}\mathbb{P}(s(k) = i)}{\mathbb{P}(s(k+1) = j)}.
\end{aligned} \tag{2.72}$$

Similar to the derivation of (2.62), observe that $\ell(k)$ is independent of $X(k)$ and $s(k)$, and the statistical properties of $X(k)$ given $s(k)$ do not change by further knowing $s(k+1)$.

Then, (2.72) simplifies to

$$\begin{aligned}
&\mathbb{E}\big[X(k+1)X(k+1)^{\mathrm{T}}|s(k+1)=j\big] \\
&\quad=\sum_{i=1}^{J}\sum_{\ell=1}^{L}(\mathbf{G}_i)^{\ell}\mathbb{E}\big[X(k)X(k)^{\mathrm{T}}|\,s(k)=i\big]\big((\mathbf{G}_i)^{\ell}\big)^{\mathrm{T}}\mathbb{P}\big(\ell(k)=\ell\big) \\
&\qquad\times\frac{q_{ij}\mathbb{P}(s(k)=i)}{\mathbb{P}(s(k+1)=j)}.
\end{aligned}\tag{2.73}$$

Now define $\mathbf{S}_j(k) := \mathbb{E}\big[X(k)X(k)^{\mathrm{T}}|\,s(k)=j\big]\mathbb{P}(s(k)=j) \in \mathbb{R}^{n(M+1)\times n(M+1)}$. Then (2.73) becomes

$$\mathbf{S}_j(k+1)=\sum_{i=1}^{J}\sum_{\ell=1}^{L}q_{ij}(\mathbf{G}_i)^{\ell}\mathbf{S}_i(k)\big((\mathbf{G}_i)^{\ell}\big)^{\mathrm{T}}\mathbb{P}\big(\ell(k)=\ell\big),\quad j=1,2,\ldots,J.\tag{2.74}$$

Notice that

$$\mathbb{E}\big[X(k)X(k)^{\mathrm{T}}\big]=\sum_{j=1}^{J}\mathbb{E}\big[X(k)X(k)^{\mathrm{T}}|s(k)=j\big]\mathbb{P}\big(s(k)=j\big)=\sum_{j=1}^{J}\mathbf{S}_j(k).\tag{2.75}$$

The second moment is a matrix-valued quantity and further transformations are needed in order to characterize its stability. We again use the vec operator defined in (2.27) and form the following augmented vector

$$\hat{S}(k)=\Big[\Big(\mathrm{vec}\big(\mathbf{S}_1(k)\big)\Big)^{\mathrm{T}},\ \ldots,\ \Big(\mathrm{vec}\big(\mathbf{S}_J(k)\big)\Big)^{\mathrm{T}}\Big]^{\mathrm{T}},\tag{2.76}$$

where $\hat{S}(k)\in\mathbb{R}^{J(n(M+1))^2}$. Using the definition (2.76) we reformulate Eq. (2.74) as

$$\hat{S}(k+1)=\mathbf{D}\,\hat{S}(k),\tag{2.77}$$

where the matrix $\mathbf{D}\in\mathbb{R}^{J(n(M+1))^2\times J(n(M+1))^2}$ is given by

$$\mathbf{D}=\big(\mathbf{Q}\otimes\mathbf{I}_{(n(M+1))^2}\big)\Big[\sum_{\ell=1}^{L}\mathrm{diag}\Big((\mathbf{G}_i)^{\ell}\otimes(\mathbf{G}_i)^{\ell}\Big)\,\mathbb{P}\big(\ell(k)=\ell\big)\Big].\tag{2.78}$$

Using definition (2.63) and noting that $\big(\mathbf{G}_i^{\ell}\otimes\mathbf{G}_i^{\ell}\big)=\big(\mathbf{G}_i\otimes\mathbf{G}_i\big)^{\ell}$, (2.78) can be written as

$$\mathbf{D}=\big(\mathbf{Q}\otimes\mathbf{I}_{(n(M+1))^2}\big)\mathrm{diag}\Big(f\big(\mathbf{G}_i\otimes\mathbf{G}_i\big)\Big).\tag{2.79}$$

If $\rho(\mathbf{D}) < 1$, system (2.77) is stable meaning that $\hat{S}(k) \to 0$ as $k \to \infty$, which, using (2.75) and (2.76), implies $\mathbb{E}\big[X(k)X(k)^{\mathrm{T}}\big] \to 0$ as $k \to \infty$. The reverse is also true: if $\mathbb{E}\big[X(k)X(k)^{\mathrm{T}}\big] \to 0$ for any initial condition $\mathbb{E}\big[X(0)X(0)^{\mathrm{T}}\big]$, then $\rho(\mathbf{D}) < 1$. To prove this, we note that in (2.75) all $\mathbf{S}_j(k)$, $j = 1, 2, \ldots, J$, are positive semi-definite and symmetric. Therefore, from (2.75) we have

$$0 \le \mathbf{S}_j(k) \le \mathbb{E}\big[X(k)X(k)^{\mathrm{T}}\big] \quad \text{for} \quad j = 1, \ldots, J, \quad k = 0, 1, 2, \ldots. \tag{2.80}$$

Now if $\mathbb{E}\big[X(k)X(k)^{\mathrm{T}}\big] \to 0$, then (2.80) implies that $\mathbf{S}_j(k) \to 0$ as $k \to \infty$ for $j = 1, \ldots, J$. Hence, (2.76) implies that $\hat{S}(k) \to 0$ as $k \to \infty$ for any initial $\hat{S}(0)$. Consequently, the spectral radius of $\mathbf{D}$ must be less than 1, *i.e.* $\rho(\mathbf{D}) < 1$, since $\hat{S}(k) = \mathbf{D}^k \hat{S}(0)$. We summarize these results as the following.

Consider system (2.59), that is a discretization of system (2.2), where $s(k)$ is a Markov chain with transition matrix $\mathbf{Q}$ in (2.58) and domain $\{1, \ldots, J\}$, and $\ell(k)$ are *i.i.d.* random variables with domain $\{1, \ldots, L\}$. Assume further that $\ell(k)$ is independent of $s(k)$ and $X(k)$. Then,

$$\mathbb{E}\big[X(k)X(k)^{\mathrm{T}}\big] \to 0 \quad \text{as} \quad k \to \infty \qquad \text{if and only if} \qquad \rho(\mathbf{D}) < 1, \tag{2.81}$$

where $\mathbf{D}$ is defined in (2.79).

Condition (2.81) is a necessary and sufficient condition for the second moment stability of the stochastic system (2.59).

2.5.3 An example

We repeat a scalar version of system (2.2) here

$$\dot{x}(t) = a\, x(t) + b\, x(t - \tau(t)), \tag{2.82}$$

Assume the delay $\tau(t)$ in (2.82) is stochastic taking values in the set $\{2, 10, 13\}$ with transition probability matrix

$$\mathbf{Q} = \begin{bmatrix} 0 & 0.5 & 0.5 \\ 0.5 & 0 & 0.5 \\ 0.5 & 0.5 & 0 \end{bmatrix}. \tag{2.83}$$

Let $\ell(k)$ follow a geometric distribution with mean $\ell_{\text{avg}} = 7$ and set $\Delta t = 0.4$. We vary the parameters a and b in (2.82) and evaluate the stability of the mean using condition (2.69) and stability of the second moment using condition (2.81). Fig. (2.6) shows the stability

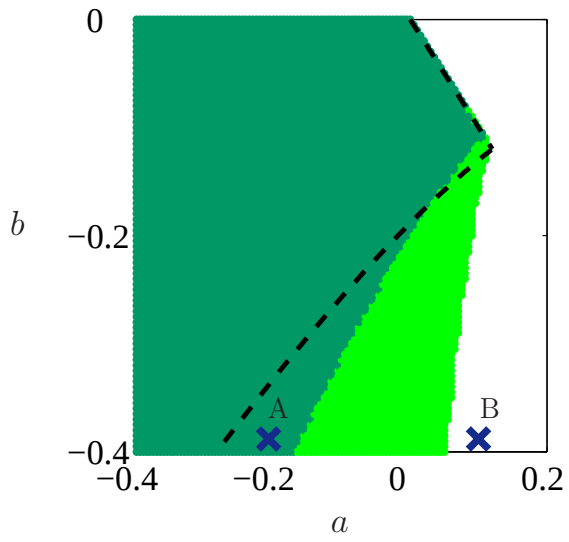

Figure 2.6: Stability chart in the plane of parameters a and b. Dark shaded area is the region of stability; *i.e.* the second moment (and the mean) are stable. Light shaded area shows the region in which only the mean (but not the second moment) is stable. The black dashed curve shows the boundary of stability region of a deterministic system with a fixed average delay $\tau_{\text{avg}} \approx 8.33$. Simulations for points A and B are displayed in panels (a) and (b) of Fig. 2.7, respectively.

region in the (a, b)-plane. The dark shaded area shows the region in which the stochastic system (2.82) is second moment stable. Light shaded area indicates the region in which the first moment (mean) is stable, but the second moment is not. The black dashed curve shows the boundary of the stable region for the deterministic system with a fixed delay $\tau_{\text{avg}} \approx 8.33$ that is equal to the average of delay values. In Fig. 2.7, we show simulations of system (2.82) with parameters associated with points A and B in Fig. 2.6. The 300 sample trajectories are plotted as thin gray curves while the mean and the standard deviation are indicated by thick black and thick red curves, respectively. Indeed, the system is stable in case A and unstable in case B.

2.6 Discussion

Delay differential equations with stochastic delay were investigated in this chapter. In particular, we considered linear systems with stochastic delay where the delay trajectories were piece-wise constant functions of time and the delay dwelt at each value for a constant time. We derived stability conditions by analyzing the mean and the second moment dynamics of the discretized version of the system. The conditions for the second moment stability also ensured almost sure stability. We applied the semi-discretization technique

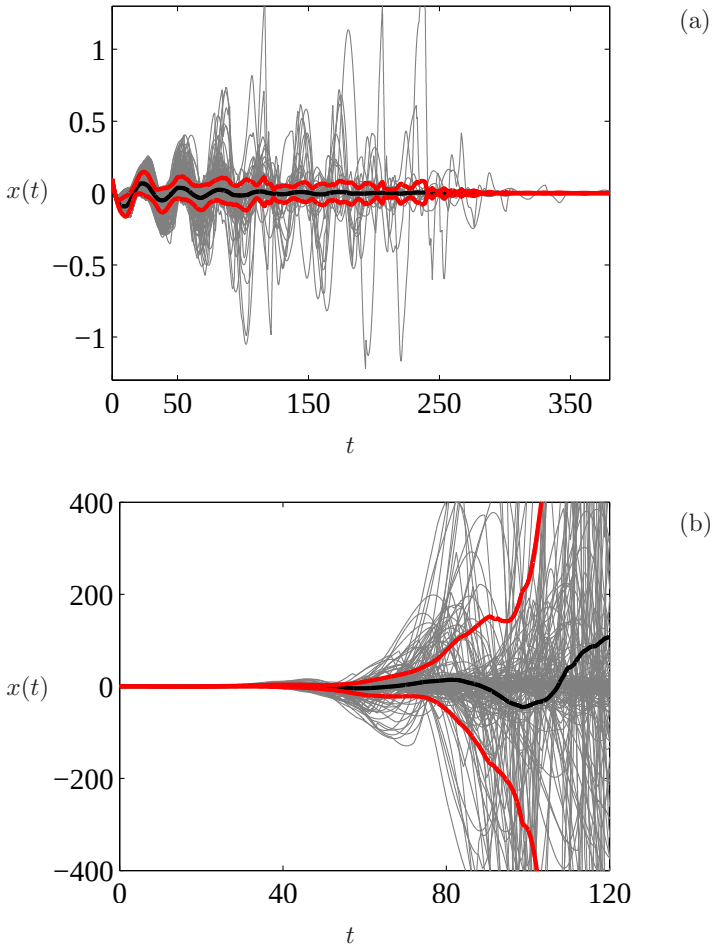

Figure 2.7: (a) Simulation results for system (2.82) using the parameters at point A in Fig. 2.6. (b) Simulation results using the parameters at point B in Fig. 2.6. The black curve shows the mean and the red curves show the mean plus and minus the standard deviation based on the gray sample trajectories.

and demonstrated convergence of stability charts when the size of the discretization time step tends to zero.

While we were able to derive continuous-time mean dynamics (although only for the case where the dwelling time is smaller than the minimum delay), such continuous-time equation does not exist for the second moment dynamics. However, we will obtain continuous-time versions of the stability conditions in Chapter 3. We remark that the stochastic delay system studied in this chapter can also be viewed as a hybrid system where switching between various delayed differential equations happen in a stochastic fashion. Work has been done on the stability analysis of hybrid systems with constant time delays [48, 52, 87, 89] or with deterministically time-varying delays [65]; however, modeling stochastic delay systems such as ours is less explored in the hybrid systems literature.

We showed that if the delay dwelling time is less than the minimum delay, then the mean dynamics can be described by a deterministic, distributed delay system. On the other hand, we showed that approximating a stochastic delay system with a deterministic, distributed delay system is not always warranted. In particular, this approximation is not valid if the dwelling time is larger than the minimum delay in the system. Furthermore, as the dwelling time increases, the approximation gets worse. This finding showed that a stochastic behavior of the delay can bring about non-intuitive consequences to the stability of the system.

In the last section of the chapter, we generalized our method to the case where the dwelling time was a random variable and the delay switchings followed a Markov chain rule rather than being *i.i.d.*. This showed that the method we developed in the chapter can be used in a more general setting and that more complicated delay behaviors can be analyzed. We obtained necessary and sufficient stability conditions for the second moment of the system and showed the application of the results with an example.

The results in this chapter show that the stability of a stochastic delay system cannot be simply speculated from the behavior of a deterministic system with the average delay or with distributed delay. The results of this chapter find their importance in the stability analysis and control design in applications such as connected vehicle systems [66], wireless communication systems [60, 42], and biological circuits [34, 27] where stochastic delays are shown to exist in the dynamics of the system.

CHAPTER 3

Stochastic delays in continuous time

3.1 Introduction

The problem of the stability analysis and control design for continuous-time systems with stochastic delays has been raised in many applications. For instance, in networked control systems, data are often transferred with random communication delay [60, 42]. In connected vehicle systems, the information from vehicles ahead is received at random times due to packet loss in wireless communication. Also, driver reaction time may change stochastically with time [66, 4]. Random delays also arise in gene regulatory networks since the execution times of transcription and translation processes are influenced by the noisy cell environment [54, 34, 46].

While the stability analysis of discrete-time systems with stochastic delay has been investigated thoroughly in literature, *e.g.* [42, 60, 69, 26], exact stability analysis—finding necessary and sufficient stability conditions—of continuous-time systems with stochastic delay is lacking in general. In other words, finding exact boundaries of stable regions in desired parameter spaces is not solved. It should be mentioned that, the stability analysis of continuous-time systems with stochastic delay has been studied [36, 47, 40, 37, 76], using Lyapunov-based theorems. However, such theorems result in only sufficient stability conditions that are typically very conservative and the results based on them can be far from real stability boundaries. Moreover, the results based on Lyapunov theorems are difficult to apply in most cases due to the difficulty of finding suitable Lyapunov functions or functionals. To overcome these problems, we present necessary and sufficient stability conditions for continuous-time linear systems with stochastic delay by investigating the stability of the second moment. One of the works where necessary and sufficient conditions are derived for a continuous-time system with stochastic delay is [82]. However, the results of [82] are applicable only for a very specific type of delay behavior. In this chapter, we consider the same delay behavior described in Chapter 2.

In Chapter 2, we derived necessary and sufficient stability conditions using discretization of the continuous-time system. In this chapter, we provide necessary and sufficient stability conditions without discretizing the system. We find the stability conditions in terms of the spectral radius of a particular combination of the solution operators associated to different delay values. Similar to Chapter 2, the delay can only assume finitely many values and it switches between these values based on a fixed probability distribution. We derive the time evolution of the second moment of the state using tensor products of infinite-dimensional solution operators and by calculating the spectral radii of these operators we construct necessary and sufficient conditions for stability. To construct stability charts, one can discretize the solution operators and find finite-dimensional versions of the stability conditions that can be evaluated numerically. The tools developed in this chapter are demonstrated with some examples where we use the semi-discretization method that was described in Chapter 2. In the last section of the chapter, we provide almost sure stability criteria of the systems under investigation and discuss the differences between second moment and almost sure stability of such systems with an emphasis on the computational aspects.

3.2 Problem statement

Consider the linear system

$$\dot{x}(t) = \mathbf{a}\, x(t) + \mathbf{b}\, x(t - \tau(t)), \tag{3.1}$$

where $x \in \mathbb{R}^n$, $\mathbf{a}, \mathbf{b} \in \mathbb{R}^{n\times n}$, and the delay $\tau(t) \in \mathbb{R}$ changes stochastically with time. We assume that the delay can take values from a finite set $\Omega = \{\tau_1, \tau_2, \ldots, \tau_J\}$ where $0 < \tau_1 < \tau_2 < \cdots < \tau_J = \tau_{\max}$. The initial condition is given by

$$x(\theta) = \phi(\theta), \quad -\tau_{\max} \le \theta \le 0, \tag{3.2}$$

where $\phi \in \mathcal{C}\big([-\tau_{\max}, 0], \mathbb{R}^n\big)$ and $\mathcal{C}$ denotes the space of continuous functions.

Before switching to a different value, the delay stays at the current value for a duration of time, t_{d}, which we call dwelling time. Therefore the value of the delay at each interval $[kt_{\mathrm{d}}, (k+1)t_{\mathrm{d}})$, $k = 0, 1, 2, \ldots$, is constant. The probability distribution $w = [w_1\ w_2\ \ldots\ w_J]$ governs the switchings of the delay where w_j is the probability of switching to the delay τ_j. The probability distribution w is assumed to be stationary which means the switchings of the delay are independent, identically distributed (*i.i.d.*). Fig. 3.1a

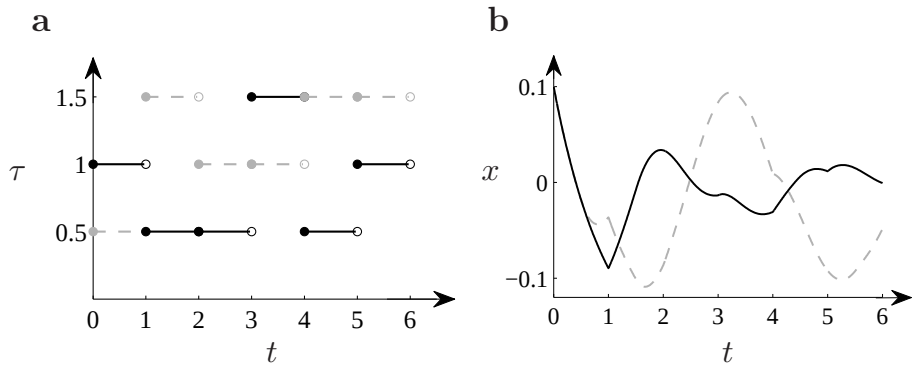

Figure 3.1: **a** Two sample paths of the delay with dwelling time $t_{\rm d} = 1$ and delay values $\{0.5, 1, 1.5\}$. **b** Trajectories of the scalar version of system (3.1) with $\mathbf{a} = -1$ and $\mathbf{b} = -2$ corresponding to sample paths of the delay shown in Fig. 3.1a and initial condition $\phi(\theta) = 0.1$, $-1.5 \leq \theta \leq 0$.

shows two sample paths of the delay and Fig. 3.1b shows the corresponding trajectories, $x(t)$, of a scalar version (*i.e.* for $n = 1$) of system (3.1), with parameters and initial conditions stated in the caption of Fig. 3.1.

Our goal is to study the stability of the stochastic system (3.1). In particular, we study the stability of the mean, $\mathbb{E}[x(t)]$, and the second moment, $\mathbb{E}[x(t)x^{\rm T}(t)]$, where $\mathbb{E}[.]$ denotes the expected value of a random variable. To this aim, we need a proper representation of system (3.1) given the delay behavior as described. In the next section, we construct this representation using solution operator formulation of delay differential equations and provide a suitable definition of the second moment using tensor products of appropriate operators.

3.3 Solution operator representation of the system

First we recall the definition of the solution operator for a deterministic delay differential equation. Consider the linear system

$$\begin{aligned} \dot{x}(t) &= \mathbf{a}\, x(t) + \mathbf{b}\, x(t-\tau), \\ x(\theta) &= \phi(\theta), \quad -\tau \leq \theta \leq 0, \end{aligned} \tag{3.3}$$

where $\phi \in \mathcal{C}([-\tau, 0], \mathbb{R}^n)$. The solution operator for system (3.3) is defined by

$$\big(\mathcal{T}(t)\phi\big)(\theta) = x(t+\theta), \quad -\tau \leq \theta \leq 0, \quad t \geq 0. \tag{3.4}$$

The operator $\mathcal{T}(t)$, $t \geq 0$, is bounded and linear and the family of operators $\mathcal{T}(t)$ is a strongly continuous semigroup that has the properties

$$\begin{aligned} &\mathcal{T}(t) : \mathcal{C}([-\tau, 0], \mathbb{R}^n) \to \mathcal{C}([-\tau, 0], \mathbb{R}^n), \quad \forall\, t \geq 0, \\ &\mathcal{T}(0) = \mathcal{I}, \\ &\mathcal{T}(t_1 + t_2) = \mathcal{T}(t_1)\mathcal{T}(t_2), \quad \forall\, t_1, t_2 \geq 0; \end{aligned} \tag{3.5}$$

see [30] for more details. Now consider the deterministic systems

$$\begin{aligned} &\dot{x}(t) = \mathbf{a}\, x(t) + \mathbf{b}\, x(t - \tau_j), \\ &j = 1, \ldots, J, \end{aligned} \tag{3.6}$$

with their respective solution operators $\mathcal{T}_j(t) : \mathcal{C}([-\tau_j, 0], \mathbb{R}^n) \to \mathcal{C}([-\tau_j, 0], \mathbb{R}^n)$, $\forall\, t \geq 0$. As described in Section 3.2, the delay is constant in each interval $[kt_{\mathrm{d}}, (k+1)t_{\mathrm{d}})$, $k = 0, 1, 2, \ldots$. Therefore, the stochastic system (3.1), in the time interval $[kt_{\mathrm{d}}, (k+1)t_{\mathrm{d}})$, evolves according to one of the systems in (3.6). In other words, if $\tau(t) = \tau_j$ in the time interval $[kt_{\mathrm{d}}, (k+1)t_{\mathrm{d}})$, the operator $\mathcal{T}_j(t_{\mathrm{d}})$ progresses the solution forward from $t = kt_{\mathrm{d}}$ to $t = (k+1)t_{\mathrm{d}}$. In order to obtain an appropriate representation of the stochastic system (3.1), we extend the operators $\mathcal{T}_j$, $j = 1, \ldots, J$, in a way that the new, extended operators share a common domain.

Let $\Gamma := \max\{\tau_{\max}, t_{\mathrm{d}}\}$ and denote by $\mathcal{C}$ the space $\mathcal{C}([-\Gamma, 0], \mathbb{R}^n)$ and by $\mathcal{C}_j$ the space $\mathcal{C}([-\tau_j, 0], \mathbb{R}^n)$, $j = 1, \ldots, J$. Now, first we define the auxiliary operators $\mathcal{U}_j : \mathcal{C} \to \mathcal{C}_j$ by

$$(\mathcal{U}_j \phi)(\theta) = \phi(\theta), \quad -\tau_j \leq \theta \leq 0, \quad \forall\, \phi \in \mathcal{C}, \tag{3.7}$$

for $j = 1, \ldots, J$. In other words, the operator $\mathcal{U}_j$ acts on a continuous function ϕ from $\mathcal{C}$ and outputs the segment of ϕ corresponding to $-\tau_j \leq \theta \leq 0$. Now choose $h > 0$ such that $t_{\mathrm{d}} = \ell h$ where $\ell \in \mathbb{N}$ is a positive integer and $h < \tau_j$, $j = 1, \ldots, J$, and $h < t_{\mathrm{d}}$. Next define the operators $\mathcal{G}_j : \mathcal{C} \to \mathcal{C}$ by

$$(\mathcal{G}_j \phi)(\theta) = \begin{cases} \big(\mathcal{T}_j(h)\mathcal{U}_j \phi\big)(\theta) & -\tau_j \leq \theta \leq 0 \\ \phi(\theta + h) & -\Gamma \leq \theta < -\tau_j, \end{cases} \tag{3.8}$$

for $j = 1, \ldots, J$. The operators $\mathcal{G}_j$ are in fact extensions of the operators $\mathcal{T}_j(h)$ from the domain $\mathcal{C}_j$ to domain $\mathcal{C}$. This extension is performed with a shift term—the bottom line in (3.8). Finally we define the operators

$$\mathcal{A}_j \phi = (\mathcal{G}_j)^{\ell} \phi, \quad \forall\, \phi \in \mathcal{C}, \tag{3.9}$$

for $j = 1, \ldots, J$. The operator $\mathcal{A}_j : \mathcal{C} \to \mathcal{C}$ is ℓ consecutive applications of the operator $\tilde{\mathcal{T}}_j$. Note that the operators $\mathcal{A}_j$, that are constructed through (3.7)-(3.9), are linear and bounded because the original operators $\mathcal{T}_j$ are bounded and linear. Now assume that the stochastic system (3.1) is realized up to the time $t = kt_{\mathrm{d}}$. Let us define

$$x_t(\theta) := x(t + \theta), \quad -\Gamma \leq \theta \leq 0, \tag{3.10}$$

as the "state" of the system at time t, where $x_t \in \mathcal{C}$. Then, assuming that $\tau(t) = \tau_j$ in the time interval $[kt_{\mathrm{d}}, (k + 1)t_{\mathrm{d}})$, we can write $x_{(k+1)t_{\mathrm{d}}} = \mathcal{A}_j x_{kt_{\mathrm{d}}}$. Consequently one can construct the stochastic system

$$x_{(k+1)t_{\mathrm{d}}} = \mathcal{A}(k) x_{kt_{\mathrm{d}}}, \tag{3.11}$$

where

$$\begin{aligned} &\mathbb{P}\big(\mathcal{A}(k) = \mathcal{A}_j\big) = w_j, \\ &j = 1, \ldots, J, \quad \text{and} \quad k = 0, 1, 2, \ldots, \end{aligned} \tag{3.12}$$

where $\sum_{j=1}^{J} w_j = 1$ and with the initial condition

$$x_0(\theta) = \phi(\theta), \quad -\Gamma \leq \theta \leq 0, \quad \phi \in \mathcal{C}. \tag{3.13}$$

Here $\mathbb{P}$ denotes probability. Note that we cannot arrive at a stochastic system of the form (3.11), if we want to use the original solution operators $\mathcal{T}_j$ due to the fact that they don't have a common domain. In the next section, we study the stability of the mean and the second moment of system (3.11).

3.4 Stability analysis

In this section, we derive stability conditions for the mean and the second moment of the stochastic system (3.11). First we provide a standard definition as well as a standard result that we will use in this section.

Definition 3.1. System

$$x_{k+1} = \mathcal{A}\, x_k, \tag{3.14}$$

where $\mathcal{A} : \mathcal{X} \to \mathcal{X}$ is a bounded, linear operator from the Banach space $\mathcal{X}$ to itself, is exponentially stable if for every initial condition $x_0 \in \mathcal{X}$, there exist $M \geq 1$ and $0 \leq r < 1$

such that

$$\|x_k\| \leq Mr^k, \quad k = 0, 1, 2, \ldots; \tag{3.15}$$

see for instance [64].

A standard result on the stability of system (3.14) is provided in the following lemma; see Theorem 2.1 in [64].

Lemma 3.1. Consider system (3.14). Let $\sigma(\mathcal{A})$ denote the spectrum of $\mathcal{A}$ and

$$\rho(\mathcal{A}) = \sup\left\{|\lambda| : \lambda \in \sigma(\mathcal{A})\right\} \tag{3.16}$$

denote the spectral radius of $\mathcal{A}$. Then, system (3.14) is exponentially stable if and only if

$$\rho(\mathcal{A}) < 1. \tag{3.17}$$

Now we consider the mean of the stochastic system (3.11). By taking the expected value of (3.11), we have

$$\mathbb{E}[x_{(k+1)t_\mathrm{d}}] = \mathbb{E}[\mathcal{A}(k)x_{kt_\mathrm{d}}]. \tag{3.18}$$

Note that the operator $\mathcal{A}(k)$ only depends on the delay value in the time interval $\big[kt_\mathrm{d}, (k+1)t_\mathrm{d}\big)$, *i.e.* if $\tau(t) = \tau_j$ in this time interval, then $\mathcal{A}(k) = \mathcal{A}_j$. On the other hand, x_{kt_d} depends on the delay values in the time intervals $\big[k't_\mathrm{d}, (k'+1)t_\mathrm{d}\big)$, $k' = 0, 1, 2, \ldots, k-1$. Since the delay value in the time interval $\big[kt_\mathrm{d}, (k+1)t_\mathrm{d}\big)$ is independent of the delay values in other time intervals (due to the *i.i.d.* assumption), the operator $\mathcal{A}(k)$ is independent of x_{kt_d}. Thus from (3.18), we arrive at

$$\mathbb{E}[x_{(k+1)t_\mathrm{d}}] = \mathbb{E}[\mathcal{A}(k)]\mathbb{E}[x_{kt_\mathrm{d}}], \tag{3.19}$$

where $\mathbb{E}[\mathcal{A}(k)] : \mathcal{C} \to \mathcal{C}$ is given by

$$\mathbb{E}[\mathcal{A}(k)] = \sum_{j=1}^{J} w_j \mathcal{A}_j. \tag{3.20}$$

Now applying Lemma 3.1 on system (3.19) results in a necessary and sufficient condition for the stability of the mean of the stochastic system (3.11). This is provided in the proposition below.

Proposition 3.1. Consider system (3.11) with initial condition

$$x_0(\theta) = \phi(\theta), \quad -\Gamma \leq \theta \leq 0, \quad \phi \in \mathcal{C}, \tag{3.21}$$

and $\mathbb{P}\big(\mathcal{A}(k) = \mathcal{A}_j\big) = w_j$, $\forall\, j \in \{1, \ldots, J\}$ and $\forall\, k \in \{0, 1, 2, \ldots\}$. Then, there exist $M \geq 1$ and $0 \leq r < 1$ such that

$$\big\|\mathbb{E}[x_{kt_{\mathrm{d}}}]\big\|_{\sup} \leq M r^k,\ \forall\, k \in \{0, 1, 2, \ldots\} \tag{3.22}$$

if and only if

$$\rho\Big(\sum_{j=1}^{J} w_j \mathcal{A}_j\Big) < 1. \tag{3.23}$$

Here $\|.\|_{\sup}$ denotes the sup norm on $\mathcal{C}$, *i.e.*

$$\|\phi\|_{\sup} = \sup_{-\Gamma \leq \theta \leq 0} \|\phi(\theta)\|_{\infty}, \quad \phi \in \mathcal{C}, \tag{3.24}$$

where $\|.\|_{\infty}$ denotes the ∞-norm (or max norm) on $\mathbb{R}^n$, *i.e.*

$$\|x\|_{\infty} = \max_{1 \leq i \leq n} |x^i|, \tag{3.25}$$

where x^i is the i^{th} component of $x \in \mathbb{R}^n$.

Proof. The proof is immediately obtained by the application of Lemma 3.1 on system (3.19). Note that the operator $\mathbb{E}[\mathcal{G}_k]$, defined in (3.20), is a finite summation of bounded and linear operators $\mathcal{A}_j$ and so is bounded and linear, and moreover it is defined on the Banach space $\mathcal{C}$. □

Our main goal is to derive necessary and sufficient conditions for the stability of the second moment of system (3.11). For a proper description of the second moment dynamics, we use the tensor product of the Banach space $\mathcal{C}$ with itself equipped with an appropriate cross norm. The connection between the second moment and the tensor product space lies in the definition of the norm.

Let $\mathcal{X}$ denote a Banach space and $\mathcal{X} \otimes \mathcal{X}$ the tensor product of $\mathcal{X}$ with itself. A standard norm on tensor product spaces is the injective norm that is given by

$$\|u\|_{\text{inj}} = \sup\Big\{\Big|\sum_{m=1}^{M} f(x_m) g(y_m)\Big| :\ f, g \in B_{\mathcal{X}^*}\Big\}, \tag{3.26}$$

where $u = \sum_{m=1}^{M} x_m \otimes y_m$ is a tensor in $\mathcal{X} \otimes \mathcal{X}$ and $B_{\mathcal{X}^*}$ is the closed unit ball on $\mathcal{X}^*$ (the normed dual of $\mathcal{X}$). In other words, f and g are bounded, linear functionals defined on $\mathcal{X}$ with norm less than or equal to 1, and the supremum in (3.26) is taken over all such f and g. Furthermore, in the definition (3.26), one can substitute $B_{\mathcal{X}^*}$ with a norming set.

A subset $\mathcal{N}$ of $B_{\mathcal{X}^*}$ is said to be a norming set if $\|x\| = \sup\{|f(x)| : f \in \mathcal{N}\}$ for every $x \in \mathcal{X}$; here $\|.\|$ is the norm defined on the Banach space $\mathcal{X}$. See [68], chapter 3, for more details about the injective norm on tensor product spaces.

Now we first define a norm on the tensor space $\mathcal{C} \otimes \mathcal{C}$ and then show that it is in fact the injective norm on $\mathcal{C} \otimes \mathcal{C}$.

Definition 3.2. Let $u = \sum_{m=1}^{M} \phi_m \otimes \psi_m$ belong to $\mathcal{C} \otimes \mathcal{C}$. We define the c-norm on $\mathcal{C} \otimes \mathcal{C}$ to be

$$\|u\|_c = \sup_{\substack{-\Gamma \le \theta_1, \theta_2 \le 0 \\ 1 \le i_1, i_2 \le n}} \Big| \sum_{m=1}^{M} \phi_m^{i_1}(\theta_1)\, \psi_m^{i_2}(\theta_2) \Big|. \tag{3.27}$$

In particular, for a simple tensor of the form $u = \phi \otimes \phi$, we have

$$\|\phi \otimes \phi\|_c = \sup_{\substack{-\Gamma \le \theta_1, \theta_2 \le 0 \\ 1 \le i_1, i_2 \le n}} \Big| \phi^{i_1}(\theta_1)\, \phi^{i_2}(\theta_2) \Big|. \tag{3.28}$$

The connection between the second moment and the c-norm defined in (3.27) can be seen from (3.28) where $\|\phi \otimes \phi\|_c$ contains the products of the values of the function ϕ at different arguments. The second moment in the infinite-dimensional setting of functions may also be understood as the expected value of the product of a function with itself at different argument values.

Next we show that the c-norm defined in (3.27) is the injective norm on $\mathcal{C} \otimes \mathcal{C}$.

Lemma 3.2. The norm $\|.\|_c$, defined in (3.27), is equivalent to the injective norm $\|.\|_{\text{inj}}$, defined in (3.26).

Proof. Let $\phi \in \mathcal{C}$. Consider the linear functionals

$$\delta_\theta^i(\phi) = \phi^i(\theta), \tag{3.29}$$

where $\phi^i(\theta)$ is the i^{th} component of $\phi(\theta)$, $i = 1, \ldots, n$ and $-\Gamma \le \theta \le 0$. Define the set $\mathcal{N} := \big\{\delta_\theta^i : -\Gamma \le \theta \le 0,\, i = 1, \ldots, n\big\}$. $\mathcal{N}$ is a subset of $B_{\mathcal{C}^*}$, because we have $|\delta_\theta^i(\phi)| = |\phi^i(\theta)| \le \|\phi(\theta)\|_\infty \le \|\phi\|_{\sup}$, $\forall\, \phi \in \mathcal{C}$, which implies $\|\delta_\theta^i\| \le 1$. Furthermore, the set $\mathcal{N}$ is a norming set, because for every $\phi \in \mathcal{C}$

$$\|\phi\|_{\sup} = \sup_{-\Gamma \le \theta \le 0} \|\phi(\theta)\|_\infty = \sup_{-\Gamma \le \theta \le 0} \Big\{ \max_{1 \le i \le n} |\phi^i(\theta)| \Big\} = \sup \Big\{ \big|\delta_\theta^i(\phi)\big| : \delta_\theta^i \in \mathcal{N} \Big\}. \tag{3.30}$$

Therefore, we can substitute $B_{\mathcal{C}^*}$ with $\mathcal{N}$ in (3.26). As a result, (3.26) yields (3.27). □

We denote by $\mathcal{C} \otimes_c \mathcal{C}$ the tensor product space equipped with the c-norm (injective norm) and by $\mathcal{C} \hat{\otimes}_c \mathcal{C}$ the completion of this space under the c-norm. It is important to note that

one may define other norms on the tensor product space $\mathcal{C} \otimes \mathcal{C}$; however, the connection between the second moment and the injective norm makes the injective norm a suitable choice. This connection will be further illuminated in the remainder of this section.

Consider the bounded and linear operator $\mathcal{A}_j : \mathcal{C} \to \mathcal{C}$. For each $j = 1, \ldots, J$, there exists (see Proposition 3.2 in [68]) a unique, bounded, and linear operator $\mathcal{A}_j \otimes_c \mathcal{A}_j : \mathcal{C}\hat{\otimes}_c\mathcal{C} \to \mathcal{C}\hat{\otimes}_c\mathcal{C}$ such that

$$(\mathcal{A}_j \otimes_c \mathcal{A}_j)(\phi \otimes \psi) = (\mathcal{A}_j\phi) \otimes (\mathcal{A}_j\psi), \quad \forall\, \phi, \psi \in \mathcal{C}. \tag{3.31}$$

Now assuming that system (3.11) is realized up to the time $t = kt_{\mathrm{d}}$ and in the interval $\big[kt_{\mathrm{d}}, (k+1)t_{\mathrm{d}}\big)$, the delay is $\tau(t) = \tau_j$, we have

$$x_{(k+1)t_{\mathrm{d}}} = \mathcal{A}_j x_{kt_{\mathrm{d}}}. \tag{3.32}$$

On the other hand, using the operator in (3.31), one can write

$$(\mathcal{A}_j \otimes_c \mathcal{A}_j)(x_{kt_{\mathrm{d}}} \otimes x_{kt_{\mathrm{d}}}) = (\mathcal{A}_j x_{kt_{\mathrm{d}}}) \otimes (\mathcal{A}_j x_{kt_{\mathrm{d}}}). \tag{3.33}$$

Eqs. (3.32-3.33) result in

$$x_{(k+1)t_{\mathrm{d}}} \otimes x_{(k+1)t_{\mathrm{d}}} = (\mathcal{A}_j \otimes_c \mathcal{A}_j)(x_{kt_{\mathrm{d}}} \otimes x_{kt_{\mathrm{d}}}). \tag{3.34}$$

Therefore, one can construct the stochastic map

$$x_{(k+1)t_{\mathrm{d}}} \otimes x_{(k+1)t_{\mathrm{d}}} = \big(\mathcal{A}(k) \otimes_c \mathcal{A}(k)\big)(x_{kt_{\mathrm{d}}} \otimes x_{kt_{\mathrm{d}}}), \tag{3.35}$$

where

$$\begin{aligned} &\mathbb{P}(\mathcal{A}(k) \otimes_c \mathcal{A}(k) = \mathcal{A}_j \otimes_c \mathcal{A}_j) = w_j, \\ &\quad j = 1, \ldots, J, \quad \text{and} \quad k = 0, 1, 2, \ldots, \end{aligned} \tag{3.36}$$

with the initial condition $x_0 \otimes x_0 = \phi \otimes \phi$.

Now we can take the expected value of Eq. (3.35) that results in

$$\mathbb{E}[x_{(k+1)t_{\mathrm{d}}} \otimes x_{(k+1)t_{\mathrm{d}}}] = \mathbb{E}\Big[\big(\mathcal{A}(k) \otimes_c \mathcal{A}(k)\big)(x_{kt_{\mathrm{d}}} \otimes x_{kt_{\mathrm{d}}})\Big]. \tag{3.37}$$

Due to the independence of $\mathcal{A}(k)$ and $x_{kt_{\mathrm{d}}}$, $\mathcal{A}(k) \otimes_c \mathcal{A}(k)$ is independent of $x_{kt_{\mathrm{d}}} \otimes x_{kt_{\mathrm{d}}}$ and therefore

$$\mathbb{E}[x_{(k+1)t_{\mathrm{d}}} \otimes x_{(k+1)t_{\mathrm{d}}}] = \mathbb{E}\big[\mathcal{A}(k) \otimes_c \mathcal{A}(k)\big]\mathbb{E}\big[x_{kt_{\mathrm{d}}} \otimes x_{kt_{\mathrm{d}}}\big], \tag{3.38}$$

where

$$\mathbb{E}\big[\mathcal{A}(k) \otimes_c \mathcal{A}(k)\big] = \sum_{j=1}^{J} w_j \, \mathcal{A}_j \otimes_c \mathcal{A}_j. \tag{3.39}$$

Note that $\mathbb{E}\big[\mathcal{A}(k) \otimes_c \mathcal{A}(k)\big]$ is a bounded, linear operator on the Banach space $\mathcal{C}\hat{\otimes}_c\mathcal{C}$. Now we can state a theorem that provides a necessary and sufficient condition for the stability of the second moment of (3.11).

Theorem 3.1. Consider system (3.11) which is repeated below

$$x_{(k+1)t_\mathrm{d}} = \mathcal{A}(k)x_{kt_\mathrm{d}}, \tag{3.40}$$

where

$$\begin{aligned} &\mathbb{P}\big(\mathcal{A}(k) = \mathcal{A}_j\big) = w_j, \\ &j = 1, \ldots, J, \quad \text{and} \quad k = 0, 1, 2, \ldots, \end{aligned} \tag{3.41}$$

with initial condition

$$x_0(\theta) = \phi(\theta), \quad -\Gamma \leq \theta \leq 0, \quad \phi \in \mathcal{C}. \tag{3.42}$$

There exist $M \geq 1$ and $0 \leq r < 1$ such that

$$\sup_{\substack{-\Gamma \leq \theta_1, \theta_2 \leq 0 \\ 1 \leq i_1, i_2 \leq n}} \Big| \mathbb{E}\big[x^{i_1}_{kt_\mathrm{d}}(\theta_1) x^{i_2}_{kt_\mathrm{d}}(\theta_2)\big] \Big| \leq Mr^k, \tag{3.43}$$

$\forall\, k \in \{0, 1, 2, \ldots\}$ if and only if

$$\rho\Big(\sum_{j=1}^{J} w_j \, \mathcal{A}_j \otimes_c \mathcal{A}_j \Big) < 1, \tag{3.44}$$

where $\mathcal{A}_j$'s are given by (3.9).

Proof. By application of Lemma 3.1 to system (3.38), we can say that there exist $M \geq 1$ and $0 \leq r < 1$ such that

$$\Big\| \mathbb{E}[x_{kt_\mathrm{d}} \otimes x_{kt_\mathrm{d}}] \Big\|_c \leq Mr^k, \tag{3.45}$$

$\forall\, k \in \{0, 1, 2, \ldots\}$ if and only if

$$\rho\Big(\sum_{j=1}^{J} w_j \, \mathcal{A}_j \otimes_c \mathcal{A}_j \Big) < 1. \tag{3.46}$$

On the other hand, from the definition of the c-norm in (3.27), we have

$$\Big\|\mathbb{E}\big[x_{kt_{\rm d}}\otimes x_{kt_{\rm d}}\big]\Big\|_c = \sup_{\substack{-\Gamma\le\theta_1,\theta_2\le 0\\ 1\le i_1,i_2\le n}}\Big|\mathbb{E}\big[x^{i_1}_{kt_{\rm d}}(\theta_1)x^{i_2}_{kt_{\rm d}}(\theta_2)\big]\Big|, \tag{3.47}$$

that completes the proof. □

Theorem 3.1 provides a necessary and sufficient condition, *i.e.* condition (3.44), for the second moment stability of system (3.11). The second moment stability is expressed by Eq. (3.43). Note that using the tensor product provided us with appropriate means to construct a linear map such as (3.35) for the second moment stability analysis. While $\mathbb{E}[x_{kt_{\rm d}}\otimes x_{kt_{\rm d}}]$ may be interpreted as the "second moment," it is not exactly the case. However, the norm defined on the tensor product space $\mathcal{C}\hat{\otimes}_c\mathcal{C}$ enables us to provide a supremum norm on the second moment of system (3.11); cf. (3.47).

Now we recall that the original question in Section 3.2 was concerned with the stability of $\mathbb{E}[x(t)x^{\rm T}(t)]$, *i.e.* the second moment of the stochastic system (3.1). In the following corollary, we show that condition (3.44) of Theorem 3.1 is truly a necessary and sufficient condition for the second moment stability of system (3.1).

Corollary 3.1. Consider system (3.1) with the delay behavior as described in Section 3.2. There exists $M\ge 1$ and $\omega>0$ such that

$$\sup_{1\le i_1,i_2\le n}\Big|\mathbb{E}\big[x^{i_1}(t)x^{i_2}(t)\big]\Big|\le M{\rm e}^{-\omega t},\quad \forall\, t\ge 0, \tag{3.48}$$

if and only if

$$\rho\Big(\sum_{j=1}^{J} w_j\,\mathcal{A}_j\otimes_c\mathcal{A}_j\Big)<1, \tag{3.49}$$

where $\mathcal{A}_j$'s are given by (3.9).

Proof. Assume $\rho\Big(\sum_{j=1}^{J} w_j\,\mathcal{A}_j\otimes_\epsilon\mathcal{A}_j\Big)<1$. Then from Theorem 3.1, there exists $M\ge 1$ and $0\le r<1$ such that (3.43) holds for any $k\in\{0,1,\ldots\}$. Now for any $t\ge 0$, there exists $\tilde{k}\in\{1,2,\ldots\}$, such that $(\tilde{k}-1)t_{\rm d}\le t<\tilde{k}t_{\rm d}$. Thus, by choosing $\theta_1=\theta_2=-\tilde{k}t_{\rm d}+t$ in (3.43) and recalling that $x_{\tilde{k}t_{\rm d}}(\theta)=x(\tilde{k}t_{\rm d}+\theta)$, we have

$$\sup_{1\le i_1,i_2\le n}\Big|\mathbb{E}\big[x^{i_1}(t)x^{i_2}(t)\big]\Big|\le Mr^{\tilde{k}}. \tag{3.50}$$

Also, since $t/t_{\rm d} < \tilde{k}$, then $r^{\tilde{k}} < r^{t/t_{\rm d}} = {\rm e}^{(\frac{1}{t_{\rm d}}\log r)t}$. Thus, (3.50) can be written as

$$\sup_{1\leq i_1,i_2\leq n}\Big|\mathbb{E}\big[x^{i_1}(t)x^{i_2}(t)\big]\Big| \leq M{\rm e}^{-\tilde{\omega}t}, \quad \forall\, t\geq 0, \tag{3.51}$$

where $\tilde{\omega} = -\frac{1}{t_{\rm d}}\log r$.

To show the reverse, assume that there exists $M \geq 1$ and $\omega > 0$ such that (3.48) holds. Choose $M_1 > 0$ such that $\sup_{1\leq i_1,i_2\leq n}\left|\phi^{i_1}(t)\,\phi^{i_2}(t)\right| \leq M_1$, $\forall\, t \in [-\Gamma, 0]$. Note that since $\phi \in \mathcal{C}$ (ϕ is the initial condition of system (3.1)), we know that such M_1 exists. Let $M_2 = \max\{M, M_1\}$. Hence,

$$\sup_{1\leq i_1,i_2\leq n}\Big|\mathbb{E}\big[x^{i_1}(t)x^{i_2}(t)\big]\Big| \leq M_2{\rm e}^{-\omega t}, \quad \forall\, t\geq -\Gamma. \tag{3.52}$$

In fact (3.52) is the extension of (3.48) to the interval $t \geq -\Gamma$. Now consider any $k \in \{0, 1, 2, \ldots\}$ and the time interval $[kt_{\rm d} - \Gamma, kt_{\rm d}]$. Setting $i_1 = i_2 = i$ in (3.52) and using the notation $x_{kt_{\rm d}}(\theta) = x(kt_{\rm d} + \theta)$, we get

$$\Big|\mathbb{E}\big[x^i_{kt_{\rm d}}(-kt_{\rm d}+t)\,x^i_{kt_{\rm d}}(-kt_{\rm d}+t)\big]\Big| \leq M_2{\rm e}^{-\omega t}, \tag{3.53}$$

$\forall\, t \in [kt_{\rm d} - \Gamma, kt_{\rm d}]$ and $\forall\, i \in \{1, \ldots, n\}$. Observe that since $t \geq kt_{\rm d} - \Gamma$, then ${\rm e}^{-\omega t} \leq {\rm e}^{-\omega(kt_{\rm d}-\Gamma)} = {\rm e}^{\omega\Gamma}({\rm e}^{-\omega t_{\rm d}})^k$. Therefore, by defining $\theta = -kt_{\rm d} + t$, (3.53) can be written as

$$\Big|\mathbb{E}\Big[\big(x^i_{kt_{\rm d}}(\theta)\big)^2\Big]\Big| \leq \tilde{M}\tilde{r}^k, \tag{3.54}$$

$\forall\, \theta \in [-\Gamma, 0]$ and $\forall\, i \in \{1, \ldots, n\}$, where $\tilde{M} = M_2{\rm e}^{\omega\Gamma}$ and $\tilde{r} = {\rm e}^{-\omega t_{\rm d}}$. On the other hand, from Cauchy-Schwarz inequality, we have

$$\Big|\mathbb{E}\Big[x^{i_1}_{kt_{\rm d}}(\theta_1)x^{i_2}_{kt_{\rm d}}(\theta_2)\Big]\Big| \leq \left(\mathbb{E}\Big[\big(x^{i_1}_{kt_{\rm d}}(\theta_1)\big)^2\Big]\mathbb{E}\Big[\big(x^{i_2}_{kt_{\rm d}}(\theta_2)\big)^2\Big]\right)^{\frac{1}{2}} \tag{3.55}$$

$\forall\, \theta_1, \theta_2 \in [-\Gamma, 0]$ and $\forall\, i_1, i_2 \in \{1, \ldots, n\}$. Substituting (3.54) in the right hand side of (3.55), we get

$$\Big|\mathbb{E}\big[x^{i_1}_{kt_{\rm d}}(\theta_1)\,x^{i_2}_{kt_{\rm d}}(\theta_2)\big]\Big| \leq \tilde{M}\tilde{r}^k, \tag{3.56}$$

$\forall\, \theta_1, \theta_2 \in [-\Gamma, 0]$ and $\forall\, i_1, i_2 \in \{1, \ldots, n\}$. Hence,

$$\sup_{\substack{-\Gamma\leq\theta_1,\theta_2\leq 0\\ 1\leq i_1,i_2\leq n}}\Big|\mathbb{E}\big[x^{i_1}_{kt_{\rm d}}(\theta_1)x^{i_2}_{kt_{\rm d}}(\theta_2)\big]\Big| \leq \tilde{M}\tilde{r}^k, \tag{3.57}$$

$\forall\, k \in \{0, 1, 2, \ldots\}$. According to the result of Theorem 3.1, (3.57) implies

$$\rho\Big(\sum_{j=1}^{J} w_j\, \mathcal{A}_j \otimes_c \mathcal{A}_j\Big) < 1. \tag{3.58}$$

□

Condition (3.23) in Proposition 3.1 and condition (3.44) in Theorem 3.1 are, respectively, necessary and sufficient conditions for the stability of the mean and the second moment of the stochastic system (3.1). However, in practice these conditions cannot be investigated directly due to the infinite-dimensional nature of the relevant operators. In the next section, we provide finite-dimensional versions of the stability conditions obtained in this section.

3.5 Finite-dimensional approximations

By discretizing system (3.1) in time, one can obtain a finite-dimensional approximation of system (3.1) and finite-dimensional approximations of the operators $\mathcal{A}_j$ given by (3.9). There are many well-established time discretization techniques for delay differential equations, such as Runge-Kutta techniques [7] and semi-discretization technique [32], that one can use. In this section, we provide finite-dimensional approximations of the stability conditions obtained in Section 3.4 independent of the specific discretization method used.

Assume that one applies a discretization method with a constant step-size mesh and obtains

$$X(k+1) = \mathbf{A}(k)X(k), \tag{3.59}$$

as a finite-dimensional approximation of system (3.11) where $X(k) \in \mathbb{R}^N$ and $\mathbf{A}(k) \in \mathbb{R}^{N\times N}$, $k = 0, 1, 2, \ldots$. Note that in Section 2.2.2 one way for how to obtain a finite-dimensional system such as (3.59) is provided (see (2.18)). However, one may use other discretization methods to obtain a finite-dimensional system, too. The integer $N \in \mathbb{N}$ is a parameter of the discretization method that is a function of the step size Δt, the largest delay $\tau_{\max}$ or the dwelling time $t_{\rm d}$ (whichever is greater), and the dimension n of the vector x in system (3.1). Similar to system (3.11), here $\mathbb{P}(\mathbf{A}(k) = \mathbf{A}_j) = w_j$, $j = 1, \ldots, J$. Moreover, the matrix $\mathbf{A}(k)$ and vector $X(k)$ are independent (due to the *i.i.d.* assumption on the delay switchings). Therefore, by taking the expected value of (3.59), we arrive at

$$\mathbb{E}[X(k+1)] = \mathbb{E}[\mathbf{A}(k)]\,\mathbb{E}[X(k)], \tag{3.60}$$

where

$$\mathbb{E}[\mathbf{A}(k)] = \sum_{j=1}^{J} w_j \mathbf{A}_j. \tag{3.61}$$

Based on (3.60-3.61), we know that $\mathbb{E}[X(k)]$ is exponentially stable if and only if

$$\rho\Big(\sum_{j=1}^{J} w_j \mathbf{A}_j\Big) < 1; \tag{3.62}$$

cf. (2.23) and (2.24). Condition (3.62) is a finite-dimensional approximation of the mean stability condition (3.23) given by Proposition 3.1.

To derive a finite-dimensional approximation of the second moment stability condition, observe that the tensor product becomes the Kronecker product in finite dimensional spaces. Therefore, from (3.59) one can write

$$\begin{aligned} X(k+1) \otimes X(k+1) &= \mathbf{A}(k)X(k) \otimes \mathbf{A}(k)X(k) \\ &= \big(\mathbf{A}(k) \otimes \mathbf{A}(k)\big)\big(X(k) \otimes X(k)\big), \end{aligned} \tag{3.63}$$

where $\otimes$ denotes the Kronecker product, $X(k) \otimes X(k) \in \mathbb{R}^{N^2}$, and $\mathbf{A}(k) \otimes \mathbf{A}(k) \in \mathbb{R}^{N^2 \times N^2}$. System (3.63) is a finite-dimensional approximation of system (3.35), where $\mathbb{P}\big(\mathbf{A}(k) \otimes \mathbf{A}(k) = \mathbf{A}_j \otimes \mathbf{A}_j\big) = w_j$, $j = 1, \ldots, J$. By taking the expected value of Eq. (3.63) and using the independence of $\mathbf{A}(k)$ and $X(k)$, we have

$$\mathbb{E}\big[X(k+1) \otimes X(k+1)\big] = \mathbb{E}\big[\mathbf{A}(k) \otimes \mathbf{A}(k)\big]\, \mathbb{E}\big[X(k) \otimes X(k)\big], \tag{3.64}$$

where

$$\mathbb{E}\big[\mathbf{A}(k) \otimes \mathbf{A}(k)\big] = \sum_{j=1}^{J} w_j \mathbf{A}_j \otimes \mathbf{A}_j. \tag{3.65}$$

Based on (3.64-3.65), we know that $\mathbb{E}[X(k) \otimes X(k)]$ is exponentially stable if and only if

$$\rho\Big(\sum_{j=1}^{J} w_j \mathbf{A}_j \otimes \mathbf{A}_j\Big) < 1; \tag{3.66}$$

cf. (2.31) and (2.32). Condition (3.66) is a finite-dimensional approximation of the second moment stability condition (3.44) given by Theorem 3.1.

After discretization of system (3.1) and obtaining the matrices $\mathbf{A}_j$, one can use condition (3.62) and (3.66) to evaluate the stability of the mean and the second moment of system (3.1), respectively. Conditions (3.62) and (3.66) can, for instance, be used to ob-

tain approximate stability boundaries in desired parameter spaces. The stability boundaries obtained using conditions (3.62) and (3.66) converge by decreasing the time step of the underlying discretization technique. Note that the convergence properties, such as the order of convergence, of $\rho\Big(\sum_{j=1}^{J} w_j \mathbf{A}_j\Big)$ to $\rho\Big(\sum_{j=1}^{J} w_j \mathcal{A}_j\Big)$ and $\rho\Big(\sum_{j=1}^{J} w_j \, \mathbf{A}_j \otimes \mathbf{A}_j\Big)$ to $\rho\Big(\sum_{j=1}^{J} w_j \, \mathcal{A}_j \otimes_c \mathcal{A}_j\Big)$ follow the convergence properties of the individual matrices $\mathbf{A}_j$ to the operators $\mathcal{A}_j$ and thus depend on the discretization technique used. We refer the reader to [10] (for Runge-Kutta techniques) and [32] (for semi-discretization technique) for more details about the convergence of the matrices $\mathbf{A}_j$ to the operators $\mathcal{A}_j$ and other approximation properties. We remark that a full characterization of the convergence properties is a subject of future work. In the next section, we demonstrate the application of the stability conditions using some examples.

3.6 Examples

In this section, we provide two examples demonstrating the application of the stability criteria obtained in Sections 3.4 and 3.5.

3.6.1 Scalar system

Consider the scalar version of system (3.1), that is,

$$\dot{x}(t) = a\, x(t) + b\, x(t - \tau(t)), \tag{3.67}$$

where $x, a, b \in \mathbb{R}$. Assume that the delay can take two values from the set $\Omega = \{0.5, 1\}$ with probability distribution $w_1 = w_2 = 0.5$, and the dwelling time of the delay is $t_{\mathrm{d}} = 0.25$. We use the semi-discretization technique with a step size of $\Delta t = 0.025$ to discretize system (3.67) and obtain matrices $\mathbf{A}_1$ and $\mathbf{A}_2$ associated with the two delay values (see Section 2.2.2 for how to obtain these matrices). We want to draw stability charts in the space of parameters a and b. Note that matrices $\mathbf{A}_1$ and $\mathbf{A}_2$ are functions of the parameters a and b. For the stability of the mean of system (3.67) we check the condition given by Proposition 3.1 that reduces here to

$$\rho\big(\frac{1}{2}\mathbf{A}_1 + \frac{1}{2}\mathbf{A}_2\big) < 1, \tag{3.68}$$

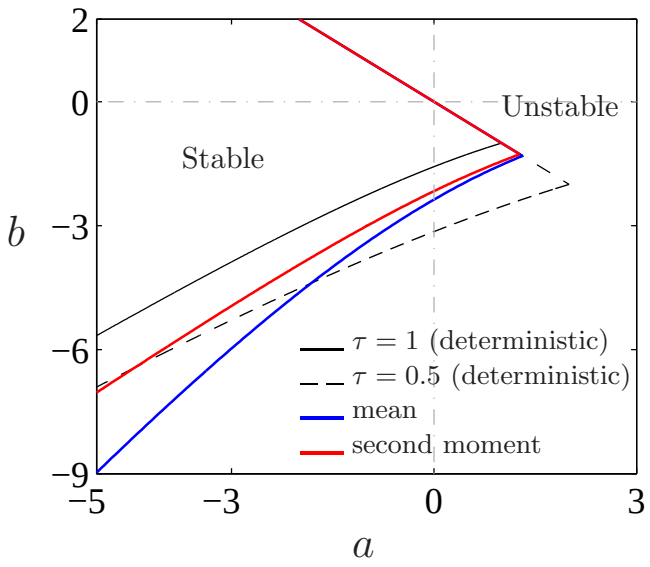

Figure 3.2: Stability charts for system (3.67). The blue curve is the boundary of the mean stable area. The red curve is the boundary of the second moment stable area. For comparison, the stable areas of deterministic versions of system (3.67) with delays equal to $\tau = 0.5$ and $\tau = 1$ are shown with dashed and solid black boundaries, respectively.

and for the stability of the second moment of system (3.67) we check the condition given by Theorem 3.1 that reduces here to

$$\rho\big(\frac{1}{2}\mathbf{A}_1 \otimes \mathbf{A}_1 + \frac{1}{2}\mathbf{A}_2 \otimes \mathbf{A}_2\big) < 1. \tag{3.69}$$

In Fig. 3.2, the stable and unstable areas of the mean (based on condition (3.68)) and the second moment (based on condition (3.69)) are shown with blue and red curves, respectively. Note that the area on the left of the boundaries that is limited by the line $b = -a$ from top is the stable region. The second moment stable region is inside the mean stable region as the second moment stability is sufficient for the mean stability. For comparison, the stable regions of a deterministic version of system (3.67) with deterministic delays $\tau = 0.5$ and $\tau = 1$ are shown by dashed black and solid black curves, respectively.

3.6.2 A vector (2-D) system

In this section, we consider a linear second order system in the general canonical reachable form

$$\dot{x}(t) = \begin{bmatrix} 0 & 1 \\ -a_2 & -a_1 \end{bmatrix} x(t) + \begin{bmatrix} 0 \\ 1 \end{bmatrix} u(t - \tau(t)), \tag{3.70}$$

where $x \in \mathbb{R}^2$ and $u \in \mathbb{R}$ is the control action that is applied with a delay $\tau(t)$. Using feedback control law

$$u(t) = [-k_1 \ \ -k_2]\, x(t), \tag{3.71}$$

the closed-loop system is

$$\dot{x} = \mathbf{a}x(t) + \mathbf{b}x(t - \tau(t)), \tag{3.72}$$

where

$$\mathbf{a} = \begin{bmatrix} 0 & 1 \\ -a_2 & -a_1 \end{bmatrix}, \quad \mathbf{b} = \begin{bmatrix} 0 & 0 \\ -k_1 & -k_2 \end{bmatrix}. \tag{3.73}$$

Let us assume that the delay takes values from the set $\Omega = \{0.7, 0.85, 1, 1.15, 1.3\}$ with equal probabilities $w_i = 1/5$, $i = 1, \ldots, 5$ and the dwelling time is $t_{\mathrm{d}} = 0.5$. We use the semi-discretization technique with time step $\Delta t = 0.05$ to obtain matrices $\mathbf{A}_1, \ldots, \mathbf{A}_5$ associated with 5 delay values. Refer to Section 2.2.2 for how to obtain matrices $\mathbf{A}_1, \ldots, \mathbf{A}_5$.

To investigate the second moment stability of system (3.72-3.73) with the given delay parameters, we use the finite-dimensional version of the second moment stability condition given by Eq. (3.66), that is,

$$\rho\Big(\sum_{j=1}^{5} \frac{1}{5} \mathbf{A}_j \otimes \mathbf{A}_j\Big) < 1. \tag{3.74}$$

First we pick point $(a_1, a_2) = (0.25, 30)$ in the (a_1, a_2) parameter space and seek for the values of control gains (k_1, k_2) for which the closed loop system (3.72) is second moment stable (by condition (3.74)). The red curve in Fig. 3.3a encircles the stable area. Note that such a boundary can be obtained by checking the (k_1, k_2) space point by point or by finding an initial point on the boundary and obtaining the rest of it using numerical continuation. Here we have used the latter exploiting the continuation routine embedded in the software package DDE-BIFTOOL [17],[71]. The black curve encloses the stable area of a deterministic version of system (3.72) with delay $\tau = 1$ that is the average delay in the set Ω. Note that in the case of the deterministic system, condition (3.74) can still be applied using matrix $\mathbf{G}_3$ that corresponds to the delay value $\tau = 1$. In this case since there is only one delay value, condition (3.74) reduces to $\rho(\mathbf{A}_3) < 1$. The difference between the red and black boundaries in Fig. 3.3a shows that the control gains that stabilize the system with stochastic delay do not necessarily stabilize the same system with the average delay, and vice versa.

Next we choose the control gains $(k_1, k_2) = (10, -0.25)$ (indicated by point P in Fig. 3.3a) and investigate the values of system parameters (a_1, a_2) for which these control gains stabilize the closed loop system (3.72). The condition (3.74) is used again to assess stability. In Fig. 3.3b, the red curve is the boundary between second moment stable

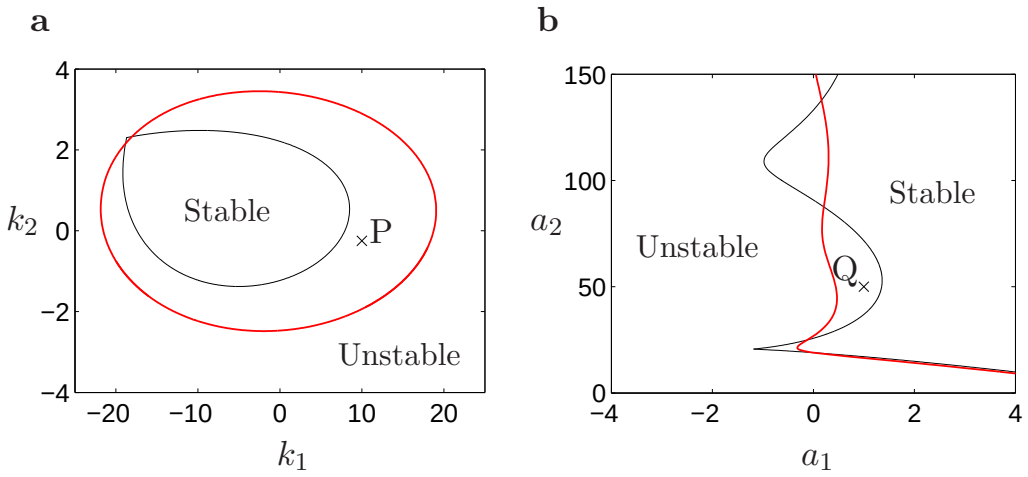

Figure 3.3: Stability charts for system (3.70-3.71). The red curve is the boundary of the second moment stable area. For comparison, the stability boundary of a deterministic version of system (3.70-3.71) with delay $\tau = 1$ (the average delay) is also shown by a black curve. **a** Stable and unstable areas in the (k_1, k_2) space for system parameters associated with point Q in panel b. **b** Stable and unstable areas in the (a_1, a_2) space for control gains indicated by point P in panel a.

and unstable regions. For comparison the black curve shows the stability boundary for a deterministic system with delay $\tau = 1$ (the average delay). The point Q in Fig. 3.3b corresponds to the parameters (a_1, a_2) for which the stabilizing control gains in Fig. 3.3a are obtained.

Note that as the time step Δt used in the time discretization technique gets smaller, the size of matrices $\mathbf{A}_j$ in condition (3.66) gets larger (cf. Section 2.2.2). In both examples in this section, we used values of Δt that are, while being computationally affordable, small enough so that the boundaries shown in Figs. 3.2 and 3.3 converged to a desired accuracy. One may make Δt values even smaller to obtain more precise boundaries, if one has access to stronger computational resources.

3.7 Note on almost-sure stability

In this section we discuss the differences between almost sure stability and second moment stability of system (3.1) from a computational point of view. To this end, we first give a well-known result about almost sure stability.

Consider system (3.59) that is the discretized version of system (3.1). The following theorem is a well-known result on almost sure stability of system (3.59); for example, see [14].

Theorem 3.2. Consider system

$$X(k+1) = \mathbf{A}(k)X(k), \quad k = 0, 1, \ldots, \tag{3.75}$$

with $X(0) = x_0 \in \mathbb{R}^N$ and $\mathbf{A}(k) \in \mathbb{R}^{N\times N}$ where $\mathbb{P}\big(\mathbf{A}(k) = \mathbf{A}_j\big) = w_j$, for $j = 1, \ldots, J$ and $k = 0, 1, \ldots$. System (3.75) is almost surely stable if and only if there exists $q \in \mathbb{N}$ such that

$$\prod_{i_1,i_2,\ldots,i_q=1}^{J} \left\|\mathbf{A}_{i_1}\mathbf{A}_{i_2}\cdots\mathbf{A}_{i_q}\right\|^{w_{i_1}w_{i_2}\cdots w_{i_q}} < 1, \tag{3.76}$$

where $\|.\|$ is an induced matrix norm.

Condition (3.76) can be checked for the values of $q = 1, 2, \ldots$, in a consecutive manner. One can see that condition (3.76) for each individual value of q is in fact a sufficient condition for almost sure stability. In practice as q increases, the computational burden blows up exponentially as the number of matrix products to be calculated is J^q.

Let us consider the scalar system given in the example in Section 3.6.1. In this example, there are two delay values, so $J = 2$, and $\mathbf{A}_1$ and $\mathbf{A}_2$ are the two matrices, obtained through time discretization, associated with the two delay values. To investigate almost sure stability of this system at a particular set of parameter values, we check condition (3.76) for $q = 1, 2, \ldots, q_{\max} = 15$, in a consecutive manner. If condition (3.76) holds for a specific value of q, we stop and declare the system almost sure stable; otherwise, we continue up to $q_{\max} = 15$ (we could not exceed $q = 15$ due to our computational limitations). If condition (3.76) does not hold for any value $q = 1, \ldots, q_{\max}$, we cannot still conclude that the system is not almost sure stable, due to the fact that larger values of q are not checked yet. Therefore, the collection of conditions provided by Eq. (3.76) for individual values $q = 1, \ldots, q_{\max}$, is still a sufficient stability condition.

In Fig. 3.4a, the cyan curve is the boundary of the almost sure stable area obtained by the procedure described above. The red curve is the boundary of the second moment stable area (same as in Fig. 3.2). Note that the true almost sure stable area is larger than the one shown in Fig. 3.4a, because we only checked a series of sufficient conditions. As a matter of fact, in the linear switched system (3.59), that is a discretized version of system (3.1), the second moment stability implies almost sure stability; see [44] or [13] for this established result. Consequently, the second moment stable region must be inside the true almost sure stable region. As another example, Fig. 3.4b shows the second moment stable and almost sure stable regions of the same system except that the dwelling time is larger: $t_{\mathrm{d}} = 2$ (rather than $t_{\mathrm{d}} = 0.25$ used in Fig. 3.4a). In this case, the almost sure stable area, obtained using condition (3.76) for $q = 1, \ldots, q_{\max} = 15$, is a bit larger than the second moment stable

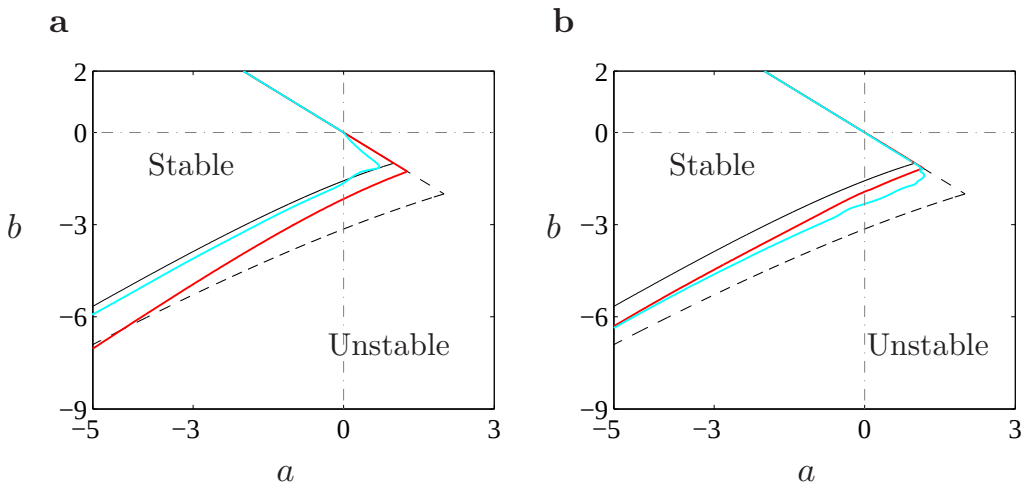

Figure 3.4: Stable and unstable regions of system (3.67) in the sense of the second moment and almost sure stability where the red curve is the boundary of the second moment stable area and the cyan curve is the boundary of the almost sure stable area. **a** The parameters are the same as in Fig. 3.2. **b** The parameters are the same as in Fig. 3.2 except that $t_{\mathrm{d}} = 2$ (slower delay switchings). For comparison, stable regions of the deterministic version of system (3.67) with delays $\tau = 0.5$ and $\tau = 1$ are also shown by dashed and solid black curves, respectively.

area. However, since we haven't checked the larger values of q, we still do not know how conservative our estimate of the almost sure stable region is.

The results shown in Fig. 3.4 demonstrate that the second moment stability criteria proposed in this chapter, that are necessary and sufficient, may be more practical for linear switched systems than almost sure stability criteria, that are just sufficient. The reason is that the second moment stability provides a sufficient condition for almost sure stability. Therefore by finding the second moment stable region, we also obtain an estimate of the almost sure stable region. However, finding the almost sure stable region does not give us any information about the second moment stable region as the almost sure stability criteria are not exact. Furthermore, the condition for almost sure stability, due to its higher computational burden, may become too conservative especially if the dimension of matrices $\mathbf{A}_j$ in (3.76) is large. As a result, the estimate for almost sure stable region obtained using condition (3.76) can be even more conservative than the estimate given by the second moment stable region itself.

3.8 Discussion

We obtained necessary and sufficient conditions for a class of continuous-time linear systems subject to stochastic delay. We considered the stability of second moment of the system as stability criteria. The stability conditions are in the form of checking the spectral radius of an operator that is a linear combination of tensor products of augmented solution operators associated with each individual delay. We presented finite-dimensional approximations of the proposed stability criteria which can be used to draw stability charts in the parameter space. The class of systems we considered has one delayed term where the delay is stochastic. The method can be generalized to the case where there are one or more terms with deterministic delays and one or more terms with stochastic delays in a straightforward fashion.

For the linear systems considered, the stability of the second moment also provides a sufficient condition for almost sure stability. Therefore, if an assessment of almost sure stability is desired, the result of this chapter can be useful. Moreover, as shown through an example, the almost sure stability region obtained by assessing the second moment stability might be less conservative than the region obtained by using the established results for almost sure stability due to the higher computational burden of the almost sure stability conditions.

The assumed delay behavior is flexible to approximate different kinds of stochastic behavior in the sense that there are three parameters to tune: delay values, the probability distribution, and the dwelling time. Furthermore, the generalization of this delay behavior to the case where the dwelling time is a random variable as well as the case where the jump probabilities follow a Markov rule can be done using the same machinery presented in this chapter. However, we also remark that the type of the problem of the stability analysis of a continuous-time system with stochastic delay depends on the form of the delay variations. In other words, if one assumes a different type of stochastic process for the delay trajectories, such as Gaussian noise, *etc.*, one may end up with an essentially different problem at hand.

CHAPTER 4

Applications of the method on gene regulation dynamics

4.1 Introduction

In this chapter, we apply the mathematical tools developed in Chapters 2 and 3 to investigate the stability properties of a negative feedback auto-regulatory gene. The model describing the auto-regulation through negative feedback is a delay differential equation where the delay, that is the protein production time, is a stochastic variable. In the Appendix, a traditional mass-action kinetic model of the auto-regulatory gene, that is obtained based on instantaneous molecular reactions, is given and it is shown that how one can obtain the model used in this chapter from chemical kinetics. We produce stability charts for equilibria on the plane of some model parameters for different distributions of the stochastic delay. The stability results are also validated by numerical simulations of linearized and nonlinear models.

4.2 Stochastic delays in a gene regulatory network

We analyze the stability of genetic circuits where a protein regulates its own production. The two major processes involved are called transcription and translation [15]. During transcription, a gene (a section of the DNA) is copied into messenger RNA (mRNA) one nucleotide at a time by an enzyme called RNA polymerase. Then during translation, ribosomes "read" the genetic code from the messenger RNA to sequentially assemble proteins from amino acids. That is, transcription and translation involve sequential biochemical reactions [2]. Although each individual reaction generally happens on a fast time-scale, the large number of reactions required and their sequential nature can result in significant delays [83]. Further processes, such as protein folding and modification, can also impact

the time it takes to produce a fully mature protein [58, 62]. Proteins can regulate (activate or repress) the production of other proteins by binding to the promoter region of the corresponding genes. Here we study the case where a protein represses its own production as shown by the diagram in Fig. 4.1. It has been shown that this single feedback system may produce oscillatory behavior and that time delays play a crucial role in the dynamics [75]. We construct two different models: a simpler model where the mRNA dynamics are neglected and another one where they are included. These examples allow us to highlight nontrivial dynamics caused by the stochastic delay variations.

We begin by describing how delays arise in protein production. We model the sequential biochemical reactions involved in protein production by the chain of reactions

$$\begin{aligned} P_0 &\xrightarrow{c_1} P_1\,, \\ P_1 &\xrightarrow{c_2} P_2\,, \\ &\vdots \\ P_{N-1} &\xrightarrow{c_N} P_N\,, \end{aligned} \tag{4.1}$$

where P_i denotes the number of molecules in the i-th state of the process and N is the number of reactions in the chain. For example, one may consider P_0 as the transcription initiation state and P_N as the fully mature protein. The parameter c_i is the reaction rate of the i-th reaction. The probability of reaction i happening during the time interval $[t,\ t+\mathrm{d}t]$ is proportional to the firing rate c_i and the number of proteins P_{i-1} in the $(i-1)$-th state.

In Appendix A, we assume that the time elapsed between reactions are independent and exponentially distributed and we consider the simplification $c_i = c$ for $i = 1, \ldots, N$ and the initial condition $P_0 = 1$, $P_i = 0$, for $i = 1, \ldots, N$. Then we show that the stochastic delay, *i.e.* the total time elapsed between the first reaction and the last reaction in system (4.1) follows the Erlang distribution

$$w_{\mathrm{e}}(\sigma) = \frac{c^N \sigma^{N-1} \mathrm{e}^{-c\sigma}}{(N-1)!}\,; \tag{4.2}$$

see also [21]. Numerically, we find that Eq. (4.2) still describes the delay distribution well for different initial conditions. To demonstrate this we consider $N = 50$ reactions, $c = 5$ reactions per second, the initial condition $P_0 = 10000$, $P_i = 0$, for $i = 1, \ldots, N$, and we simulate the reactions using a Gillespie algorithm [25]. The corresponding normalized histogram of the delay is overlaid with the distribution (4.2) in Fig. 4.2(a). We remark that in this case we still measure the delay as the time difference between the first reaction and the N-th reaction rather than tracing individual molecules in the simulation.

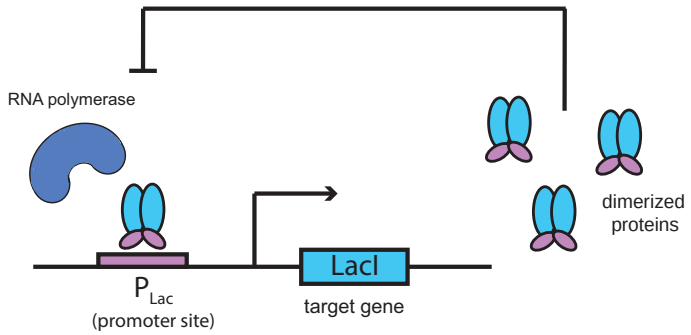

Figure 4.1: An auto-regulatory gene network. The target gene codes for the protein *LacI* that represses its own production by blocking the RNA polymerase from binding.

To characterize the Erlang distribution (4.2) we calculate its mean

$$E := \int_0^\infty w_{\mathrm{e}}(\sigma)\,\sigma\,\mathrm{d}\sigma = \frac{N}{c}\,, \tag{4.3}$$

and variance

$$V := \int_0^\infty w_{\mathrm{e}}(\sigma)\,(\sigma - E)^2 \mathrm{d}\sigma = \frac{N}{c^2}\,. \tag{4.4}$$

Notice that the relative variance

$$R := \frac{V}{E^2} = \frac{1}{N}\,, \tag{4.5}$$

is inversely proportional to the number of reactions N but does not depend on the transcription rate c; see [1].

4.3 Model of an auto-regulatory gene circuit

After characterizing the stochastic delay arising from sequential reactions, we analyze the dynamics of the auto-regulatory gene circuit (also called auto-repressor) depicted in Fig. 4.1 under such stochastic delay variations. Neglecting the mRNA dynamics, we consider the model

$$\dot{p}(t) = -\gamma\, p(t) + \frac{\kappa}{1 + \big(p\big(t - \tau(t)\big)/p_{\mathrm{h}}\big)^2}\,, \tag{4.6}$$

where p denotes the concentration of fully matured proteins. The linear term on the right hand side accounts for the protein degradation while the nonlinear term represents the protein production. Here, γ denotes the degradation rate, κ is the maximum production rate, and p_{h} is the protein concentration corresponding to half repression. The nonlinearity is in the form of a Hill function where the power 2 in the denominator represents repres-

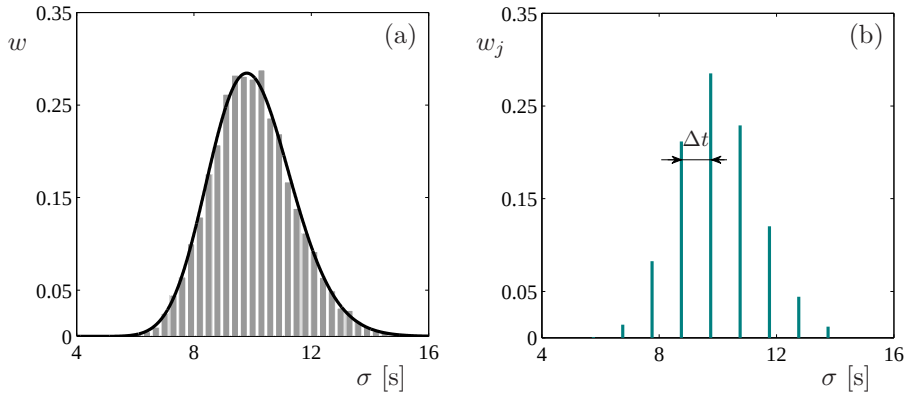

Figure 4.2: (a) A normalized histogram of the delay obtained with running a Gillespie simulation for system (4.1) with $N = 50$ reactions and $c = 5$ reactions per second using the initial condition $P_0 = 10000$, $P_i = 0$, for $i = 1, \ldots, N$. The black curve shows the Erlang distribution (4.2) for the same parameters with mean $E = N/c = 10\,[\mathrm{s}]$ and variance $V = N/c^2 = 2\,[\mathrm{s}^2]$. (b) Discretization of the Erlang distribution using Dirac deltas separated by $\Delta t = 1\,[\mathrm{s}]$.

sion strength. This model has been studied in the literature [15, 75] with constant delay $\tau(t) \equiv \tau$ and can be shown to admit one of two behaviors: asymptotic convergence to a positive equilibrium or convergence to a limit cycle [51] depending on the parameters γ, κ, and p_{h}. Here, we assume that the delay follows a stationary stochastic process with Erlang distribution (4.2) and show that this system demonstrates similar behavior in the stochastic sense. More details about the reactions involved in system (4.6) can be found in Appendix A where the parameters γ, κ, and p_{h} are related to reaction rates using mass-action kinetics. For the stability charts shown in the following section, we set $p_{\mathrm{h}} = 100$ proteins per cell and vary γ and κ while assuming $\gamma > 0$ and $\kappa > 0$.

The model (4.6) has a unique equilibrium $p(t) \equiv p_*$ where p_* is the real solution of the cubic equation

$$p_*^3 + p_{\mathrm{h}}^2\, p_* - \frac{\kappa p_{\mathrm{h}}^2}{\gamma} = 0. \tag{4.7}$$

To study the stability of this equilibrium, we define the perturbation $x(t) = p(t) - p_*$ and linearize the system (4.6) about the equilibrium. This yields

$$\dot{x}(t) = a\, x(t) + b\, x(t - \tau(t))\,, \tag{4.8}$$

with

$$\begin{aligned} a &= -\gamma\,, \\ b &= \frac{-2\kappa\, p_{\mathrm{h}}^2\, p_*}{(p_{\mathrm{h}}^2 + p_*^2)^2}\,. \end{aligned} \tag{4.9}$$

Indeed, Eq. (4.8) has the same form as Eq. (2.33) but here the delay follows the Erlang distribution (4.2) instead of the uniform distribution used in Sec. 2.3.1.

As shown in Chapter 2, if $t_{\mathrm{d}} \leq \tau_{\min}$, system (2.5) describes continuous-time mean dynamics. While $\tau_{\min} = 0$ for the Erlang distribution, for the examples considered in this section the distribution is very close to zero for $\sigma \leq E - 3\sqrt{V}$; see Fig. 4.2(a) as an example and also the Appendix for some quantitative details. Thus, we assume $t_{\mathrm{d}} < E - 3\sqrt{V}$ and use (2.5) with continuous distribution (4.2). Using the trial solution $\bar{x}(t) = \kappa \mathrm{e}^{st}$, $\kappa, s \in \mathbb{C}$, we obtain the characteristic equation

$$s - a - b\,\frac{c^N}{(s+c)^N} = 0\,, \tag{4.10}$$

which has finitely many (in particular $N+1$) solutions for the eigenvalues s. It can be shown that when the Erlang distribution is perturbed with perturbation size ϵ, additional spectra appear in the neighborhood of these eigenvalues such that the size of the neighborhood is proportional to ϵ. Additional eigenvalues may also appear to the left of a vertical line located at $\Re(s) = -1/\epsilon$; see [20] for more details.

We check for two types of stability loss. First we substitute $s = 0$ into (4.10) which results in $b = -a$. But when using equations (4.7) and (4.9) no feasible solutions can be found in the (γ, κ) parameter plane. Second, we substitute $s = \mathrm{i}\omega$ into (4.10) and we obtain the stability boundary

$$\begin{aligned} a &= \frac{\omega \cos(N\theta)}{\sin(N\theta)}\,, \\ b &= \frac{-\omega}{\sin(N\theta)} \left(1 + \frac{\omega^2}{c^2}\right)^{\frac{N}{2}}\,, \end{aligned} \tag{4.11}$$

where

$$\theta = \tan^{-1}\left(\frac{\omega}{c}\right). \tag{4.12}$$

Now using equations (4.7) and (4.9) one may obtain

$$\begin{aligned} \gamma &= -a\,, \\ \kappa &= -2p_{\mathrm{h}}\frac{a^2}{b}\left(\frac{b}{2a-b}\right)^{3/2}\,, \end{aligned} \tag{4.13}$$

which result in a stability curve in the positive quadrant in (γ, κ)-plane; see black dashed curves in Fig. 4.3.

In order to apply the stability analysis developed in Section 2.3, the delay distribution must have finite support. To achieve this, we truncate and discretize the Erlang distribution $w_{\mathrm{e}}(\sigma)$ given in (4.2). Again, noticing that the distribution is close to zero when σ is more than three standard deviations away from the mean, we set weights at $\sigma_i = E - 3\sqrt{V} + (i-1)\Delta t$ to be

$$\tilde{w}_i = \begin{cases} \Delta t\, w_{\mathrm{e}}(\sigma_i)\,, & \text{if} \quad |\sigma_i - E| \le 3\sqrt{V}\,, \\ 0\,, & \text{if} \quad |\sigma_i - E| > 3\sqrt{V}\,, \end{cases} \tag{4.14}$$

for $i = 1, 2, \ldots$ such that $\tilde{w}_i \neq 0$ only for $i = q, \ldots, Q$. Finally, we normalize the distribution by

$$w_j = \frac{\tilde{w}_{q+j-1}}{\sum_{k=q}^{Q} \tilde{w}_k}\,, \tag{4.15}$$

for $j = 1, \ldots, J$ where $J = Q - q + 1$. Fig. 4.2(b) depicts the discretization of the Erlang distribution shown in Fig. 4.2(a) with $\Delta t = 1$ [s].

Once the delay distribution w is characterized for system (4.8),(4.9), we may construct the discretized systems (2.22),(2.23) for the mean and (2.30),(2.31) for the second moment to analyze their stability using the characteristic equations (2.40) and (2.41), respectively. The results are shown in Fig. 4.3 in the (γ, κ) parameter plane. The blue and red curves show the stability boundaries of the mean and the second moment, respectively. The dark gray region is where the second moment (and the mean) is stable. The light gray region is where the mean is stable but not the second moment. We vary the mean E and the relative variance R, as indicated, in order to inspect the effects of changing the probability distribution of the delay. Note that the delay distribution used in Fig. 4.3(g) corresponds to the case shown in Fig. 4.2(b). We kept Δt constant for all plots in Fig. 4.3 so that the effect of changing the delay values is reflected accurately. When we discretize the continuous delay distribution (4.2), we use the same time step as the time discretization step Δt. In all panels in Fig. 4.3, we set $\Delta t = 1[\mathrm{s}]$ and also $t_{\mathrm{d}} = 1[\mathrm{s}]$.

As explained above, the mean loses stability only via Hopf stability loss where the angular frequency ω increases along the stability boundary from left to right (blue curves

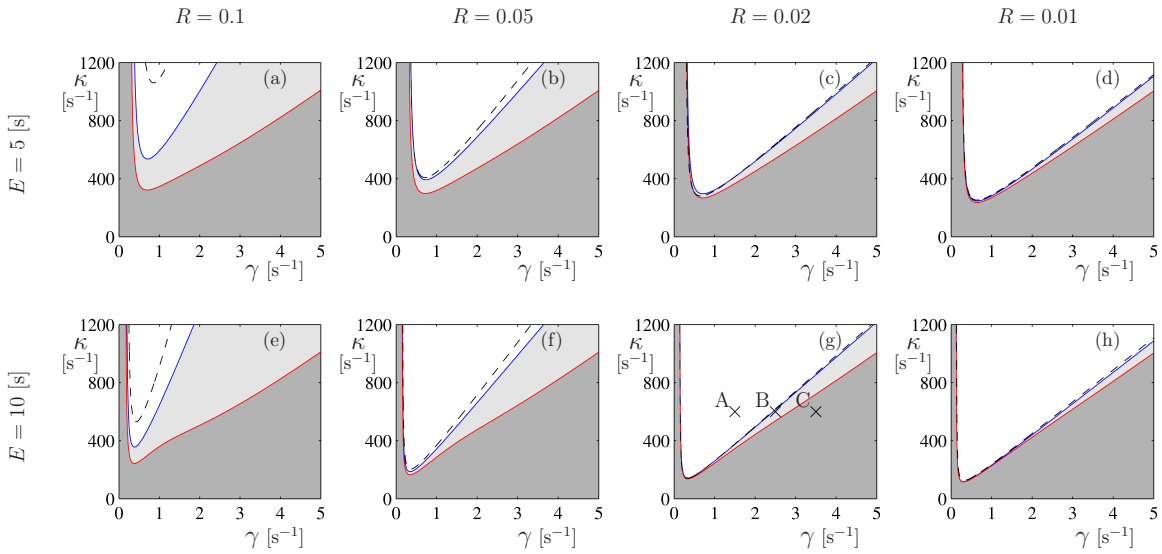

Figure 4.3: Stability charts for system (4.8),(4.9) when the delay follows the Erlang distribution (4.2) for different values of the mean delay $E = N/c$ and relative variance $R = 1/N$. The dwelling time is set to $t_{\mathrm{d}} = 1\,[\mathrm{s}]$ and $\Delta t = 1\,[\mathrm{s}]$. The dark gray region is where the second moment and the mean are stable. The light gray region is where the mean is stable but not the second moment. The dashed black curve is the boundary of the stability for the continuous-time mean dynamics described by Eqs. (4.13).

obtained by the semi-discretization and the black dashed curves obtained through (4.10)-(4.13)). For the second moment, only fold stability loss occurs and the corresponding red curves are obtained by the semi-discretization. In general, the stability regions shrink when increasing the mean delay $E = N/c$ and when decreasing relative variance $R = 1/N$. Also, when decreasing R the difference between mean stability and second moment stability decreases as indicated by the size of the light gray area. This corresponds to the fact that as the delay distribution is getting narrower, the dynamics get closer to the dynamics of a system with a single delay $\tau \equiv E$. Moreover, notice that the size of the dark gray domain, where the second moment is stable, increases with R indicating that the stochasticity in the delay may stabilize the system. Similar results relating to noise induced stability have been shown in other works [3, 6, 45, 50].

We remark that our stability analysis may require large computational effort when calculating the largest eigenvalues (*i.e.* the spectral radius) of the matrix $\bar{\bar{\mathbf{A}}}$ in (2.31). This may cause problems especially if both large and small delays exist in the system. In particular, Δt should be smaller than the minimum delay $\tau_{\min}$ in the system so that $\lfloor \frac{\tau_{\min}}{\Delta t} \rfloor \geq 1$. Otherwise all the delays that are smaller than Δt will be neglected in the analysis. On the other hand, if $\tau_{\max} \gg \tau_{\min}$ the size of matrix $\bar{\bar{\mathbf{A}}}$, that is proportional to $(\lfloor \frac{\tau_{\max}}{\Delta t} \rfloor)^2$, gets un-

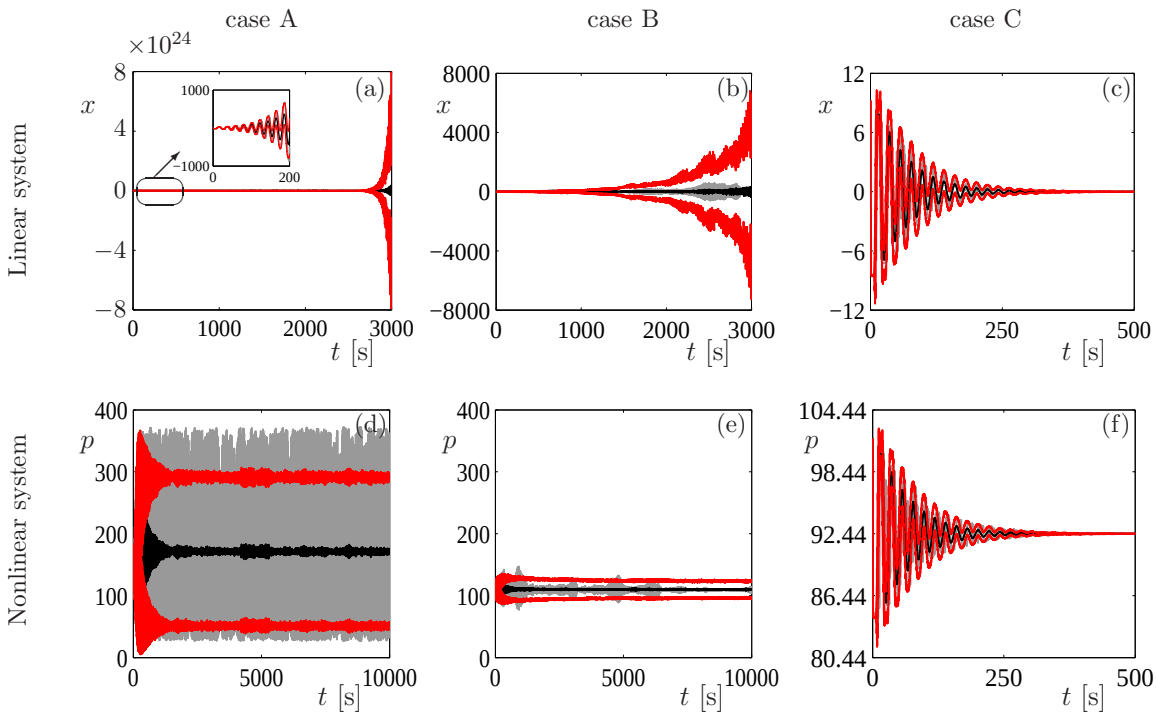

Figure 4.4: (a–c) Numerical simulations of the linear model (4.8),(4.9) for points A $(\gamma, \kappa) = (1.5, 600)$, B $(\gamma, \kappa) = (2.5, 600)$, and C $(\gamma, \kappa) = (3.5, 600)$ marked in Fig. 4.3(g). (d–f) Corresponding simulation results of the nonlinear model (4.6). In each panel (a–f), the black trajectory indicates the mean while the red trajectories enclose mean $\pm$ standard deviation for 1000 runs and the gray curve shows a sample realization.

manageably large. In panels (b-d) and (f-h), $\Delta t = 1$[s] is small enough. Consequently, the blue curves obtained by the semi-discretization approximate well the black dashed curves obtained using the continuous-time mean dynamics (4.11)-(4.13). On the other hand for the wide distributions used in Fig. 4.3(a,e), $\Delta t = 1$[s] is not small enough. In particular, in case (a), we have $\tau_{\min} = E - 3\sqrt{V} \approx 0.26$. Therefore ideally Δt should be smaller than 0.26.

In order to demonstrate the time evolution of the linear system (4.8),(4.9) and the original nonlinear system (4.6), we use numerical simulation that is based on semi-discretization, *i.e.* we assume the delayed term stays constant in the time interval $[i\Delta t, (i+1)\Delta t]$. Since in (4.6), the delayed term is contained in the only nonlinearity, the resulting ODE can still be solved analytically in each interval. The Erlang distribution is also discretized as in (4.14)-(4.15). We set $E = 10$ [s] and $R = 0.02$ and choose three points marked as A $(\gamma = 1.5, \kappa = 600)$, B $(\gamma = 2.5, \kappa = 600)$, and C $(\gamma = 3.5, \kappa = 600)$ in different regions in Fig. 4.3(g). The initial condition is set to $x(t) \equiv 0.1p_*$ in the linear system (4.8) (that corresponds to $p(t) \equiv 1.1p_*$ in the nonlinear system (4.6)) along the time domain $t \in [-\tau_J, 0]$

where p_* is the equilibrium obtained from (4.7).

The results are summarized in Fig. 4.4 where the black curve indicates the mean and the red curves bound the mean plus and minus the standard deviation computed from 1000 simulations. A sample realization is shown by a gray curve in each panel. Fig. 4.4(a–c) show the results for the linear system (4.8),(4.9). In case A, the equilibrium is unstable and both the mean and the standard deviation diverge. In case B, the mean converges to zero while the standard deviation diverges. In case C, both the mean and the standard deviation converge to zero corresponding to almost sure stability of the equilibrium. The corresponding simulation results for the nonlinear system (4.6) are displayed in Fig. 4.4(d–f). The results are qualitatively similar to the linear ones except that in cases A and B the standard deviation does not go to infinity but saturates due to the saturating nonlinear terms. The corresponding nonlinear oscillations shown by the gray sample trajectories resemble those found for a deterministic system with distributed delay in [51]. For example, by doing Fast Fourier Transform (FFT) analysis, the main frequency of the nonlinear oscillations is found to be close to the Hopf frequency at which the continuous-time mean dynamics lose stability. Note that in case C, almost sure stability of the equilibrium is ensured by our analysis at the linear level only, but the nonlinear system also demonstrates almost sure stability.

4.4 Auto-regulatory gene network with mRNA dynamics and dual delayed feedback

We now consider a model where we incorporate mRNA dynamics, resulting in a non-scalar example. Additionally, we assume that the system has two distinct regulatory pathways with distinct signaling delays [49, 81].

In particular, we consider the model

$$\begin{aligned} \dot{\hat{m}}(t) &= -\gamma_m\, \hat{m}(t) + \frac{\alpha_m}{1 + (p(t-\tau(t))/p_{\mathrm{h}})^2} \\ \dot{p}(t) &= -\gamma_p\, p(t) + \alpha_p\, \hat{m}(t), \end{aligned} \tag{4.16}$$

where $\hat{m}$ is the concentration of mRNA in the transcriptional initiation phase, p is the concentration of fully matured protein, and γ_m and γ_p are mRNA and protein degradation rates, respectively. The nonlinear term in the first equation in (4.16) incorporates the feedback due to self-repression where the delay $\tau(t)$ still represents the total delay in the feedback loop and α_m is the maximum mRNA production rate. According to the second equation

in (4.16), the protein production is assumed to be proportional to the mRNA concentration with rate α_p. Assuming that mRNA dynamics are fast relative to the protein dynamics, *i.e.* assuming that the first equation in (4.16) approaches steady state quickly, the model (4.16) can be reduced to (4.6) with $\kappa = \alpha_p \alpha_m / \gamma_m$ as shown in Appendix A.

As mentioned above, we assume two distinct signaling pathways. Thus, the delay $\tau(t)$ will have a bimodal distribution where each mode resembles an Erlang distribution. To simplify the model we consider a bimodal distribution with two distinct delay values τ_1 and τ_2, that is, the probability density function

$$w(\sigma) = u\,\delta(\sigma - \tau_1) + (1-u)\,\delta(\sigma - \tau_2), \tag{4.17}$$

where $0 \leq u \leq 1$ represents the likelihood of the protein being produced through pathway 1 and it can be tuned through a combination of relative plasmid copy numbers, promoter strengths, and ribosome binding strengths. The steady state protein concentration is the real solution of the cubic equation

$$p_*^3 + p_{\rm h}^2 p_* - \frac{\alpha_m \alpha_p p_{\rm h}^2}{\gamma_m \gamma_p} = 0, \tag{4.18}$$

that is, the equilibrium point of (4.16) is the same as that of (4.6) since $\kappa = \alpha_m \alpha_p / \gamma_m$. The steady state mRNA concentration is $m_* = (\gamma_p / \alpha_p) p_*$. Defining the perturbation $x = [\hat{m} - m_*,\ p - p_*]$, we linearize (4.16) around the steady state obtaining the form (2.2) with matrices

$$\mathbf{a} = \begin{bmatrix} -\gamma_m & 0 \\ \alpha_p & -\gamma_p \end{bmatrix}, \qquad \mathbf{b} = \begin{bmatrix} 0 & \frac{-2\kappa\, p_{\rm h}^2\, p_*}{(p_{\rm h}^2 + p_*^2)^2} \\ 0 & 0 \end{bmatrix}. \tag{4.19}$$

Figure 4.5(a–c) show stability plots for different values of the parameter u of the distribution (4.17). The delay dwelling time is assumed to be $t_{\rm d} = 5\,[\rm s]$ and a time step of $\Delta t = 1\,[\rm s]$ is used for the semi-discretization. Figure 4.5(a) and (b) show the second moment stable region (the dark grey shaded area) for $u = 1$ and $u = 0$, respectively. The values $u = 1$ and $u = 0$ correspond to the deterministic systems with delays $\tau = 10$ [s] and $\tau = 20$ [s], respectively. Figure 4.5(c) shows the stable region for the stochastic system with $u = 0.75$.

We mark point Q at $(\gamma_p, \alpha_m) = (0.5, 70)$ in the parameter space, which pertains to instability of system (4.16) for the single delay feedback with $\tau = 10\,[\rm s]$ and $\tau = 20\,[\rm s]$. However, our stability analysis predicts a stable system for $u = 0.75$ where the delay stochastically varies between these two values. Fig. 4.5(d–f) shows the simulations of the nonlinear model (4.16) where the protein concentration is shown as a function of time for

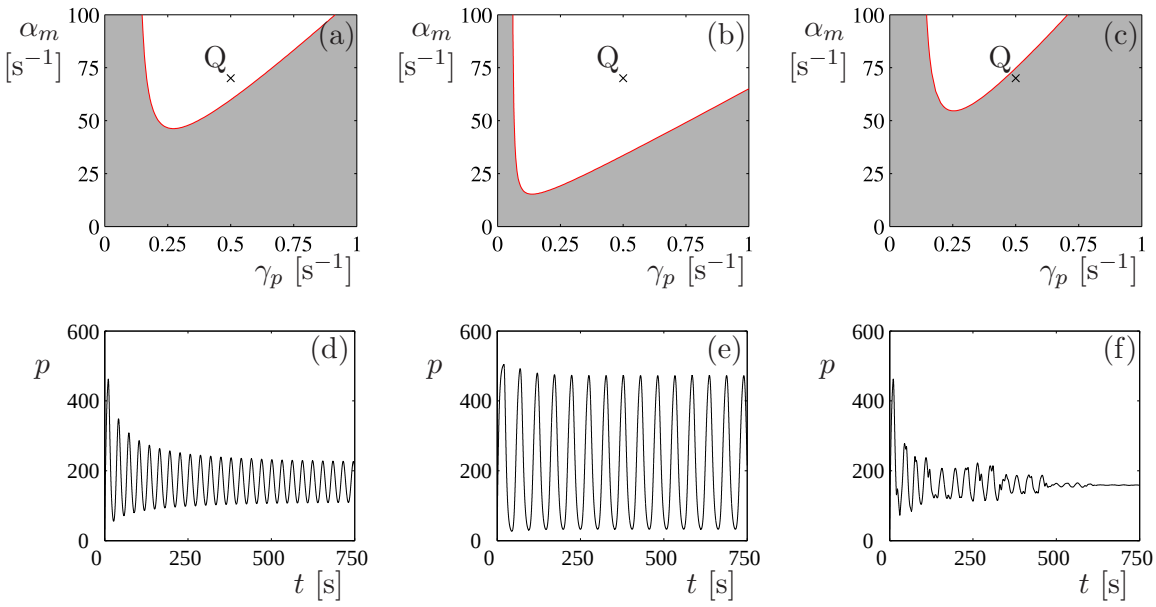

Figure 4.5: Top panels: stability boundaries for the linearized system (2.2,4.19) with $\tau_1 = 10\,[\mathrm{s}]$ and $\tau_2 = 20\,[\mathrm{s}]$ and probability distribution $w_1 = u$, $w_2 = 1 - u$ for (a) $u = 1$, (b) $u = 0$, and (c) $u = 0.75$. Bottom panels: simulation results of the nonlinear model (4.16) for parameter values associated with point Q: $(\gamma_p, \alpha_m) = (0.5, 70)$. A sample trajectory of proteins as a function of time for (d) $u = 1$, (e) $u = 0$, and (f) $u = 0.75$. Note that panels (d) and (e) correspond to the deterministic systems with the single delay $\tau = 10\,[\mathrm{s}]$ and $\tau = 20\,[\mathrm{s}]$, respectively.

the parameter values associated with point Q for dwelling time $t_\mathrm{d} = 5\,[\mathrm{s}]$. We use the semi-discretization to simulate the continuous-time nonlinear system (4.16) with the parameters $\gamma_m = 0.25\,[\frac{1}{\mathrm{s}}]$, $\alpha_p = 1\,[\frac{1}{\mathrm{s}}]$, $p_\mathrm{h} = 100$ proteins per cell, and initial conditions $\hat{m}(\xi) = 1.1 m_*$, $p(\xi) = 0.2 p_*$, for $-\tau_\mathrm{max} \le \xi \le 0$. In panels (d) and (e), the simulations with a single deterministic delay $\tau = 10$ [s] and $\tau = 20$ [s] are shown, respectively. In these cases, the equilibrium point is unstable and we see oscillations in the protein concentration. Panel (f) shows the simulation when the delay varies stochastically between the two values with $u = 0.75$. In this case, the equilibrium becomes stable.

Fig. 4.6(a) shows the spectral radius of matrix $\bar{\bar{\mathbf{A}}}$ as a function of the distribution parameter u. Notice that as u decreases from 1 to 0 the spectral radius initially decreases (that is, the stable regime grows), but then begins to increase again (the stable regime shrinks again). In the parameter regime $0.59 < u < 0.88$ the stochastic system is stable. Fig. 4.6(b) shows the spectral radius of matrix $\bar{\bar{\mathbf{A}}}$ as a function of the dwelling time t_d. It is seen that system (4.16) can be destabilized by increasing the delay dwelling time t_d. This may be explained noting that for large t_d values the system dwells in an unstable system pertaining

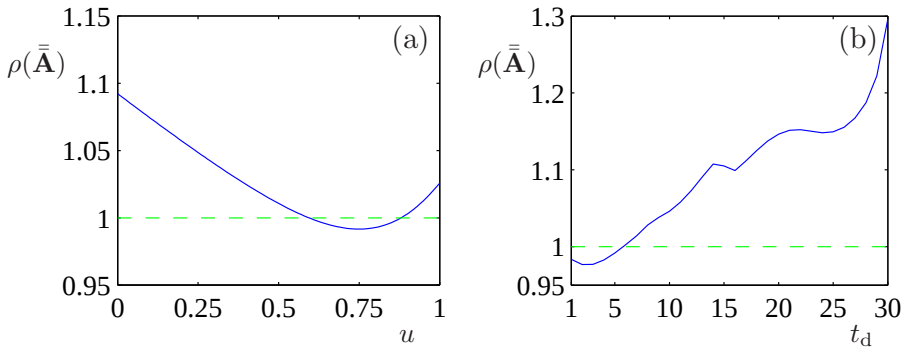

Figure 4.6: (a) The spectral radius of $\bar{\bar{\mathbf{A}}}$ versus the weight u in the probability distribution. (b) The spectral radius of $\bar{\bar{\mathbf{A}}}$ versus the dwelling time t_{d}.

to each delay value. The dynamics are only stabilized by the switching events between the two unstable systems.

4.5 Discussion

The theoretical tools developed in Chapters 2 and 3 were applied to simple auto-regulatory gene networks where stochastic delays appear due to sequential biochemical reactions. We showed that the resultant delay distribution is well approximated by an Erlang distribution. We first investigated an auto-regulatory gene circuit described by a scalar model. We found that increasing the stochasticity in the delay (characterized by the relative variance of the distribution) increased the size of the almost sure stable region indicating that stochasticity in the delay may stabilize unstable equilibria. Our findings were justified using numerical simulations of the linearized and full nonlinear system. We also investigated the auto-regulatory circuit taking into account mRNA dynamics where we included a bimodal delay distribution. We found that even if both the regulatory delays are individually destabilizing, the stochastic combination of these two delays can make the system stable. Furthermore, we found that the longer the dwelling times, the more unstable the network became. The developed tools are anticipated to be useful in analyzing the dynamics of more complicated synthetic and natural gene regulatory networks.

CHAPTER 5

Dynamics of microbial consortia

5.1 Introduction

A major goal of synthetic biology is the construction of genetic circuits that endow cells and organisms with novel functions. Synthetic gene circuits provide the basis for technologies such as gene therapy [86], biofuel and biopharmaceutical production [91], and have a range of environmental applications [53]. In addition, they allow for unprecedented control of biological systems thus opening new avenues in biological research [73]. The majority of currently available synthetic gene circuits have been built within a single strain and operate at the single-cell level. However, to realize the full potential of synthetic biology we need to be able to design consortia of interacting cells and organisms. Cooperating cells can specialize and assume different responsibilities within a consortium [84]. This allows bacterial consortia to be more efficient, and have a wider range of functions than monocultures. In such consortia, the signals within and between bacterial populations shape the response of genetic networks within cells. The activity of the population, in turn, arises from the coordinated activity of individuals [12, 28]. Consortia can thus perform computations and make decisions that are far more sophisticated than those of a single bacterium [67, 41].

To understand the behaviors of naturally occurring microbial consortia and to engineer synthetic consortia for practical applications, it is necessary to develop mathematical and computational models that describe their behavior. Such multi-scale models must simultaneously describe transcriptional dynamics within cells, interactions between cells due to cell-to-cell communication, and population-level dynamics that arise as different cell types compete for limited resources [35, 9]. To further complicate matters, each of these levels of organization is linked to the others. Transcriptional dynamics within single cells are affected by intercellular signaling molecules. The concentrations of signaling molecules, in turn, are determined by gene network activity and total strain density. Strain density is also affected by transcriptional dynamics, as protein production can affect the growth

rate of cells [78, 70, 59]. Therefore, to understand and predict the dynamics of microbial consortia, one must consider the dynamic interplay of multiple levels of organization.

In this chapter, we introduce a class of models describing the dynamics of synthetic microbial consortia in which two strains transcriptionally repress each other. We first introduce a deterministic model to describe the average behavior of cells within each population, their global interactions, and the resulting emergent dynamics. Furthermore, we show how to extend this model to include stochastic effects due to small population size and small molecular counts within each cell. This stochastic model has the deterministic model as its mean field approximation while it is able to capture fluctuations within cells and across strains as well as strain extinctions.

The co-repressive microbial consortium is a generalization of the well-known synthetic toggle switch that operates in a single bacterium [23] (See Fig. 5.1a). In single cells, the co-repressive toggle switch can exhibit transcriptional bistability with two mutually exclusive gene expression states: 1) expression of *tetR* and repression of *lacI*; or 2) expression of *lacI* and repression of *tetR*. The analogous synthetic co-repressive microbial consortium, shown in Fig. 5.1b, might be constructed with two strains using two orthogonal quorum sensing systems (here *cinI/R* and *rhlI/R*) [56, 85], and two transcriptional inverters [77]. When one strain is active, it produces an intercellular signal that transcriptionally represses the opposing strain. Unlike its bistable single strain counterpart, the co-repressive consortium may exhibit more complicated behaviors. In particular, we show that the co-repressive consortium can oscillate if the growth rates of the strains depend on their transcriptional state, which can occur when heterologous protein is produced [78, 70].

While we only consider the dynamics of co-repressive microbial consortia, our modeling approach proposed in this chapter can be extended to any consortia of fixed size when spatial effects are negligible. Both our deterministic and stochastic models can be easily modified to describe different gene circuits and cell-to-cell interactions. We thus provide a general framework for modeling and analyzing the interplay between population and gene circuit dynamics that drives the behavior of microbial consortia.

5.2 Dynamics of a two-strain co-repressive consortium

We first consider the deterministic dynamics of a two-strain consortium growing in a small, well-mixed turbidostat, such as a microfluidic trap [8]. Since such traps have fixed volume, we assume that the total population size and cellular volume of the consortium remain constant. To maintain a fixed population size whenever a cell divides, we assume that a randomly chosen cell from the consortium exits the chamber. For simplicity, we assume

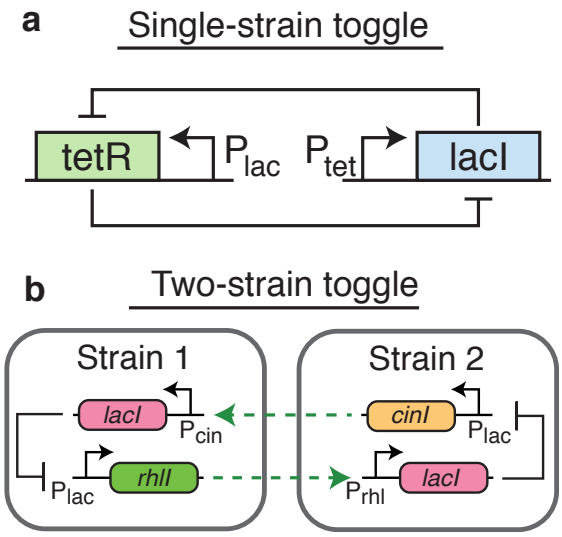

Figure 5.1: Single- and two-strain toggle switch. **a** Gene circuit diagram of a single cell co-repressive toggle switch [23]. **b** Proposed synthetic microbial consortium with a co-repressive network. Each strain contains a transcriptional inverter (mediated by LacI) and an enzyme that creates a quorum sensing molecule. Repression occurs when the quorum sensing molecule from one strain diffuses into the other strain, up-regulating the target transcriptional inverter (green dashed arrows). That inverter down-regulates production of the second, orthogonal quorum sensing molecule.

that all cells in the consortium have equal size. The fraction of strain 1 within the chamber is then defined by the ratio $r = V_1/V = n_1/N$ where V_1 is the volume occupied by strain 1, V is the total volume, n_1 is the number of cells in strain 1, and N is the total number of cells. Note that the ratio r is treated as a real number that can vary between 0 and 1. Moreover, denoting the volume occupied by strain 2 by V_2 and the number of cells in strain 2 by n_2, we have $V_1 + V_2 = V$ and $n_1 + n_2 = N$. Therefore, the fraction of strain 2 in the chamber is given by $1 - r = V_2/V = n_2/N$.

We model the dynamics of a single gene within each strain. We assume that the production of an enzyme that creates a signaling molecule is repressed by the presence of the signaling molecule produced by the other strain. Further, the concentration of a signaling molecule is assumed to be spatially homogeneous and directly proportional to the total concentration of its enzyme within the culture (*i.e.*, the product of the average intracellular concentration of the enzyme and the number of cells containing it). Therefore the time evolution of the average concentrations x_1 and x_2 of the corresponding enzymes can be

described by

$$\begin{aligned} \dot{x}_1 &= \alpha f_1(x_2, r) - \beta_1 x_1, \\ \dot{x}_2 &= \alpha f_2(x_1, r) - \beta_2 x_2, \end{aligned} \tag{5.1}$$

where

$$f_1(x_2, r) = \frac{1}{1 + \big((1-r)Nx_2/\theta\big)^n}, \quad f_2(x_1, r) = \frac{1}{1 + \big(rNx_1/\theta\big)^n}. \tag{5.2}$$

Here α is the maximal production rate of the proteins, β_1 and β_2 are the growth rates of strains 1 and 2, respectively, θ is a scaling parameter that determines half-maximal repression, and n is the Hill coefficient. The proteins are assumed to be stable and decrease in concentration only through cellular growth and division at a rate proportional to the growth rates. It is assumed that the volume is measured in units of single cells so that the total cellular volume is $V = N$. Moreover, we assume that there is a linear relation between the expression of the signaling molecule and protein within a single cell. Therefore protein production in strain 2 is repressed in proportion to the total protein signal $V_1 x_1 = rVx_1 = rNx_1$ from strain 1. Similarly, the protein production in strain 1 is repressed by the total protein signal $(1-r)Nx_2$ from strain 2. Note that this approximation for the amount of signaling molecule assumes that: 1) the transient dynamics of the signaling molecule are fast with respect to changes in the corresponding protein concentration x_i, and 2) the quasi-equilibrium concentration of the signaling molecule is linearly proportional to the amount of enzyme making it. The first approximation is generally valid provided that the growth chamber is small enough and that diffusion across cell walls is fast. The second approximation is valid provided that the presence of the signaling molecule does affect the enzyme's ability to make it.

Next, we describe a deterministic model of the dynamics of the population ratio r assuming that the number of cells within each strain can be described by a birth–death process. A new cell is born at cell division, while a "death" occurs when a cell is removed from the chamber. Recall that n_1 and n_2 are the number of cells in strains 1 and 2, respectively, so that $n_1 + n_2 = N$ is constant. Left on their own, the two strains would grow exponentially with rates $\beta_1 n_1$ and $\beta_2 n_2$, respectively. To keep the total population size constant, we set the total rate at which cells are removed from the population to $\beta_1 n_1 + \beta_2 n_2$. If all cells are equally likely to be removed, the probability that a cell is removed from strain i is n_i/N, giving a death rate of $(\beta_1 n_1 + \beta_2 n_2)\frac{n_i}{N}$. The deterministic birth-death process of the strain 1 can then be described by the differential equation

$$\dot{n}_1 = \beta_1 n_1 - (\beta_1 n_1 + \beta_2 n_2)\frac{n_1}{N}. \tag{5.3}$$

Substituting $n_1 = rN$ and $n_2 = (1-r)N$ into (5.3), we obtain the logistic equation

$$\dot{r} = (\beta_1 - \beta_2) r(1-r), \tag{5.4}$$

for the ratio r of the strain 1 in the chamber.

5.2.1 Bistability in the absence of metabolic loading

There are many reasons why protein production might influence the growth rate of a cell. For instance, heterologous protein expression may slow growth due to metabolic loading [78, 70], or transcription of a suicide gene may be linked to one of the two states [88, 5]. For simplicity, we will refer to these phenomena collectively as "metabolic loading" – a burden imposed by the production of heterologous protein.

In the absence of metabolic loading, the growth rates of the two strains are not affected by the production of the enzymes and hence will remain constant. If the two strains grow at the same rate $\beta_1 = \beta_2$, Eq. (5.4) implies that the ratio r will remain fixed at its initial value. Then we can treat r as a parameter in system (5.1) and the equilibria $x_1(t) = x_1^*$ and $x_2(t) = x_2^*$ are given by

$$\begin{aligned} \beta_1 x_1^* &= \alpha f_1(x_2^*, r), \\ \beta_2 x_2^* &= \alpha f_2(x_1^*, r). \end{aligned} \tag{5.5}$$

Indeed, the equilibria are the solutions of $x_1^* = h_1(h_2(x_1^*))$, where $h_i = \alpha f_i/\beta_i$. Since h_1 and h_2 are monotonically decreasing sigmoidal functions, $h_1 \circ h_2$ is a monotonically increasing sigmoidal function and it intersects the diagonal in 1, 2, or 3 points which correspond to the equilibria.

Fig. 5.2a shows a typical example of how x_1^* changes with the ratio r. If the ratio r is high or low, there exists a unique equilibrium (solid line) and one of the strains dominates the trap; the dominant strain will be expressed and the opposite strain repressed. For mid values of r, the system is bistable with two stable equilibria (solid lines) and an unstable equilibrium in the middle (dashed line). This region of bistability is bounded by bifurcations at which two of the equilibria disappear in a saddle-node collision. That is, the consortium behaves like a toggle switch for a range of strain ratios. Unlike switches that operate on the level of single cells, bistability in the present case depends on the ratio of the strains in the trap.

Fig. 5.2b shows simulations of system (5.1) with equal growth rates $\beta_1 = \beta_2$ for two different sets of initial conditions where the ratio r is chosen from the bistable domain. If

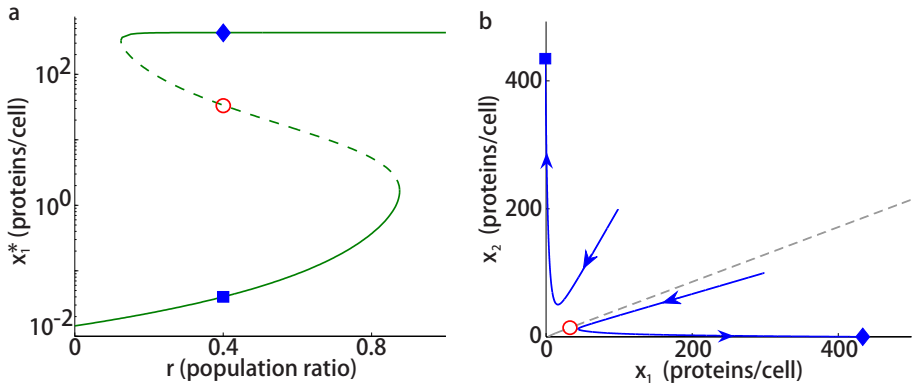

Figure 5.2: Two-strain population toggle with equal growth rates. **a** The equilibrium x_1^* as a function of population ratio r. The dashed and solid lines correspond to unstable and stable equilibria, respectively. **b** Two trajectories of Eq. (5.1) approaching one of the two stable equilibria marked by ♦ and ■ based on the initial conditions. The third, unstable equilibrium is denoted by ○. The gray dashed line shows the separatrix between the two basins of attraction of the stable equilibria. The parameters are chosen as $\beta_1 = \beta_2 = 0.023\,[\text{min}^{-1}]$ corresponding to *E. coli*'s cell cycle of approximately 30 minutes, $\alpha = 10\,[\text{min}^{-1}]$, $\theta = 500$, $N = 200$, and $n = 2$. The simulations are carried out for constant population ratio $r = 0.4$ and initial conditions $\big(x_1(0), x_2(0)\big) = (100, 200)$ proteins per cell and $\big(x_1(0), x_2(0)\big) = (300, 100)$ proteins per cell.

the initial conditions fall below the gray dashed separatrix (given by the stable manifold of the unstable equilibrium denoted by ○), the system approaches the equilibrium denoted by ♦. The simulations starting above the separatrix approach the other stable equilibrium denoted by ■. Note that the slope of the separatrix is equal to 1 for ratio $r = 0.5$, and decreases with decreasing r.

When the difference $\beta_1 - \beta_2$ between the growth rates of the two strains is small, r changes slowly according to Eq. (5.4). Let us assume that

$$\begin{aligned} \beta_1 &= \beta_0(1+\epsilon), \\ \beta_2 &= \beta_0, \end{aligned} \tag{5.6}$$

where ϵ reflects the relative difference between the growth rates of the two strains. We only consider $\epsilon \geq 0$, since if $\epsilon < 0$ the roles of strains 1 and 2 can be reversed. When ϵ is small, (5.1), (5.2), and (5.4) form a slow-fast system. Thus, the concentrations x_1 and x_2 track a stable equilibrium until it disappears in a saddle-node bifurcation [31] (see Fig. 5.2a). Once an equilibrium disappears, the system jumps to the other stable equilibrium, and a switch in expression levels occurs. For example, as shown in Fig. 5.3b,c, when $\epsilon > 0$ and r

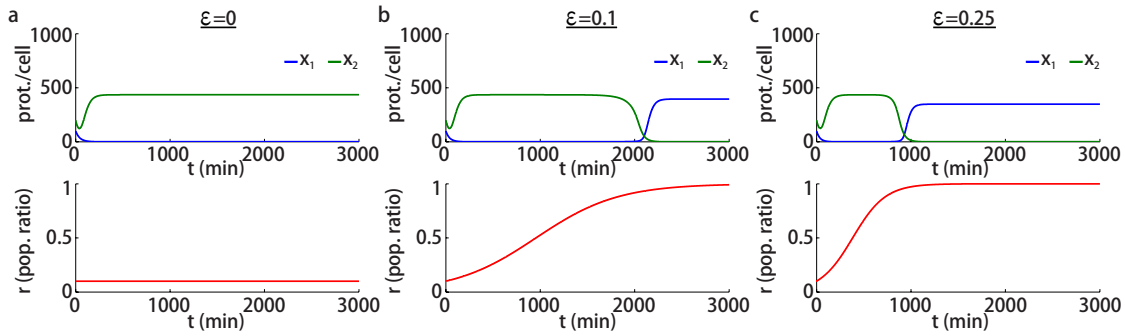

Figure 5.3: Two-strain population toggle with different growth rates. Simulations of system (5.1),(5.2),(5.4),(5.6) with $\beta_0 = 0.023\,[\text{min}^{-1}]$ and different ϵ values as indicated. Other parameters are the same as in Fig. 5.2. Initial protein concentrations are $\big(x_1(0), x_2(0)\big) = (100, 200)$ proteins per cell and initial population ratio is $r(0) = 0.1$.

is initially close to 0, the concentration x_1 initially approaches the lower equilibrium value (repressed state) and stays close to it as r increases slowly due to the larger growth rate of the first population. After the ratio r passes through the critical value at which the lower equilibrium disappears, x_1 switches to the higher equilibrium (expressed state). Fig. 5.3b,c show such transitions for small and intermediate differences in growth rates. Notice that the transition occurs earlier in time as ϵ increases. On the other hand, when the growth rates are equal, no transition occurs as the ratio r remains constant; see Fig. 5.3a. While the dynamics for different values of $\epsilon > 0$ are similar, the slow-fast approach is valid only when ϵ is small.

When the two strains have identical growth rates, the two-strain microbial consortium behaves like a single-strain toggle switch: gene expression in the two strains is bistable for a range of population ratios r. However, if one strain has a larger growth rate, the opposite strain eventually disappears from the trap. Even before it is driven to extinction, the less numerous strain becomes fully repressed.

5.2.2 Impact of metabolic loading on population toggle dynamics

We next investigate the dynamics of the co-repressive consortium in the presence of metabolic loading, *i.e.*, when the growth rates of the two strains depend on their transcriptional states. If a balance of population sizes is necessary to maintain a particular behavior then any change in the growth rates can affect the dynamics of the consortium. To imagine how metabolic loading in the two-strain toggle consortium can lead to relaxation oscillations, assume that the cells with higher expression rate experience an increased metabolic burden, and thus grow slower. This, in turn, allows cells in the repressed state to increase their rel-

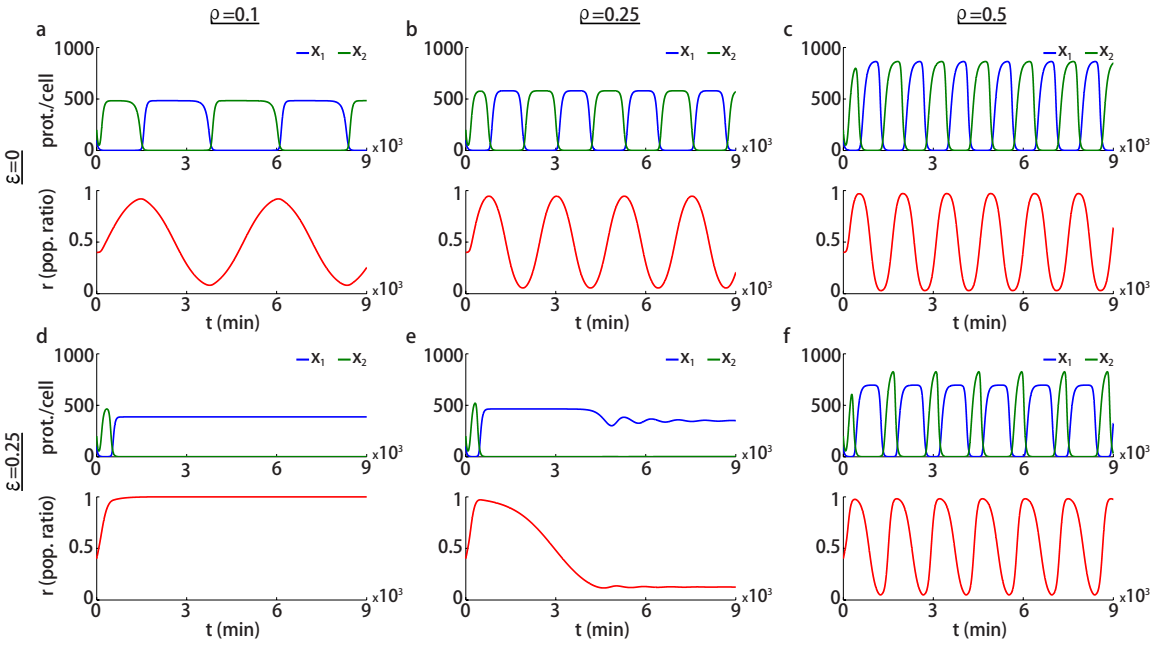

Figure 5.4: Metabolic loading leading to relaxation oscillations. Simulations of system (5.1),(5.2),(5.4),(5.7) for different values of ϵ and ρ as indicated. Parameters are $\beta_0 = 0.023\,[\text{min}^{-1}]$, $\alpha = 10\,[\text{min}^{-1}]$, $\theta = 500$, $N = 200$, and $n = 2$. Initial conditions are $\big(x_1(0), x_2(0)\big) = (100, 200)$ proteins per cell and $r(0) = 0.4$.

ative population size. Once these cells dominate the trap, they are no longer repressed. As they reach high expression levels, they experience higher metabolic load and the process repeats.

To demonstrate such relaxation oscillations in the co-repressive consortium, we assume that the growth rates of both strains depend on the rate of expression of each gene, f_1 and f_2 defined in Eq. (5.2). In particular Eq. (5.6) is replaced by

$$\begin{aligned} \beta_1 &= \beta_0(1+\epsilon)\big(1-\rho f_1(x_2, r)\big), \\ \beta_2 &= \beta_0\big(1-\rho f_2(x_1, r)\big), \end{aligned} \tag{5.7}$$

where the parameter $0 < \rho < 1$ determines the impact of the metabolic load on the growth rates, such that $\rho \approx 0$ corresponds to a low and $\rho \approx 1$ corresponds to a high impact. The growth rate of a strain is therefore largest when gene expression is at its minimum. Here the parameter ϵ determines the difference between the maximal growth rates of the two strains.

Fig. 5.4 shows solutions of system (5.1),(5.2),(5.4),(5.7) for different values of the parameters ϵ and ρ. When $\epsilon = 0$, the system exhibits oscillations for all values of $\rho > 0$, see Fig. 5.4a–c (recall that for the case $\rho = 0$, we have the bistable system shown in Fig. 5.2a). The frequency and amplitude of these oscillations increase with the impact of the metabolic

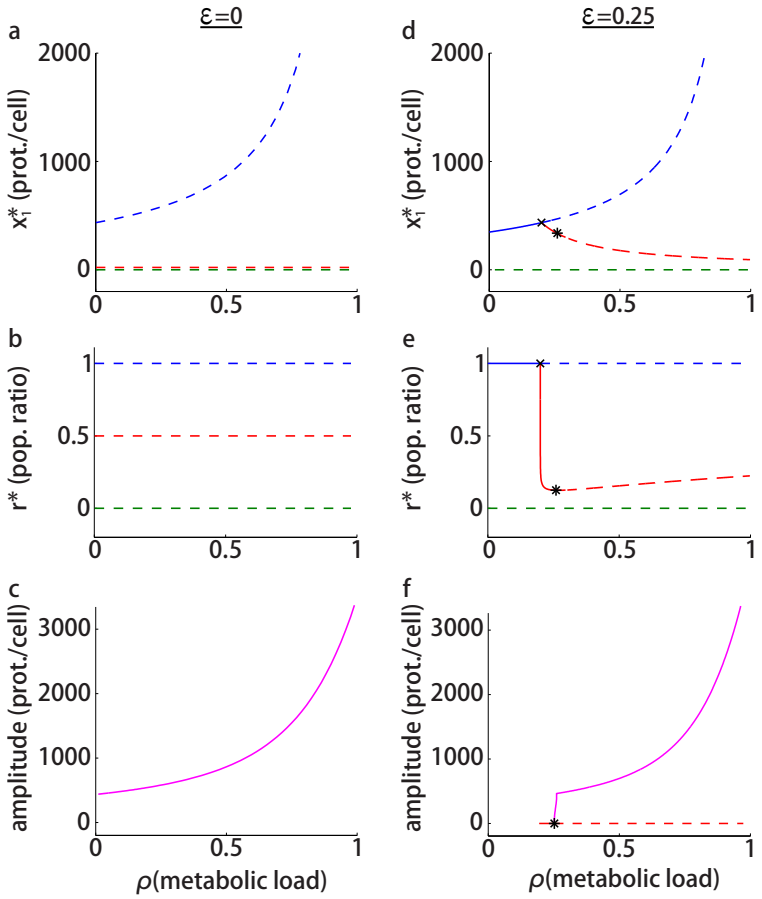

Figure 5.5: Bifurcation diagrams for the two-strain toggle under metabolic load. In panels **a,b,d,e**, solid and dashed lines denote stable and unstable equilibria, respectively. In panels **d,e,f**, the markers $\times$ and $*$ indicate transcritical and Hopf bifurcations, respectively. The solid magenta line in panels **c,f** shows the amplitude of the periodic solution. In panel **f** the periodic solution emerges from a Hopf bifurcation. Parameters are the same as in Fig. 5.4.

loading ρ. Fig. 5.5a–c show the bifurcation diagrams while using ρ as the bifurcation parameter for the case $\epsilon = 0$. In Fig. 5.5a, three unstable equilibria are shown as a function of ρ. Fig. 5.5b shows the value of the population ratio r for these unstable equilibria. Fig. 5.5c shows the amplitude of the oscillations as a function of ρ.

Fig. 5.4d–f shows numerical simulations of (5.1),(5.2),(5.4),(5.7) for different ρ values where $\epsilon = 0.25$ is kept fixed. We observe that when $\epsilon > 0$, oscillations occur only when metabolic loading is sufficiently large. The bifurcation diagrams for the case $\epsilon = 0.25$ are shown in Fig. 5.5d–f. When ρ is close to zero the equilibrium $r^* = 1$ is stable. An increased metabolic load, ρ, leads to the appearance of a stable equilibrium for which $0 < r^* < 1$ (the red curve that emerges via a transcritical bifurcation indicated by $\times$ in Fig. 5.5d,e). This equilibrium is stable over a small range of the parameter ρ, then undergoes a supercritical

Hopf bifurcation (marked by $*$) leading to stable oscillations. Note that if we continued the equilibrium shown by the red branch to lower ρ values, the corresponding population ratio r^* would be larger than 1 and physically not meaningful. Therefore, this branch section is not shown here. The amplitude of the periodic orbit is shown in Fig. 5.5f where the middle equilibrium (red branch) is included with zero amplitude. The amplitude of the oscillations arising from the Hopf bifurcation grows explosively over a small parameter range after the bifurcation. We conjecture that this is due to a *canard explosion* [43].

5.3 Small population effects

In smaller traps, or confined geometries, the number of cells may be sufficiently small for stochastic fluctuations in population size and gene expression to become appreciable. We therefore describe a stochastic model of the dynamics of intracellular proteins, as well as the birth and removal of cells in the two strains. We work under the same assumptions as in the previous section: the number of cells, $n_1 + n_2 = N$, in the trap is fixed, and is maintained by following each birth by a removal of a randomly chosen cell. We again neglect spatial effects.

We model protein dynamics separately in each cell. Let $x_{i,j}$ be the number of proteins in cell j of strain i, so that $i \in \{1, 2\}$, and $j \in \{1, 2, \cdots, n_i\}$. We therefore have a set of N birth processes modeling protein production

$$\begin{array}{llll} \emptyset & \xrightarrow{\alpha f_1} & x_{1,1}, & \emptyset \xrightarrow{\alpha f_2} x_{2,1}, \\ \emptyset & \xrightarrow{\alpha f_1} & x_{1,2}, & \emptyset \xrightarrow{\alpha f_2} x_{2,2}, \\ & \vdots & & \vdots \\ \emptyset & \xrightarrow{\alpha f_1} & x_{1,n_1}, & \emptyset \xrightarrow{\alpha f_2} x_{2,n_2}. \end{array} \tag{5.8}$$

The rate of protein production in each cell in strain i is αf_i, where

$$f_1 = \frac{1}{1 + \left(\frac{x_{2,1}+x_{2,2}+\cdots+x_{2,n_2}}{\theta}\right)^n}, \quad \text{and} \quad f_2 = \frac{1}{1 + \left(\frac{x_{1,1}+x_{1,2}+\cdots+x_{1,n_1}}{\theta}\right)^n}, \tag{5.9}$$

cf. (5.2). Note that we do not model protein degradation explicitly, as we assume that proteins are relatively stable. Approximately fixed concentrations are maintained by dilution through division, as explained further below.

We separately model the division (birth) and removal (death) of cells from the trap. The rates of these processes are as described in the derivation of (5.3). The number of cells n_1

and n_2 in each strain is governed by the coupled birth and death processes

$$\begin{aligned}
&\emptyset \xrightarrow{\beta_1 n_1} \text{One cell in strain 1 divides and } \begin{cases} \text{a cell from strain 1 is removed with probability } n_1/N, \\ \text{a cell from strain 2 is removed with probability } n_2/N, \end{cases} \\
&\emptyset \xrightarrow{\beta_2 n_2} \text{One cell in strain 2 divides and } \begin{cases} \text{a cell from strain 1 is removed with probability } n_1/N, \\ \text{a cell from strain 2 is removed with probability } n_2/N. \end{cases}
\end{aligned} \tag{5.10}$$

The two population sizes therefore follow Moran dynamics [57, 61]: whenever a cell divides, another randomly chosen cell is removed.

We use Gillespie algorithm to sample trajectories of the system described by (5.8),(5.10). At each step of the Gillespie algorithm, the possible events and their probabilities are given by these two equations. There are $N + 2$ possible events that can occur in each step of the algorithm: a birth (division) in either strain, accompanied by the removal of a random cell, and a birth (formation) of a protein in one of the N cells. The rate at which a division occurs in strain i is given by $\beta_i n_i$ where β_i were given by (5.7), *i.e.*

$$\begin{aligned}
\beta_1 &= \beta_0(1+\epsilon)(1-\rho f_1), \\
\beta_2 &= \beta_0(1-\rho f_2),
\end{aligned} \tag{5.11}$$

where the protein production rates, f_1 and f_2, are defined in (5.9).

When a cell divides, its cellular material, including all proteins, is divided between the two daughter cells. Let the index pair (i, j) correspond to cell j in strain i, so that $i \in \{1, 2\}$ and $j \in \{1, 2, \ldots, n_i\}$. If an event corresponds to division in strain 1, we pick a random cell in that strain with index $(1, b)$, to be divided into two. If the cell to be removed comes from the same strain, say it has index $(1, d)$, we replace cell $(1, d)$ with a new cell, and divide the proteins from cell $(1, b)$ into two groups by sampling from a binomial distribution. One of the two groups is assigned to cell $(1, b)$, while the other is transferred to the new cell with index $(1, d)$. In this case, the cell counts n_1 and n_2 remain constant. If one of the cells in the strain 2 is chosen to be removed, say cell $(2, d)$, we add an additional cell with index $(1, n_1 + 1)$ to strain 1. We again partition the proteins from the dividing cell $(1, b)$ between the mother and daughter cell. We then remove the cell $(2, d)$ from strain 2 and renumber the remaining cells in strain 2 to close the resulting gap, that is, $x_{2,j} \to x_{2,j+1}$, for $j = d, d + 1, \ldots, n_2$. In this second case, n_1 increases by 1 and n_2 decreases by 1. The algorithm is equivalent if a cell divides in strain 2. Also, a modeling assumption in this algorithm is that the birth and removal of cells happen concurrently, not allowing for the cell that is just born to be removed.

Next we explore stochastic dynamics of the two-strain consortium.

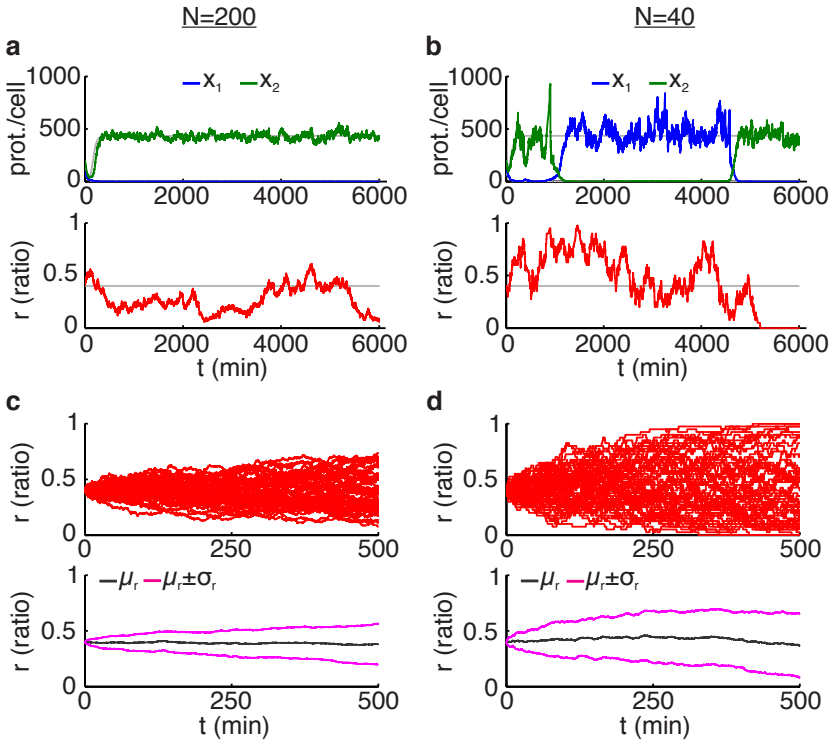

Figure 5.6: Stochasticity in the dynamics of the two-strain toggle consortium. **a,b** Simulations of system (5.8)-(5.11) with no metabolic loading ($\rho = 0$) and equal growth rates ($\epsilon = 0$) for different population sizes as indicated. The blue and green curves show the mean number of proteins in strains 1 and 2, respectively. The red curve shows the population ratio. Simulations of the deterministic system (5.1),(5.2),(5.4) are also shown using gray curves. Parameters are the same as in Fig. 5.4. Initial protein counts are $x_{1,i}(0) = 100$, $i = 1, \ldots, n_1$, $x_{2,j}(0) = 200$, $j = 1, \ldots, n_2$, and initial ratio of strain 1 is $r(0) = 0.4$. **c,d** Stochastic simulations of the population ratio r corresponding to the parameters in panels **a,b**, respectively. The mean of the simulations (μ_r) and the mean plus and minus the standard deviation ($\mu_r \pm \sigma_r$) are also shown as functions of time.

5.3.1 Stochastic dynamics in the absence of metabolic loading

With no metabolic loading, *i.e.* when $\rho = 0$, the growth rates of the two strains are constant. The slower growing strain is more likely to disappear from the trap. However, even if the two growth rates are equal, random fluctuations eventually lead to the extinction of one strain.

When the two strains of bacteria have equal growth rates, the probability of a strain dominating the whole population is equal to the initial proportion of that strain in the trap [61]. For example, the probability that the strain 1 will take over is $n_1(0)/N$. Fig. 5.6 shows simulations of the stochastic model (5.8)-(5.11) with $\rho = 0$ and when the two strains have equal growth rates, *i.e.* $\epsilon = 0$, for different population sizes N. In Fig. 5.6a,b, the blue and

green curves show the mean number of proteins in strains 1 and 2, respectively. The gray curves represent the solutions of corresponding deterministic system (5.1),(5.2),(5.4) with the same parameters. When the population size is smaller the effects of random fluctuations are more pronounced. This can be observed when comparing Fig. 5.6a and Fig. 5.6b. In Fig. 5.6a, where the total cell number N is larger, the protein concentrations x_1 and x_2 follow the deterministic model (shown by the gray curves) fairly close so that x_1 approaches the repressed state and x_2 approaches the expressed state. The ratio r oscillates around the initial value of $r = 0.4$. In Fig. 5.6b, initially the genes in strain 2 are expressed while the genes in strain 1 are repressed. However, as the total cell population is smaller, the fluctuations in the population ratio r are larger and the likelihood of a switch taking place in the gene expression states is bigger. Therefore, we observe more switches between the gene expression states. This behavior cannot be predicted by the deterministic model. In larger cell populations, the fluctuations in the population ratio are not strong enough and a switch in the gene expression states is less likely to occur. Furthermore, in a stochastic model random fluctuations always drive one population to extinction. However, in the deterministic model when growth rates are equal, no extinctions occur as the ratio remains constant.

Fig. 5.6c,d show the time evolution of the population ratio r obtained by running 50 simulations of the stochastic model (5.8)-(5.11). For $N = 200$, the variability in the population ratio is observed to be smaller than that for $N = 40$. In the bottom plots in Fig. 5.6c,d, the mean of the population ratio (μ_r) is shown by a black curve and the mean plus and minus the standard deviation ($\mu_r \pm \sigma_r$) is shown by a magenta curve. When the total population size is smaller (panel d), the variance of population ratio grows faster with time.

When the two strains have different growth rates, the likelihood that the strain with a lower growth rate goes extinct increases. Fig. 5.7 shows the simulations of the stochastic model (5.8)-(5.11) for cases $\epsilon = 0.1$ and $\epsilon = 0.25$ each with population sizes $N = 200$ and $N = 40$. Simulations of the corresponding deterministic model (5.1),(5.2),(5.4),(5.6) with the same parameters are also shown as gray curves. As predicted by the deterministic model, starting from 0.1, the population ratio r increases and crossing a critical value a switch happens in the gene expression states. However, the time at which this switch occurs depends on the random fluctuations in the population ratio and could be either before or after the time predicted by the deterministic model. It can also be the case that strain 1 goes extinct (r becomes 0) and no switches occur. When ϵ is larger (Fig. 5.7c,d), the switch occurs faster and the stochastic dynamics are closer to those of the deterministic model.

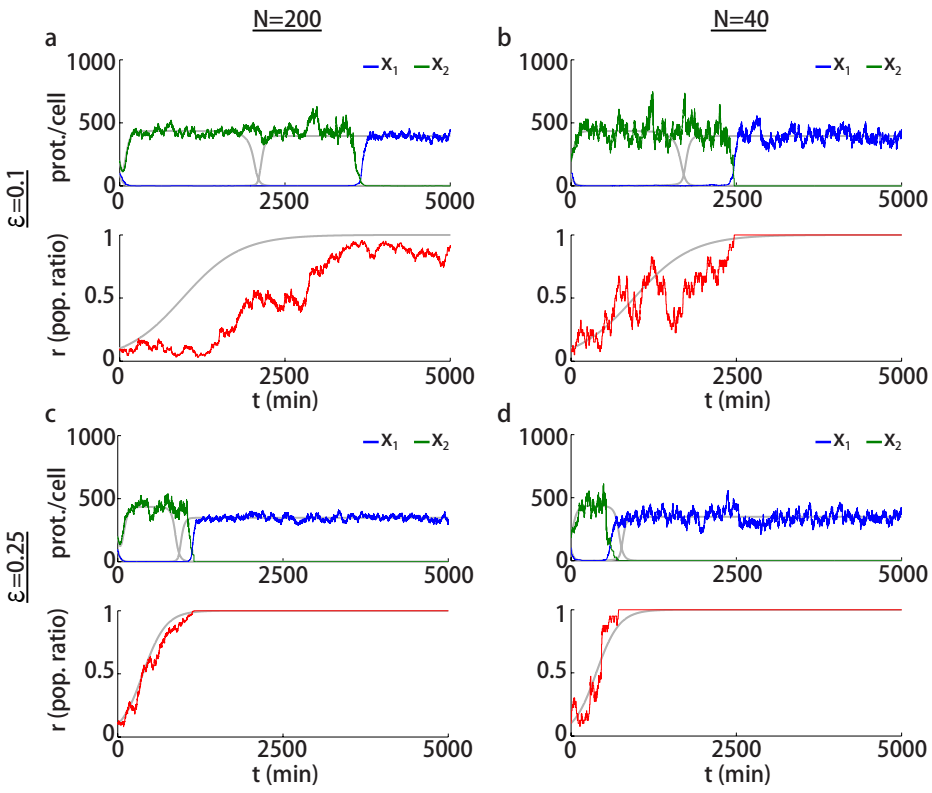

Figure 5.7: Simulations of the stochastic system (5.8)-(5.11) with unequal growth rates of the strains and no metabolic loading ($\rho = 0$) with different ϵ and N values as indicated. The gray curves show the simulations of the corresponding deterministic model (5.1),(5.2),(5.4),(5.6). Parameters are the same as in Fig. 5.4. Initial conditions are $x_{1,i}(0) = 100$ proteins, $i = 1, \ldots, n_1$, $x_{2,j}(0) = 200$ proteins, $j = 1, \ldots, n_2$, and initial ratio of strain 1 is $r(0) = 0.1$.

5.3.2 The impact of metabolic loading on stochastic growth dynamics

We next simulate the stochastic model (5.8)-(5.11) taking into account the effect of metabolic loading on the growth rates of the bacterial strains by setting $0 < \rho < 1$ in (5.11). As Fig. 5.8 shows, oscillations occur when the metabolic load is taken into account. However, when the total population size is small, the likelihood that one of the strains goes extinct increases. Therefore, as shown in Fig. 5.8(b), the oscillations can stop early due to extinction.

Next we ask whether metabolic loading affects the extinction time. Our deterministic analysis showed that metabolic loading increases the frequency of the oscillations in the population ratio r. Therefore, for smaller populations, one expects that the chance of extinction increases as the population ratio gets close to 0 or 1 more frequently. To test this hypothesis numerically, for each of the cases $\rho = 0$ (no metabolic loading), $\rho = 0.5$, and

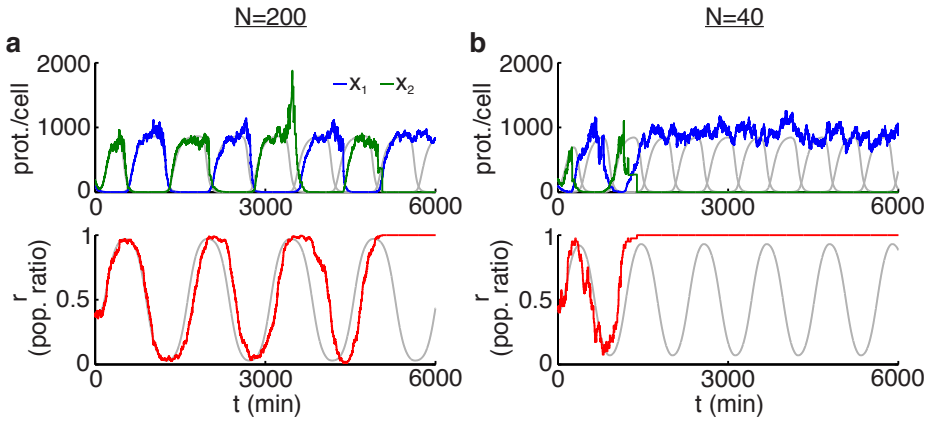

Figure 5.8: Effects of the metabolic load on the stochastic dynamics of the two-strain toggle. Simulations of the stochastic system (5.8)-(5.11) with metabolic loading $\rho = 0.5$ and $\epsilon = 0$ for different populations sizes as indicated. The gray curves show the simulations of the corresponding deterministic model (5.1),(5.2),(5.4),(5.7). Parameters are the same as in Fig. 5.4. Initial conditions are $x_{1,i}(0) = 100$ proteins, $i = 1, \ldots, n_1$, $x_{2,j}(0) = 200$ proteins, $j = 1, \ldots, n_2$, and initial ratio of strain 1 is $r(0) = 0.4$.

$\rho = 0.9$, we run 500 simulations of the stochastic model (5.8)-(5.11). The histograms of the extinction times are shown in Fig. 5.9. Note that the extinction time is determined when either one of the populations goes extinct, *i.e.* the time at which $r = 0$ or $r = 1$. We see that the distribution of the extinction times gets narrower as the metabolic load increases. For higher metabolic loads, the change in the mean and variance of the distribution is more pronounced.

5.4 Discussion

We showed in this chapter that population growth can significantly alter the dynamics of synthetic microbial consortia. Differential growth between the strains which constitute the consortium, whether due to random fluctuations or changes in growth rate due to protein production, can lead to an imbalance in population sizes and alter the strength of signals between cells. Further, when the growth rates of cells are directly affected by protein production, "hidden" feedback loops arise that can change the dynamical landscape of the consortium. For instance, the regulatory structure of the two-strain co-repressive consortium forms a positive feedback loop. Positive feedback loops generally do not permit oscillatory solutions. However, we showed that growth rate changes due to metabolic load can create a "hidden" negative feedback loop that acts on a slow time scale. Therefore, the entire system has a fast positive feedback loop (due to signaling) and a slow negative feedback

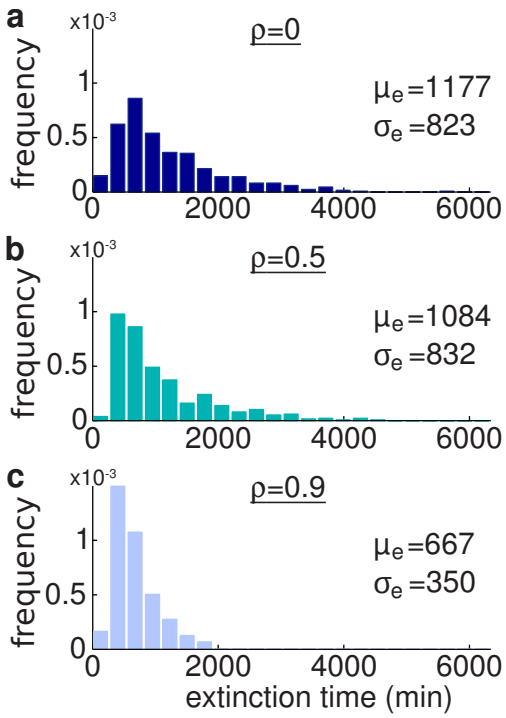

Figure 5.9: Effects of the metabolic load on the extinction times of the two-strain consortium. Normalized histograms of the extinction times for different values of metabolic loading ρ obtained from 500 simulations of the stochastic model (5.8)-(5.11) with $N = 40$ and $\epsilon = 0$. Parameters are the same as in Fig. 5.4. Initial conditions are $x_{1,i}(0) = 100$ proteins, $i = 1, \ldots, n_1$, $x_{2,j}(0) = 200$ proteins, $j = 1, \ldots, n_2$, and initial population ratio is $r(0) = 0.5$.

loop (due to metabolic loading) – the hallmark of relaxation oscillators [79]. A two-strain toggle consortium where the growth rates of the strains are affected by the metabolic load on the cells can therefore exhibit relation oscillations, a behavior that cannot be observed in the single-strain toggle switch. It is also shown that under the circumstances where the strains have an identical growth rate not affected by metabolic loading, the consortium shows bistability similar to the single-strain counterpart.

The perturbations due to the random partitioning of proteins at the time of cell division can have a strong effect on internal cell dynamics [80]. With metabolic loading internal and external fluctuations are even more strongly coupled. Variations in the ratio between the strains can change the expression within each cell. On the other hand, internal fluctuations within cells can affect growth, and thus the ratio between strains. Our model captures this interaction of fluctuations across scales, and can be extended to describe more details of local and global processes, or different dynamical behaviors.

In particular, our analysis could be extended to include spatial effects. Such effects will

be most important for consortia that are not well-mixed or are large enough to limit intercellular signaling. As strains grow and compete for space within the colony, their spatial arrangement within the colony will change in time. Therefore, the regulatory "topology" of such a system will depend on both time and space, significantly complicating resulting dynamics. Any model that accurately recapitulates such a situation must include the internal dynamics of proteins within cells, the spatiotemporal dynamics of intercellular signals, the growth rate dynamics of the strains, and the time-dependent rearrangement of boundaries between cell types.

CHAPTER 6

Conclusion

A stability theory was developed in this dissertation for systems with stochastic delays. Linear continuous-time systems with stochastic delay were considered. The delay was assumed to take values from a finite set of numbers according to some probability distribution function. The stability results were obtained in terms of spectral radii of some operators or matrices governing moment dynamics that can be used to construct stability charts in parameter domains of interest. The main strength of the stability criteria proposed in this dissertation is that they are exact—necessary and sufficient—stability conditions; however, existing stability results in literature, that are obtained from Lyapunov-based theorems, are conservative sufficient conditions. The proposed stability results can be easily implemented in Matlab or other programming software and therefore are easy to use for design purposes. While the main stability results were in terms of the stability of the second moment, almost-sure stability conditions were also discussed. In particular, we showed that from a computational point of view, the second moment stability criteria are more useful than the almost sure stability criteria for linear systems with stochastic delay. By studying generic examples, we showed that the stochasticity in the delay may have significant effects on the stability that might not be captured using approximating deterministic systems.

The stability analysis tools were applied to models of simple gene regulatory networks. The effects of stochasticity in protein production times on the stability of the steady state protein production were characterized. In particular, it was found that the stochasticity in the delay times can improve the stability of the steady state. Moreover, designing a stochastic combination of two distinct regulatory pathways with distinct delays, where each individual pathway alone is oscillatory, can lead to a stable steady state in a self-regulatory gene.

The interactions between intracellular gene expression and population dynamics in multicellular environments were investigated using deterministic and stochastic approaches. We found that in a two-strain microbial consortium, metabolic loading may provide a mechanism to create sustained oscillations in both gene expression and population levels.

APPENDIX A

Mass-action kinetics of auto-regulatory gene

Here, we use mass-action kinetics to provide some details regarding the origin of the parameters such as degradation and production rates that appear in the auto-regulatory network models (4.6) and (4.16). We first take mRNA dynamics into account to derive model (4.16). Then we show how one can simplify (4.16) to (4.6) using quasi steady state approximations. We assume that the proteins produced through transcription and translation form dimers which bind to the promoter site of the gene and repress their own transcription by blocking the RNA polymerase from binding.

The set of reactions we consider are

$$\begin{aligned}
P + P &\underset{k_-}{\overset{k_+}{\rightleftharpoons}} D\,,\\
G + D &\underset{r_-}{\overset{r_+}{\rightleftharpoons}} G_{\mathrm{d}}\,,\\
G &\xrightarrow{\nu} G + M_0\,,\\
M_0 &\xrightarrow{c} M_1\,,\\
&\vdots\\
M_N &\xrightarrow{c} M\,,\\
M &\xrightarrow{\gamma_m} \emptyset\,,\\
M &\xrightarrow{\tilde{\nu}} M + P_0\,,\\
P_0 &\xrightarrow{\tilde{c}} P_1\,,\\
&\vdots\\
P_{\tilde{N}} &\xrightarrow{\tilde{c}} P\,,\\
P &\xrightarrow{\gamma_p} \emptyset\,,
\end{aligned} \tag{A.1}$$

where P represents the number of the fully mature proteins (often called transcription factors), M represents the number of mRNA transcripts, D is the number of dimers, G is the

number of genes without dimers bound to them, and G_{d} is the number of genes with dimers bound. Finally, the symbols M_i, $i = 0, \ldots, N$, and P_i, $i = 0, \ldots, \tilde{N}$ are the numbers of molecules of mRNA and protein in the intermediate stages of synthesis in the transcription and translation processes, respectively. The variables k_+ and k_- are the associative and dissociative rate constants for dimerization, while r_+ and r_- are the reaction rates for binding and unbinding of a dimer to the promoter site. The initiation of the transcription that occurs when an RNA polymerase binds to a gene with an unoccupied promoter site occurs with reaction rate ν. For each reaction in the following sequence the reaction rate is set to c (transcription rate). The initiation of the translation occurs at rate $\tilde{\nu}$ and each reaction in the following sequence happens with rate $\tilde{c}$. The symbols γ_m and γ_p represent the mRNA and protein degradation rates, respectively. We remark that further details may be considered regarding the binding of the RNA polymerase [38] that are omitted here for simplicity.

Using the generalized mass-action kinetics for (A.1), we arrive at the following set of ordinary differential equations

$$\begin{aligned}
\frac{\mathrm{d}d}{\mathrm{d}t} &= k_+ p^2 - k_- d - r_+ g d + r_- g_{\mathrm{d}} , \\
\frac{\mathrm{d}g}{\mathrm{d}t} &= -r_+ g d + r_- g_{\mathrm{d}} , \\
\frac{\mathrm{d}m_0}{\mathrm{d}t} &= \nu g - c m_0 , \\
\frac{\mathrm{d}m_i}{\mathrm{d}t} &= c m_{i-1} - c m_i , \qquad \text{for} \quad i = 1, \ldots, N , \\
\frac{\mathrm{d}m}{\mathrm{d}t} &= -\gamma_m m + c m_N , \\
\frac{\mathrm{d}p_0}{\mathrm{d}t} &= \tilde{\nu} m - \tilde{c} p_0 , \\
\frac{\mathrm{d}p_i}{\mathrm{d}t} &= \tilde{c} p_{i-1} - \tilde{c} p_i , \qquad \text{for} \quad i = 1, \ldots, \tilde{N} , \\
\frac{\mathrm{d}p}{\mathrm{d}t} &= -\gamma_p p + \tilde{c} p_{\tilde{N}} - 2k_+ p^2 + 2k_- d ,
\end{aligned} \tag{A.2}$$

where the lower case letters denote the corresponding concentrations and the plasmid copy number $g + g_{\mathrm{d}}$ is assumed to be constant. Notice that the set of linear equations for m_i, $i = 1, \ldots, N$ and p_i, $i = 1, \ldots, \tilde{N}$ can be solved analytically to obtain $m_N(t)$ and $p_{\tilde{N}}(t)$ as a function of $m_0(t)$ and $p_0(t)$, respectively. In particular, considering zero initial conditions we have

$$m_i(t) = \int_0^t c\, \mathrm{e}^{-c(t-u)} m_{i-1}(u)\, \mathrm{d}u , \tag{A.3}$$

for $i = 1, \ldots, N$. Substituting the solution

$$m_1(t) = \int_0^t c\,\mathrm{e}^{-c(t-u)} m_0(u)\,\mathrm{d}u\,, \tag{A.4}$$

into the formula of $m_2(t)$ gives

$$m_2(t) = \int_0^t c\,\mathrm{e}^{-c(t-v)} m_1(v)\,\mathrm{d}v = \int_0^t \int_0^v c^2\,\mathrm{e}^{-c(t-u)} m_0(u)\,\mathrm{d}u\,\mathrm{d}v = \int_0^t c^2\,\sigma \mathrm{e}^{-c\sigma} m_0(t-\sigma)\,\mathrm{d}\sigma\,, \tag{A.5}$$

where we changed the order of integration and defined the new variable $\sigma = t - u$ to obtain the result. Similarly, we can obtain

$$m_3(t) = \int_0^t \frac{c^3\sigma^2 \mathrm{e}^{-c\sigma}}{2!}\, m_0(t-\sigma)\,\mathrm{d}\sigma. \tag{A.6}$$

Repeating the integration in the same manner we arrive at

$$m_N(t) = \int_0^\infty \frac{c^N \sigma^{N-1} \mathrm{e}^{-c\sigma}}{(N-1)!}\, m_0(t-\sigma)\,\mathrm{d}\sigma = \int_0^\infty w_\mathrm{e}(\sigma)\, m_0(t-\sigma)\,\mathrm{d}\sigma\,, \tag{A.7}$$

where $w_\mathrm{e}(\sigma)$ is the Erlang distribution (4.2) and we extended the integration limit to infinity since we consider $m_0(t) \equiv 0$ for $t \leq 0$. Similarly, for $p_{\tilde{N}}(t)$ we have

$$p_{\tilde{N}}(t) = \int_0^\infty \frac{\tilde{c}^{\tilde{N}} \sigma^{\tilde{N}-1} \mathrm{e}^{-\tilde{c}\sigma}}{(\tilde{N}-1)!}\, p_0(t-\sigma)\,\mathrm{d}\sigma = \int_0^\infty \tilde{w}_\mathrm{e}(\sigma)\, p_0(t-\sigma)\,\mathrm{d}\sigma\,, \tag{A.8}$$

where $\tilde{w}_\mathrm{e}(\sigma)$ is the Erlang distribution with order $\tilde{N}$ and rate $\tilde{c}$. Using (A.7) and (A.8), we can reduce (A.2) to

$$\begin{aligned}
\frac{\mathrm{d}d}{\mathrm{d}t} &= k_+\, p^2 - k_-\, d - r_+\, g\, d + r_-\, g_\mathrm{d}\,, \\
\frac{\mathrm{d}g}{\mathrm{d}t} &= -r_+\, g\, d + r_-\, g_\mathrm{d}\,, \\
\frac{\mathrm{d}m_0}{\mathrm{d}t} &= \nu\, g - c\, m_0\,, \\
\frac{\mathrm{d}m}{\mathrm{d}t} &= \gamma_m\, m + c \int_0^\infty w_\mathrm{e}(\sigma)\, m_0(t-\sigma)\,\mathrm{d}\sigma\,, \\
\frac{\mathrm{d}p_0}{\mathrm{d}t} &= \tilde{\nu}\, m - \tilde{c}\, p_0\,, \\
\frac{\mathrm{d}p}{\mathrm{d}t} &= -\gamma_p\, p + \tilde{c} \int_0^\infty \tilde{w}_\mathrm{e}(\sigma)\, p_0(t-\sigma)\,\mathrm{d}\sigma - 2k_+\, p^2 + 2k_-\, d\,.
\end{aligned} \tag{A.9}$$

This may be further reduced by using quasi-steady state approximations and singular perturbation methods. In particular, assuming that the kinetics of dimerization, promoter binding, transcription initiation, and translation initiation happen on a fast time-scale, the corresponding equations can be assumed to reach equilibrium quickly, allowing us to replace $d(t)$, $g(t)$, $m_0(t)$, and $p_0(t)$ with their respective steady-state values yielding

$$\begin{aligned} \dot{m}(t) &= -\gamma_m\, m(t) + \int_0^\infty w_{\mathrm{e}}(\sigma)\, \frac{\alpha_m}{1+\big(p(t-\sigma)/p_{\mathrm{h}}\big)^2}\, \mathrm{d}\sigma\,, \\ \dot{p}(t) &= -\gamma_p\, p(t) + \int_0^\infty \tilde{w}_{\mathrm{e}}(\sigma)\, \alpha_p\, m(t-\sigma)\, \mathrm{d}\sigma\,, \end{aligned} \tag{A.10}$$

with constants $\alpha_m = \nu(g+g_{\mathrm{d}})$, $p_{\mathrm{h}} = \sqrt{\frac{r_- k_-}{r_+ k_+}}$, and $\alpha_p = \tilde{\nu}$.

Note that equations (A.10) are the mean dynamics of the auto-regulatory network as they are obtained through mass-action kinetics. Thus, we may assume a single delay $\bar{\sigma}$ for the transcription and a single delay $\bar{\bar{\sigma}}$ for the translation to obtain

$$\begin{aligned} \dot{m}(t) &= -\gamma_m\, m(t) + \frac{\alpha_m}{1+\big(p(t-\bar{\sigma})/p_{\mathrm{h}}\big)^2}\,, \\ \dot{p}(t) &= -\gamma_p\, p(t) + \alpha_p\, m(t-\bar{\bar{\sigma}})\,. \end{aligned} \tag{A.11}$$

We can further simplify (A.11) by using the change of variables $\hat{m}(t) = m(t-\bar{\bar{\sigma}})$. This allows us to absorb the two delays into one single delay $\tau = \bar{\sigma} + \bar{\bar{\sigma}}$ and obtain

$$\begin{aligned} \dot{\hat{m}}(t) &= -\gamma_m\, \hat{m}(t) + \frac{\alpha_m}{1+\big(p(t-\tau)/p_{\mathrm{h}}\big)^2}\,, \\ \dot{p}(t) &= -\gamma_p\, p(t) + \alpha_p\, \hat{m}(t), \end{aligned} \tag{A.12}$$

which is the same as (4.16).

Finally assuming that the mRNA dynamics are fast and replacing $\hat{m}(t)$ in the second equation in (A.12) with its steady-state value we arrive at

$$\dot{p}(t) = -\gamma_p\, p(t) + \frac{\kappa}{1+\big(p(t-\tau)/p_{\mathrm{h}}\big)^2}\,, \tag{A.13}$$

where $\kappa = \alpha_m\alpha_p/\gamma_m$ that is the same as (4.6).

We remark that one may also obtain (A.13) by neglecting the mRNA dynamics in (A.1) and following the steps above yielding

$$\dot{p}(t) = -\gamma_p\, p(t) + \int_0^\infty w_{\mathrm{e}}(\sigma)\, \frac{\kappa}{1+\big(p(t-\sigma)/p_{\mathrm{h}}\big)^2}\, \mathrm{d}\sigma \tag{A.14}$$

for the mean protein dynamics.

BIBLIOGRAPHY

[1] R. F. V. ANDERSON, *The relative variance criterion for stability of delay systems*, Journal of Dynamics and Differential Equations, 5 (1993), pp. 105–128.

[2] A. ARKIN, J. ROSS, AND H. H. MCADAMS, *Stochastic kinetic analysis of developmental pathway bifurcation in Phage λ-infected Escherichia coli cells*, Genetics, 149 (1998), pp. 1633–1648.

[3] L. ARNOLD, H. CRAUEL, AND V. WIHSTUTZ, *Stabilization of linear systems by noise*, SIAM Journal on Control and Optimization, 21 (1983), pp. 451–461.

[4] F. BAI AND H. KRISHNAN, *Reliability analysis of DSRC wireless communication for vehicle safety applications*, in Intelligent Transportation Systems Conference (ITSC), IEEE, 2006, pp. 355–362.

[5] F. K. BALAGADDÉ, H. SONG, J. OZAKI, C. H. COLLINS, M. BARNET, F. H. ARNOLD, S. R. QUAKE, AND L. YOU, *A synthetic* Escherichia coli *predator-prey ecosystem*, Molecular Systems Biology, 4 (2008), p. 187.

[6] G. K. BASAK, *Stabilization of dynamical systems by adding a colored noise*, IEEE Transactions on Automatic Control, 46 (2001), pp. 1107–1111.

[7] A. BELLEN AND M. ZENNARO, *Numerical methods for delay differential equations*, Oxford University Press, 2003.

[8] M. R. BENNETT AND J. HASTY, *Microfluidic devices for measuring gene network dynamics in single cells*, Nature Review Genetics, 10 (2009), pp. 628–638.

[9] A. E. BLANCHARD, C. LIAO, AND T. LU, *An ecological understanding of quorum sensing-controlled bacteriocin synthesis*, Cellular and Molecular Bioengineering, 9 (2016), pp. 443–454.

[10] D. BREDA, *Solution operator approximations for characteristic roots of delay differential equations*, Applied Numerical Mathematics, 56 (2006), pp. 305–317.

[11] D. BREDA, S. MASET, AND R. VERMIGLIO, *Stability of linear delay differential equations – a numerical approach with MATLAB*, Springer-Verlag New York, 2015.

[12] Y. CHEN, J. K. KIM, A. J. HIRNING, K. JOSIĆ, AND M. R. BENNETT, *Emergent genetic oscillations in a synthetic microbial consortium.*, Science, 349 (2015), pp. 986–989.

[13] O.L.V. COSTA, M.D. FRAGOSO, AND R.P. MARQUES, *Discrete-time Markov jump linear systems*, Springer, 2006.

[14] X. DAI, Y. HUANG, AND M. XIAO, *Almost sure stability of discrete-time switched linear systems: a topological point of view*, SIAM Journal on Control and Optimization, 47 (2008), pp. 2137–2156.

[15] D. DEL VECCHIO AND R. M. MURRAY, *Biomolecular Feedback Systems*, Princeton University Press, 2014.

[16] O. DIEKMANN, S. A. VAN GILS, S. M. VERDUYN LUNEL, AND H. O. WALTHER, *Delay Equations: Functional-, Complex-, and Nonlinear Analysis*, vol. 110 of Applied Mathematical Sciences, Springer, 1995.

[17] K. ENGELBORGHS, T. LUZYANINA, AND D. ROOSE, *Numerical bifurcation analysis of delay differential equations using DDE-BIFTOOL*, ACM Transactions on Mathematical Software, 28 (2002), pp. 1–21.

[18] K. ENGELBORGHS AND D. ROOSE, *On stability of LMS methods and characteristic roots of delay differential equations*, SIAM Journal on Numerical Analysis, 40 (2002), pp. 629–650.

[19] T. ERNEUX, *Applied Delay Differential Equations*, vol. 3 of Surveys and Tutorials in the Applied Mathematical Sciences, Springer, 2009.

[20] M. FARKAS AND G. STÉPÁN, *On perturbation of the kernel in infinite delay systems*, Zeitschrift fur Angewandte Mathematik und Mechanik, 72 (1992), pp. 153–156.

[21] R. M. FELDMAN AND C. V. FLORES, *Applied Probability and Stochastic Processes*, Springer, 2010.

[22] H. GAO AND T. CHEN, *New results on stability of discrete-time systems with time-varying state delay*, IEEE Transactions on Automatic Control, 52 (2007), pp. 328–334.

[23] T. S. GARDNER, C. R. CANTOR, AND J. J. COLLINS, *Construction of a genetic toggle switch in* Escherichia Coli, Nature, 403 (2000), pp. 339–342.

[24] M. GHASEMI, S. ZHAO, T. INSPERGER, AND T. KALMÁR-NAGY, *Act-and-wait control of discrete systems with random delays*, in American Control Conference (ACC), 2012, pp. 5440–5443.

[25] D. T. GILLESPIE, *Exact stochastic simulation of coupled chemical reactions*, Journal of Physical Chemistry, 81 (1977), pp. 2340–2361.

[26] M. M. GOMEZ, W. B. QIN, G. OROSZ, AND R. M. MURRAY, *Exact stability analysis of discrete-time linear systems with stochastic delays*, in American Control Conference (ACC), 2014, pp. 5534–5539.

[27] M. M. GOMEZ, M. SADEGHPOUR, M. R. BENNETT, G. OROSZ, AND R. M. MURRAY, *Stability of systems with stochastic delays and applications to genetic regulatory networks*, SIAM Journal on Applied Dynamical Systems, 15 (2016), pp. 1844–1873.

[28] C. GONZÁLEZ, J. C. RAY, M. MANHART, R. M. ADAMS, D. NEVOZHAY, A. V. MOROZOV, AND G. BALÁZSI, *Stress-response balance drives the evolution of a network module and its host genome*, Molecular Systems Biology, 11 (2015), p. 827.

[29] C. GUPTA, J. M. LÓPEZ, R. AZENCOTT, M. R. BENNETT, K. JOSIĆ, AND W. OTT, *Modeling delay in genetic networks: From delay birth-death processes to delay stochastic differential equations*, The Journal of Chemical Physics, 140 (2014), p. 204108.

[30] J. K. HALE AND S. M. V. LUNEL, *Introduction to functional differential equations*, Springer-Verlag, 1993.

[31] G. HEK, *Geometric singular perturbation theory in biological practice*, Journal of Mathematical Biology, 60 (2010), pp. 347–386.

[32] T. INSPERGER AND G. STÉPÁN, *Semi-discretization for time-delay systems, stability and engineering applications*, Springer, 2011.

[33] T. INSPERGER, G. STÉPÁN, AND TURI, *State-dependent delay in regenerative turning processes*, Nonlinear Dynamics, 47 (2007), pp. 275–283.

[34] K. JOSIC, J. M. LOPEZ, W. OTT, L. J. SHIAU, AND M. BENNET, *Stochastic delay accelerates signaling in gene networks*, PLoS Computational Biology, 7 (2011).

[35] O. KANAKOV, T. LAPTYEVA, L. TSIMRING, AND M. IVANCHENKO, *Spatiotemporal dynamics of distributed synthetic genetic circuits.*, Physica D, 318-319 (2016), pp. 116–123.

[36] I. KATS, *On the stability of systems with random delay in the first approximation*, Prikladnaya Matematika i Mekhanika (P. M. M.), translated as Journal of Applied Mathematics and Mechanics, 31 (1967), pp. 447–452.

[37] V. L. KHARITONOV AND S.-I. NICULESCU, *On the stability of linear systems with uncertain delay*, IEEE Transactions on Automatic Control, 48 (2003), pp. 127–132.

[38] S. KLUMPP, *A superresolution census of RNA polymerase*, Biophysical Journal, 105 (2013), pp. 2613–2614.

[39] V. B. KOLMANOVSKII AND V. R. NOSOV, *Stability of Functional Differential Equations*, vol. 180 of Mathematics in Science and Engineering, Academic Press Inc., 1986.

[40] I. KOLMANOVSKY AND T.L. MAIZENBERG, *Stochastic stability of a class of nonlinear systems with randomly varying time-delay*, in Proceedings of the American Control Conference, Chicago, Illinois, USA, 2000.

[41] W. KONG, V. CELIK, C. LIAO, Q. HUA, AND T. LU, *Programming the group behaviors of bacterial communities with synthetic cellular communication*, Bioresources and Bioprocessing, 1 (2014), p. 24.

[42] R. KRTOLICA, Ü. ÖZGÜNER, H. CHAN, H. GÖKTAŞ, J. WINKELMAN, AND M. LIUBAKKA, *Stability of linear feedback systems with random communication delays*, International Journal of Control, 59 (1994), pp. 925–953.

[43] M. KRUPA AND P. SZMOLYAN, *Relaxation oscillation and canard explosion*, Journal of Differential Equations, 174 (2001), pp. 312–368.

[44] H. J. KUSHNER, *Introduction to stochastic control*, Holt, Rinehart and Winston, 1971.

[45] A. A. KWIECIŃSKA, *Stabilization of partial differential equations by noise*, Stochastic Processes and their Applications, 79 (1999), pp. 179–184.

[46] J. LEWIS, *Autoinhibition with transcriptional delay: a simple mechanism for the zebrafish somitogenesis oscillator*, Current Biology, 13 (2003), pp. 1398–1408.

[47] E. A. LIDSKII, *On stability of motion of a system with random delays*, Differentialnye Uravnenia, translated as Differential Equations, 1 (1965), pp. 96–101.

[48] X. LIU AND J. SHEN, *Stability Theory of Hybrid Dynamical Systems With Time Delay*, IEEE Transactions on Automatic Control, 51 (2006), pp. 620–625.

[49] D. M. LONGO, J. SELIMKHANOV, J. D. KEARNS, J. HASTY, A. HOFFMANN, AND L. S. TSIMRING, *Dual delayed feedback provides sensitivity and robustness to the nf-κb signaling module*, PLoS Computational Biology, 9 (2013).

[50] M. C. MACKEY, A. LONGTIN, AND A. LASOTA, *Noise-induced global asymptotic stability*, Journal of Statistical Physics, 60 (1990), pp. 735–751.

[51] J. MALLET-PARET AND H. L. SMITH, *The Poincaré-Bendixson theorem for monotone cyclic feedback systems*, Journal of Dynamics and Differential Equations, 2 (1990).

[52] X. MAO, *Exponential stability of stochastic delay interval systems with Markovian switching*, IEEE Transactions on Automatic Control, 47 (2002), pp. 1604–1612.

[53] C. A. MASIELLO, Y. CHEN, X. GAO, S. LIU, H.-Y. CHENG, M. R. BENNETT, J. A. RUDGERS, D. S. WAGNER, K. Z. ZYGOURAKIS, AND J. J. SILBERG, *Biochar and microbial signaling: Production conditions determine effects on microbial communication*, Environmental Science and Technology, 47 (2013), pp. 11496–11503.

[54] H. H. MCADAMS AND A. ARKIN, *It's a noisy business! genetic regulation at the nanomolar scale*, Trends in Genetics, 15 (1999), pp. 65–69.

[55] W. MICHIELS, V. VAN ASSCHE, AND S.-I. NICULESCU, *Stabilization of time-delay systems with a controlled time-varying delay*, IEEE Transactions on Automatic Control, 50 (2005), pp. 493–504.

[56] M. B. MILLER AND B. L. BASSLER, *Quorum sensing in bacteria*, Annu Rev Microbiol, 333 (2001), pp. 1315–1319.

[57] P. A. P. MORAN, *Random processes in genetics*, Mathematical Proceedings of the Cambridge Philosophical Society, 54 (1958), pp. 60–71.

[58] A. N. NAGANATHAN AND V. MUÑOZ, *Scaling of folding times with protein size*, Journal of the American Chemical Society, 127 (2005), pp. 480–481.

[59] D. NEVOZHAY, R. M. ADAMS, E. VAN ITALLIE, M. R. BENNETT, AND G. BALÁZSI, *Mapping the environmental fitness landscape of a synthetic gene circuit*, PLoS Computational Biology, 8 (2012), p. e1002480.

[60] J. NILSSON, B. BERNHARDSSON, AND B. WITTENMARK, *Stochastic analysis and control of real-time systems with random time delays*, Automatica, 34 (1998), pp. 57–64.

[61] M. A. NOWAK, *Evolutionary dynamics: exploring the equations of life*, Harvard University Press, 2006.

[62] G. OROSZ, J. MOEHLIS, AND R. M. MURRAY, *Controlling biological networks by time-delayed signals*, Philosophical Transactions of the Royal Society A, 368 (2010), pp. 439–454.

[63] P. G. PARK, *A delay-dependent stability criterion for systems with uncertain time-invariant delays*, IEEE Transactions on Automatic Control, 4 (1999), pp. 876–877.

[64] K. M. PRZYLUSKI, *Stability of linear infinite-dimensional systems revisited*, International Journal of Control, 48 (1988), pp. 513–523.

[65] X. PU AND H. ZHAO, *Stability of a kind of hybrid systems with time delay*, Advances in Electronic Engineering, Communication and Management, 139 (2012), pp. 159–165.

[66] W. B. QIN, M. M. GOMEZ, AND G. OROSZ, *Stability and frequency response under stochastic communication delays with applications to connected cruise control design*, IEEE Transactions on Intelligent Transportation Systems, 18 (2017), pp. 388–403.

[67] S. REGOT, J. MACIA, N. CONDE, K. FURUKAWA, J. KJELLEN, T. PEETERS, S. HOHMANN, E. DE NADAL, F. POSAS, AND R. SOLE, *Distributed biological computation with multicellular engineered networks*, Nature, 469 (2011), pp. 207–211.

[68] R. A. RYAN, *Introduction to tensor products of Banach spaces*, Springer, 2002.

[69] M. SADEGHPOUR AND G. OROSZ, *On the stability of continuous-time systems with stochastic delay: applications to gene regulatory circuits*, in ASME IDETC, 2014, p. V006T10A078.

[70] M. SCOTT, C. W. GUNDERSON, E. M. MATEESCU, Z. ZHANG, AND T. HWA, *Interdependence of cell growth and gene expression: origins and consequences*, Science, 330 (2010), pp. 1099–1102.

[71] J. SIEBER, K. ENGELBORGHS, T. LUZYANINA G. SAMAEY, AND D. ROOSE, *DDE-BIFTOOL v. 3.1.1 Manual–Bifurcation analysis of delay differential equations*.

[72] H. SMITH, *An introduction to delay differential equations with sciences applications to the life*, vol. 57 of Texts in Applied Mathematics, Springer, 2011.

[73] D. SPRINZAK AND M. B. ELOWITZ, *Reconstruction of genetic circuits*, Nature, 438 (2005), pp. 443–448.

[74] G. STÉPÁN, *Retarded dynamical systems: stability and characteristic functions*, vol. 210 of Pitman Research Notes in Mathematics, Longman, 1989.

[75] J. STRICKER, S. COOKSON, M. R. BENNETT, W. H. MATHER, L. S. TSIMRING, AND J. HASTY, *A fast, robust and tunable synthetic gene oscillator*, Nature, 456 (2008), pp. 516–519.

[76] Y. SUN AND J. XU, *Stability analysis and controller design for networked control systems with random time delay*, in The Ninth International Conference on Electronic Measurement and Instruments (ICEMI), 2009, pp. 136–141.

[77] J. J. TABOR, H. M. SALIS, Z. B. SIMPSON, A. A. CHEVALIER, A. LEVSKAYA, E. M. MARCOTTE, C. A. VOIGT, AND A. D. ELLINGTON, *A synthetic genetic edge detection program*, Cell, 137 (2009), pp. 1272–1281.

[78] C. TAN, P. MARGUET, AND L. YOU, *Emergent bistability by a growth-modulating positive feedback circuit*, Nature Chemical Biology, 5 (2009), pp. 842–848.

[79] B. VAN DER POL, *LXXXVIII. on "relaxation-oscillations"*, The London, Edinburgh, and Dublin Philosophical Magazine and Journal of Science, 2 (1926), pp. 978–992.

[80] A. VELIZ-CUBA, C. GUPTA, M. R. BENNETT, K. JOSIĆ, AND W. OTT, *Effects of cell cycle noise on excitable gene circuits*, Physical Biology, 13 (2016), p. 066007.

[81] O. S. VENTURELLI, H. EL-SAMAD, AND R. M. MURRAY, *Synergistic dual positive feedback loops established by molecular sequestration generate robust bimodal response*, Proceedings of the National Academy of Sciences of the United States of America, 109 (2012), pp. E3324–33.

[82] E. I. VERRIEST AND W. MICHIELS, *Stability analysis of systems with stochastically varying delays*, Systems and Control Letters, 58 (2009), pp. 783–791.

[83] U. VOGEL AND K. F. JENSEN, *The RNA chain elongation rate in Escherichia coli depends on the growth rate*, Journal of Bacteriology, 176 (1994), pp. 2807–2813.

[84] E. H. WINTERMUTE AND PAMELA A. SILVER, *Dynamics in the mixed microbial concourse*, Genes & Development, 24 (2010), pp. 2603–2614.

[85] F. WU, D. J. MENN, AND X. WANG, *Quorum-sensing crosstalk-driven synthetic circuits: From unimodality to trimodality*, Chemical Biology, 21 (2014), pp. 1629–1638.

[86] Z. XIE, L. WROBLEWSKA, L. PROCHAZKA, R. WEISS, AND Y. BENENSON, *Multi-input RNAi-based logic circuit for identification of specific cancer cells*, Science, 333 (2011), pp. 1307–1311.

[87] P. XING-CHENG AND Y. WEI, *Stability of hybrid stochastic systems with time-delay*, ISRN Mathematical Analysis, (2014). Article ID 423413.

[88] L. YOU, R. S. COX III, R. WEISS, AND F. H. ARNOLD, *Programmed population control by cell-cell communication and regulated killing*, Nature, 428 (2004), pp. 868–871.

[89] C. YUAN AND X. MAO, *Stability of stochastic delay hybrid systems with jumps*, European Journal of Control, 16 (2010), pp. 595–608.

[90] D. YUE, Y. ZHANG, E. TIAN, AND C. PENG, *Delay-distribution-dependent exponential stability criteria for discrete-time recurrent neural networks with stochastic delay*, IEEE Transactions on Neural Networks, 19 (2008), pp. 1299–1306.

[91] F. ZHANG, J. CAROTHERS, AND J. D. KEASLING, *Design of a dynamic sensor-regulator system for production of chemicals and fuels derived from fatty acids*, Nature Biotechnology, 30 (2012), pp. 354–359.